Telemark University College
Faculty of technology
M.Sc. Programme

MASTER THESIS 2008

Recommendation of a Model for Simulating & Analysis of the Influence of Particle Size Distribution on the Simulations of Bubbling Fluidized Beds

D.G.A. Sanoja U. Ariyarathna

Faculty of Technology
Address: Kjolnes Ring 56, N-3914 Porsgrunn, Norway, tel: +47 35 57 50 00, fax: +47 35 55 75 47

Telemark University College
Faculty of Technology
M.Sc. Programme

WRITTEN REPORT MASTER THESIS, COURSE CODE FMH60

Student : D.G.A. SANOJA U. ARIYARATHNA

Thesis Title : Recommendation of a Model for Simulating & Analysis of the Influence of Particle Size Distribution on the Simulations of Bubbling Fluidized Beds

Signature : . . . . . .

Number of pages : 131

Keywords : CFD, Bubbling fluidized bed, Particle size distribution, Particle segregation, Bubble behaviour, Bed expansion

Supervisor : Ass. Prof. Britt M. Halvorsen sign.: . . . . . .

2nd Supervisor : - sign.: . . . . . .

Sensor : - sign.: . . . . . .

External partner : -

Availability : <Open/Secret>

Archive approval (supervisor signature): . . . . . **Date:** . . . . . .

Abstract:

A computational study of the influence of particle size distribution on bubbling fluidized beds is performed. Several simulations are performed using Eulerian multiphase model for a two dimensional fluidized bed with an air jet as preliminary work. The commercial software FLUENT is used to perform the simulations. A combination of the models available in FLUENT is finalized as a good combination to be used in the main work.

The finalised combination of models is used to simulate a two dimensional fluidized bed with uniform distribution of air in order to check the influence of particle size distribution on simulations. The "Syamlal O'Brien Symmetric" drag model is used to introduce the solid-solid drag forces and the "Syamlal O'Brien" drag model to introduce the solid-fluid drag forces. Five simulations are performed with increasing number of particle phases in the bed, such as, one simulation with one particle phase, two simulations with two particle phases and two simulations with three and four particles phases in each. The five simulations are compared with each other and with an experiment performed by Mr. Wu W.J.

Representation of the particle size distribution in the simulations is arranged according to the particle distributions of the particle mixture used in the reference experiment except in one simulation. Each particle phase is represented by the corresponding mean particle diameter. The same mean particle diameter persists in all five simulations.

The comparison conducted in terms of the particle segregation, expansion of the particle bed and the bubble behaviour in the particle bed. All simulated mixtures have predicted particle segregation, bubbles in the bed and expansion in the particle bed, except the simulation with only one particle phase. The reason is found as the superficial gas velocity used in the simulations, which is well bellow the minimum fluidization velocity of the particles used in the bed.

Prediction of particle segregation in simulations is analyzed using contours of the particle phases as well as the plots of volume fraction (VOF) data it self. The progress of the particle segregation also analyzed using VOF data of particle phases at along the height of the bed and at selected points of the bed. Bubble behaviour prediction is analyzed in terms of bubble velocity, bubble frequency, bubble distribution in the bed and the lowest position of bubble occurrence in the bed. The bed expansion in the simulations is compared with the reference experiment using contours of the particle phases.

Comparison of the simulated results with the reference experiment showed that the higher the number of particle phases the better the prediction of particle segregation, bubble behaviour and the bed expansion in the simulations. Also it is observed that, the closer the presentation of the particle size distribution in the simulation to the mixture used in the experiment the better the prediction of the dynamics of the particle bed.

Two abstracts have been sent to the AICHE – 2008 annual meeting and SIMS 2008 conference using some of the work performed related to this study.

Recommendation of a Model for Simulating & Analysis of the Influence of Particle Size Distribution on the Simulations of Bubbling Fluidized Beds

D.G.A. Sanoja U. Ariyarathna

06. June 2008

Contents

Part I

Nomenclature

VOF = Volume fraction
frs = Frames per second
$\vec{v}$ = Velocity of a phase $\left(ms^{-1}\right)$
$\dot{m}$ = Rate of mass transfer from the one phase to another $\left(kgs^{-1}\right)$
ρ_{rq} = Phase reference density $\left(kgm^{-3}\right)$
(volume averaged density of the q^{th} phase in the solution domain)
α = Phasic volume fractions (dimensionless)
ρ = Physical density of a phases $\left(kgm^{-3}\right)$
S_q = Source term (dimensionless)
t = Time (s)
$\vec{R}_{pq}$ = Interphase force $\left(N/m^2\right)$
p = Pressure (Pa)
$\overline{\overline{\tau}}$ = Stress-strain tensor (Pa)
$\overrightarrow{g}$ = Gravitational acceleration $\left(ms^{-2}\right)$
K = Interphase momentum exchange coefficient $\left(kgs^{-1}\right)$
$\vec{F}_q$ = External body force $\left(N/m^2\right)$
$\vec{F}_{lift,q}$ = Lift force $\left(N/m^2\right)$
$\vec{F}_{vm,q}$ = Virtual mass force $\left(N/m^2\right)$
$\vec{v}_{qp}$ = Interphase velocity $\left(ms^{-1}\right)$
h = Specific enthalpy of a phase (kJ/kg)
$\vec{q}$ = Heat flux $\left(W/m^2\right)$
Q = Intensity of heat exchange between the phases (W)
$h_{pq},\ h_{qp}$ = Interphase enthalpy (kJ/kg)
C_D = Drag coefficient (dimensionless)
$\upsilon_{r,s}$ = Terminal velocity for the solid phase $\left(ms^{-1}\right)$
Re_s = Relative Reynolds number (dimensionless)
d = Diameter of the particles in a solid phase (m)
μ_l = Shear viscosity of phase fluid phase l $(Pa.s)$
e = Coefficient of restitution (dimensionless)
C_{fr} = Coefficient of friction between particles of two solid phases (dimensionless)
g_0 = Radial distribution function (dimensionless)
p_s = Solids pressure (Pa)
Θ = Granular temperature $\left(m^2/s^2\right)$
μ_{fr} = Frictional viscosity $(Pa.s)$
ϕ = Angle of internal friction (dimensionless)
I_{2D} = Second invariant of the deviatoric stress tensor $\left(s^{-2}\right)$
$\mu_{s,kin}$ = Kinetic viscosity $(Pa.s)$
$\mu_{s,\mathrm{col}}$ = Collisional viscosity $(Pa.s)$
λ_s = Granular bulk viscosity $(Pa.s)$

Part II

Recommendation of a CFD Model for Simulating the Bubbling Fluidized Beds

Chapter 1

Introduction

Fluidization is a well known mechanism in industry for the purpose of mixing the particles. This operation makes the solid to achieve a fluid like behavior while suspending it in a gas or a liquid. The fluid like behavior of solids gives a rapid and easy transportation ability with intimate gas contacting, which is the most important factor that makes the fluidization an important unit operation used in industry.

The phenomenon of fluidization can be described using some of the stages that a bed will go through during the fluidization process. The first stage is the fixed bed (Figure 1.1 (a)). The fluid is having a very low flow velocity and fills the void spaces between the stationary particles in the bed and passes through the bed slowly at this stage. When the flow rate is increased a little, particles tends to move apart and also to vibrate resulting the expanded bed stage. By increasing the flow velocity further, it is possible to get a state, where the solid particles are only suspending in the fluid, which is the minimum fluidization (Figure 1.1 (b)). The fluid flow velocity at this state is the minimum fluidization velocity. At this state the frictional force between particles and fluid just counterbalance the weight of the particles, the vertical component of the compressive force between adjacent particles disappears, and the pressure drop through any section of the bed is about equals the weight of fluid and the solid in that section of the bed [13]. When the fluid flow increases further the dynamics of the bed tends to achieves further changes, but the resultant state is more dependant on the system type.

There are mainly two types of fluidization systems. Those are the solid-liquid systems and solid-gas systems. Both systems are considered as dense phase fluidized beds as the upper surface of the bed can be clearly defined. As this study focuses the gas-solid systems, only those will be described here.

Gas-solid systems show instabilities with bubbling and channeling in the solid bed, when the fluid velocity is increased above the minimum fluidization velocity. Even though the bed doesn't expand much than the height it has at the minimum fluidization conditions, it gives better agitation as the particle movements become more violent due to the instability. Such a bed is a bubbling

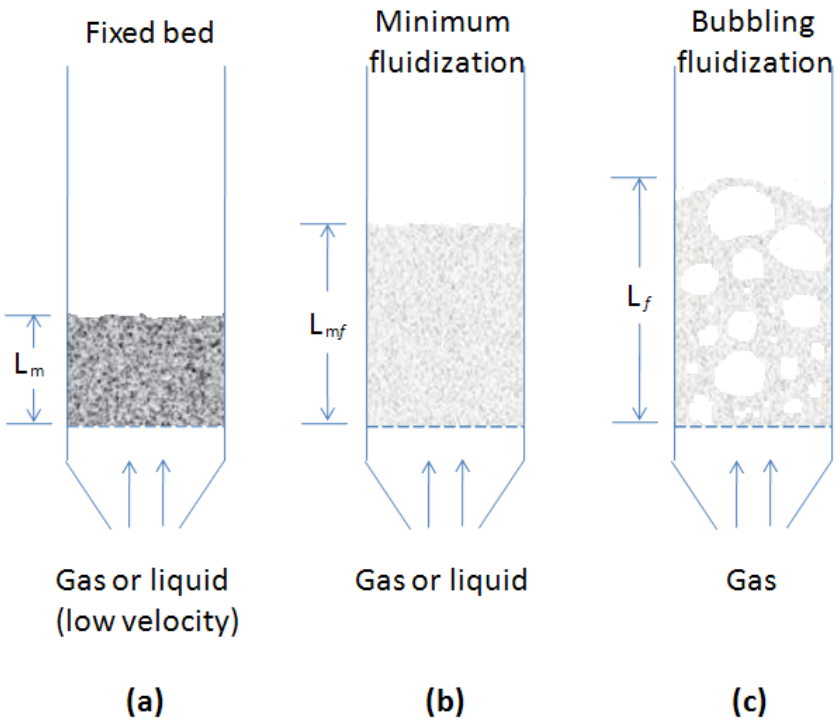

Figure 1.1: Various stages of a fluidized bed

fluidized bed (Figure 1.1 (c)), which is the main focus of this study.

Unlike the liquid-solid fluidized beds, the gas-solid fluidized beds have some unusual and useful properties compared to other contacting and mixing methods. The gas-solid fluidized beds looks very much like a boiling liquid and in many ways exhibits liquid-like behavior [13]. For example, if a large, light object is easily pushed in to a bed and released, it will pop up and float on the surface (Figure 1.2 (a)). When the container is tipped, the upper surface of the bed remains horizontal (Figure 1.2 (b)), and when two beds are connected there levels equalizes (Figure 1.2 (d)). Also, the pressure gradient between any two points in a bed is roughly equal to the static head of bed between those two points (Figure 1.2 (e)). The bed also shows liquid-like flow properties by gushing the solid in a jet from a hole in a side of the container (Figure 1.2 (c)) and by flowing like a liquid from vessel to vessel.

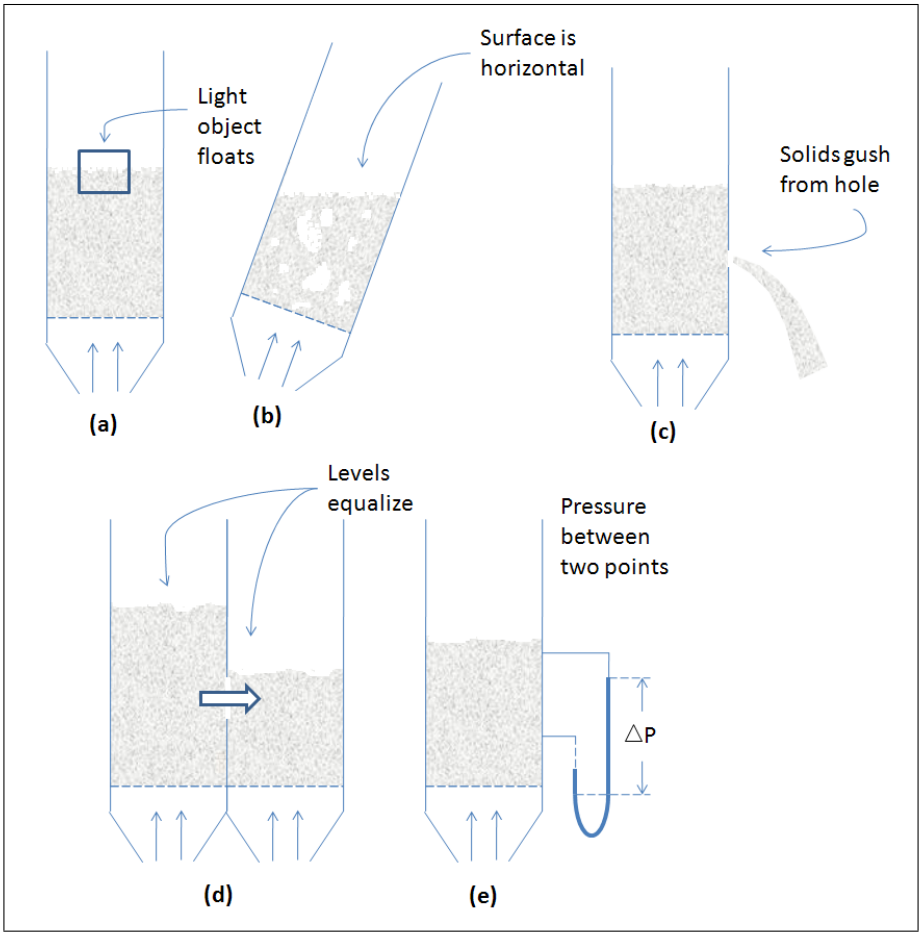

Figure 1.2: Liquid-like behavior of gas fluidized beds

1.1 Fluidization Compared with Other Mixing Methods

Fluidization is important when it comes to reactors and normal mixers due the unusual mixing abilities of the fluidized beds. Comparisons of the gas-solid fluidized beds with other types of contacting methods have shown that the gas-solid fluidized beds has excellent controlling ability of temperature which allows good operating conditions for solid catalyzed gas phase reactions compared to other contacting methods. Also, the temperature is almost constant throughout the bed while some of the other contacting types get severe temperature gradients, which is difficult to handle. Unlike the other contacting types, fluidization can handle a wide size distribution in the bed. More details about the comparisons are given in the appendix A**.**

The gas-solid fluidized systems have both pluses and minuses that should be considered. The advantages and disadvantages of fluidized beds for industrial operations are as follows [14].

1.1.1 Advantages

1. The smooth, liquid-like flow of particles allows continuous automatically controlled operations with easy handling.
2. The rapid mixing of solids leads to close to isothermal conditions throughout the reactor; hence the operation can be controlled simply and reliably.
3. In addition, the whole vessel of well mixed solids represents a large thermal flywheel that resists rapid temperature changes, responds slowly to abrupt changes in operating conditions, and gives a large margin of safety in avoiding temperature runaways for highly exothermic reactions.
4. The circulation of solids between two fluidized beds makes it possible to remove (or add) the vast quantities of heat produced (or needed) in large reactions.
5. It is suitable for large scale operations
6. Heat and mass transfer rates between gas and particles are high when compared with other modes of contacting
7. The rate of heat transfer between a fluidized bed and an immersed object is high; hence heat exchangers within fluidized beds require relatively small surface areas.

1.1.2 Disadvantages

1. For bubbling beds of fine particles, the difficult-to -describe flow of gas, with its large deviations from the plug flow, represents insufficient contacting. This becomes specially serious when high conversion of gaseous reactant or high selectivity of a reaction intermediate is required.

2. The rapid mixing of solids in the bed leads to nonuniform residence times of solids in the reactor. For continuous treatment of solids, this gives a nonuniform product and poorer performance, especially at high conversion levels. For catalytic reactions, the movement of porous catalytic particles, which continually capture and release reactant gas molecules, contributes to the back mixing of gaseous reactant, thereby reducing yield and performance.

3. Friable solids are pulverized and entrained by the gas and must be replaced.

4. Erosion of pipes and vessels from abrasion by particles can be serious.

5. For non-catalytic operations at high temperatures, the agglomeration and sintering of fine particles can be require a lowering in temperature of the operation, thereby reducing the reaction rate considerably.

1.2 Industrial Applications of Fluidized Beds

Depending on the advantages and disadvantages, there are a vast range of industrial applications, which are dependant on the gas-solid fluidization systems. A common application is to use the fluidized beds as heat exchangers, because of there unique ability to rapidly transport heat and maintain a uniform temperature. Also, it is used in industrial applications where granules to be made from the solidification of a melt. One example is the production of urea granules. In that process, the sprayed molten urea falls as droplets through a tall tower while cold air passes upwards through the tower, cooling and solidifying the droplets [14]. The few big droplets still needing to be frozen fall in to the base of the tower. They are quickly covered by a layer of small solids, move around the bed, and then get solidified.

Fluidized beds are used in industry for the purpose of coating metal objects with plastics. The importance is that the coating can be done accurately even for the uneven and heavily concave surfaces, while having thicker coating than paint. In addition, fluidization is used for coating of other objects like tablets of drugs, sweets and etc and also for growing of particles like table salt. Drying of solids is an other application of fluidization. The fluidized bed dryer is used extensively in a wide variety of industries because of its large capacity, low construction cost, easy operability, and high thermal efficiency [14]. It is suited for any kind of wet solid as long as the solid can be fluidized by hot gas.

Fluidized beds are used in industry in order to carry out synthesis reactions too. The main reason for choosing the fluidized bed rather than the fixed bed for these solid-catalyzed gas phase reactions is the demand for strict temperature control of the reaction zone [14]. There are several possible reasons for this demand like the reaction may be explosive out side a narrow temperature range, the yield of the desired product to side products may be sensitive to the temperature level of the operation, or hot spots in the catalyst may lead to the rapid

deterioration and deactivation of otherwise stable catalyst that normally does not require regeneration. The temperature control is difficult as those reactions are generally highly exothermic. Due to the poor heat transfer characteristics and very low heat capacities of gases compared to their heats of reaction, it is difficult to achieve the necessary positive temperature control in fixed beds. Consequently, extensive heat exchanger surface and large dilution of reactant gases are often required. This control is much easier to obtain due to the rapid circulation of solids of relatively high heat capacity in fluidized beds. Such a fluidized bed efficiently distributes the heat and helps eliminate potential hot spots.

Cracking of hydrocarbons is another industrial operation where the fluidized beds are in use. Catalytic or thermal break down of hydrocarbons to lower molecular weight materials is known as cracking of hydrocarbons. Those reactions are exothermic and there is a high tendency of getting carbon depositions on the nearby solids surfaces. Typically, those operations require two locations. First location is for heat absorption, reaction and carbon deposition. The second location is for burn off the deposited carbon and release heat. The heat released is normally transported back to the first location to feed the reaction with use of circulating solids. The most efficient way to carry out all those steps is to use a solid circulation system which have one or more fluidized beds. The circulating fluidized beds are preferred in this operation.

Fluidized beds are used in industry for the combustion of low grade coal and oil shale fines, fuels that cannot be burned efficiently in conventional boiler furnaces and for the incineration of solid waste. Carbonization and gasification is also an other area with importance of fluidization. Many different routs and concepts are used for the gasification of coal. Those have a variety of contacting and heat supplying methods in order to carry out the reaction. Some of those methods are involved in using fluidized bed gas generators. Activation of carbon also comes under the same area of application of fluidized beds. In addition, gasification of solid waste is performed using of fluidized beds, and well known as a better method than waste incineration as the clean up of combustion gas is far simpler and cheaper as the volume of gas produced is smaller than that of incinerators.

In addition to all those applications, fluidized beds are widely used in industrial operations where reactions involving solids take place. The latest area of application of fluidized beds is in operation of bio-fluidization, in other words the cultivation of microorganisms. Fluidized cultivation is reported to be superior to the conventional layer cultivation in the following areas [14]:

- Large effective growing surface of microorganisms
- Easy oxygen transfer results in an active metabolism
- Heat and carbon dioxide generated by this active metabolism are effectively removed
- Temperature, moisture, and pH level are easily and automatically controlled

It is expected that the bio-fluidized reactors will be increasingly used in the food and pharmaceutical industry.

1.3 Importance of Analyzes

Above discussion shows that the fluidized beds are widely used in a vast range of industrial applications. Both the fine and large particles can be used in those applications depending on the requirement. Fine particles of wide particle size distribution can be fluidized in a wide range of gas flow rates, permitting flexible operations with deep, large beds. On the contrary, beds of large uniformly sized solids often fluidized poorly, with bumping, spouting, and slugging. That may cause serious structural damage in large beds. Numerous other factors may also effect the quality of fluidizers, such as vessel geometry, gas inlet arrangement, type of solids used, and whether the solids are free flowing or liable to agglomerate. It is important to have a good understanding about those factors for the optimum use of the fluidized beds.

In addition it is emphasized that the bubbling fluidization (bubbling fluidized beds) is in a competitive position with the circulation fluidization. It is important to study about the dynamics and other properties of the bubbling fluidized beds. The later sections of this report has presented a study focused on the bubbling fluidization.

The most important property of fluidized beds compared to other contacting methods is the large contact area between phases in the beds, which enhances the heat and mass transfer as well as the chemical reactions. As a combination of those properties the efficiency of the bed gives the path for optimization of processes. The efficiency of the bubbling fluidized beds are dependant on the bubble size, bubble frequency, bubble distribution and bubble velocity in the bed. The bubble characteristics are very important in the design of fluidized beds because they govern hydrodynamics and efficiency of the operation for which the bed is used [3]. It is with a great importance to study how those things dependant on the particle size distribution.

Simulations with satisfactory results are the prime requirement for this type of studies. A CFD model for simulating bubbling fluidized beds will be built in this project work by combining different models exists in the commercial CFD software FLUENT. A comparison between the simulated and experimental results will be carried out in order to test and finalize the CFD model.

The finalized model will be used in few more simulations having particle size distributions introduced. The influence form the particle size distribution on simulations will be analyzed by comparing the simulations with each other and comparing the simulations with an experiment, which is done in a 2-D fluidized bed under the same conditions as in the simulations.

Chapter 2

Multiphase Modelling

Computational fluid dynamics has improved a lot within past years. Ahmadi et al [1] developed a thermodynamical formulation dispersed multiphase turbulent flows and Lun et al [17] introduced kinetic theories for granular flow to inelastic and slightly inelastic particles. Many other people have contributed to the study area and developed mathematical models that can be useful in simulating fluidized beds.

Fluidized beds usually consists of two phases at least (solid and gas) and can be simulated without much trouble. If the simulations having more than one solid phase in the bed, then the situation becomes complex. The multiphase modelling has to be used for simulating the Bubbling fluidized beds. Basic approaches available for multiphase modelling and the models available in FLUENT have presented in this chapter. Importance of using special features and special conditions while performing the simulations have also presented.

2.1 Basic Approaches of Multiphase Modelling

There are two approaches available currently for numerical calculations of the multiphase flows. Those are the Euler-Lagrange approach and the Euler-Euler approach.

Euler-Euler Approach

The Euler-Euler approach is especially useful and computationaly cost effective when the volume fractions (VOFs) of the phases are comparable, or when the body forces (such as gravity) act to separate phases, or when the interaction within and between the phases plays a significant role in determining the hydrodynamics of the system [19]. In the Euler-Euler Approach different phases are treated separately. As the volume occupied by a phase cannot be taken by another phase, phasial VOFs are considered for the analysis. Phasial VOFs are assumed to be continuous functions of space and time. The sum of the phasial VOFs is equal to unity. A set of conservation equations are solved including one

equation for each phase. Those set of equations are closed by using the kinetic theory of granular flow or other constitutive relations that are obtained from empirical information.

Euler-Lagrange Approach

In the Euler-Lagrange approach the fluid phase is treated as a continuum by solving the time-averaged Navier-Stokes equations. The dispersed phase is solved by considering a large number of particles, bubbles or droplets. It is considered that the dispersed phase can exchange momentum, mass, and energy with the fluid phase. The path that a particle, bubbles or droplet follows are calculated individually at specified intervals during the fluid phase calculations. According to the above features this approach is inappropriate for modeling the fluidized beds, or any application where the VOF of the secondary phase is not negligible.

2.1.1 Use of Multiphase Approaches in Research

Research have conducted using both the Euler-Euler approach and the Euler-Lagrange approach depending on the requirements. Halvorsen, B. [10] has used the Euler-Euler approach with MFIX software programme in her simulations of bubbling fluidized beds. Patil et al [20] and [21] have used Euler-Euler approach with two different closure models. Those are the constant viscosity model and a model based on the kinetic theory of granular flow. They have compared the simulated results of the two models with each other and also with the experimental results. Enwald et at [7] have presented a model using Euler-Euler approach as well as the application of the model in the simulations of bubbling and circulating fluidized beds.

Huilin et al [11] has used both approaches separately showing the results as a comparison with the experiments. Details of particle collision information are obtained through tracing particle motions based on Euler-Lagrange approach coupled with the discreet hard sphere model. A CFD model based on kinetic theory of granular flow and Euler-Euler approach is used to simulate flows in bubbling gas-solid fluidized beds.

Boemer et al [4] have developed a computer code to simulate the fluid dynamics of fluidized beds using Eularian approach. Arastoopour, H. [2] has used Eularian approach for the simulations he used to compare the predicted flow parameters with large scale experimental data of fluidized beds.

2.2 The Eulerian Model

Three different multiphase models are available under the Euler-Euler approach in FLUENT. Those are the volume of fluid model, the mixture model and the Eulerian model. Eularian model is the suitable model to simulate granular flows. The Eulerian model is used with unsteady conditions in the simulations related to this study of bubbling fluidized beds.

The Eulerian model is the most complex multiphase model in FLUENT [8]. It gives a set of equations as it solves continuity and momentum conservation equations for each phase. Pressure and momentum exchange coefficients couple the set of equations. The kinetic theory has used to introduce the properties of granular flows. Depending on the type of the mixture, the momentum transfer between phases is also modeled. The Eulerian multiphase model can be applied to bubble columns, risers, particle suspensions, and fluidized beds.

2.2.1 Use of the Eulerian Model in Simulations

Any number of phases can be used in the simulations with Eularian model depending on the memory capacity available and the convergency of the system. It is possible to use this model for simulating the bubbling fluidized beds while introducing the particle size distribution of the granular material. While the Eularian model has selected as the multiphase model, other parameters like drag coefficient, solids pressure, granular viscosity and etc have to be specified also. There are number of models available in FLUENT for most of those parameters and those models have presented in the following sections.

2.2.2 Models Available in FLUENT

In simulations of multiphase flows, the continuity, momentum and the energy equations will be solved for each phase. VOF of each phase will be calculated by solving the continuity equation. The continuity, momentum and energy equations are presented below in their general format for a case that have n number of phases. Other models to specify some of the parameters in those equations are also presented as required.

.

Continuity Equation

$$\frac{1}{\rho_{rq}}\left(\frac{\partial}{\partial t}\left(\alpha_q\rho_q\right)+\nabla.\left(\alpha_q\rho_q\vec{v}_q\right)=\sum_{p=1}^{n}\left(\dot{m}_{pq}-\dot{m}_{qp}\right)\right)+S_q$$

Here ρ_{rq} and ρ_q are the phase reference density (the volume averaged density of the q^{th} phase in the solution domain.) and the physical density of phase q respectively. α_q is the phasic volume fraction and $\vec{v}_q$ is the velocity of phase q. $\dot{m}_{pq}$ and $\dot{m}_{qp}$ represent the rate of mass transfer from the p^{th} to q^{th} phase and the q^{th} to p^{th} phase. S_q is the source term.

.

Momentum Conservation Equation

$$\begin{aligned}\frac{\partial}{\partial t}\left(\alpha_q\rho_q\vec{v}_q\right)+\nabla.\left(\alpha_q\rho_q\vec{v}_q\vec{v}_q\right) &= -\alpha_q\nabla p+\nabla.\overline{\overline{\tau_q}}+\alpha_q\rho_q\overrightarrow{g}\\ &\quad+\sum_{p=1}^{n}\left(\vec{R}_{pq}+\dot{m}_{pq}\vec{v}_{pq}-\dot{m}_{qp}\vec{v}_{qp}\right)\\ &\quad+\left(\vec{F}_q+\vec{F}_{lift,q}+\vec{F}_{vm,q}\right)\\ \sum_{p=1}^{n}\vec{R}_{pq} &= \sum_{p=1}^{n}K_{pq}\left(\vec{v}_p-\vec{v}_q\right)\end{aligned}$$

∇p is the pressure gradient and $\overline{\overline{\tau_q}}$ is the q^{th} phase stress-strain tensor. $\overrightarrow{g}$ is the gravitational acceleration, $\vec{R}_{pq}$ is the interphase force and K_{pq} is the interphase momentum exchange coefficient. $\vec{F}_q$, $\vec{F}_{lift,q}$ and $\vec{F}_{vm,q}$ represent an external body force, a lift force and a virtual mass force respectively. $\vec{v}_{qp}$ is the interphase velocity.

The momentum exchange coefficient can be either fluid-solid or solid-solid when it is for a bubbling fluidized bed with more than two phases. A Drag function is included in most of the exchange coefficients. That means the exchange coefficient varies according to the drag coefficient. Three models are available in FLUENT to specify the drag function and those have presented in the table below.

.

.

Fluid-solid exchange	
Syamlal-O'Brien model	Appropriate when the solids shear stresses are defined according to Syamlal et al
$K_{ls}=\frac{\alpha_s\rho_s\left(\frac{C_D\,\mathrm{Re}_s\,\alpha_l}{24v_{r,s}^2}\right)}{\tau_s}$, $C_D=\left(0.63+\frac{4.8}{\sqrt{\mathrm{Re}_s/v_{r,s}}}\right)^2$	
Wen and Yu model	
$K_{ls}=\frac{3}{4}C_D\frac{\alpha_s\alpha_l\rho_l\left\lvert\overrightarrow{v_s}-\overrightarrow{v_l}\right\rvert}{d_s}\alpha_l^{-2.65}$ $C_D=\frac{24}{\alpha_l\,\mathrm{Re}_s}\left[1+0.15\left(\alpha_l\,\mathrm{Re}_s\right)^{0.687}\right]$	Appropriate for the dilute systems

Gidaspow model	
$K_{ls} = \frac{3}{4} C_D \frac{\alpha_s \alpha_l \rho_l \left\vert \overrightarrow{v_s} - \overrightarrow{v_l} \right\vert}{d_s} \alpha_l^{-2.65}, \ \alpha_l > 0.8$ $C_D = \frac{24}{\alpha_l \operatorname{Re}_s} \left[1 + 0.15 \left(\alpha_l \operatorname{Re}_s \right)^{0.687} \right]$	A combination of the Wen and Yu model and the Ergun equation. Recommended for dense fluidized beds
$K_{ls} = 150 \frac{\alpha_s (1-\alpha_l) \mu_l}{\alpha_l d_s^2} + 1.75 \frac{\rho_l \alpha_s \left\vert \overrightarrow{v_s} - \overrightarrow{v_l} \right\vert}{d_s}$ $\alpha_l < 0.8$	
Solid-solid exchange	
$K_{sl} = \frac{3(1+e_{ls}) \left(\frac{\pi}{2} + C_{fr,ls} \frac{\pi^2}{8} \right) \alpha_s \rho_s \alpha_l \rho_l (d_s + d_l)^2 g_{0,ls}}{2\pi \left(\rho_l d_l^3 + \rho_s d_s^3 \right)} * \left\vert \overrightarrow{v_l} - \overrightarrow{v_s} \right\vert$	Radial distribution coefficient has to be defined

.

.

Three models to represent the radial distribution function are available in FLUENT. Those can be used to define the redial distribution coefficient, which is to be used in the solid-solid exchange coefficient of the momentum equation. In addition to that, three models for defining the solids pressure are also available in FLUENT. The value of solids pressure calculated with use of a specified model is to be used in the momentum equation.

Solids stress tensor also has to be specified to solve the momentum equation. The solids stress tensor contains the shear and bulk viscosities. Shear viscosity consists of granular viscosity and frictional viscosity of the solid phases. Three frictional viscosity models, two granular viscosity models and a granular bulk viscosity model are available in FLUENT. In addition to the available models there is a possibility to use an user defined model or even to set the parameters to constant values. Also an option is available to set that there is no frictional viscosity effects in solid phases.

Frictional pressure term is embodied in the frictional viscosity. There are three models available with FLUENT to define the frictional pressure. Also it is possible to use an user defined model or the term can be set as there is no frictional pressure available.

All those models mentioned are listed in the tables shown below.

.

Solids pressure	
$p_s = \alpha_s \rho_s \Theta_s + 2\rho_s (1+e_{ss}) \alpha_s^2 g_{0,ss} \Theta_s$	Lun et al
$p_s = 2\rho_s (1+e_{ss}) \alpha_s^2 g_{0,ss} \Theta_s$	Syamlal O'Brien
$p_s = \alpha_s \rho_s \Theta_s$ $\left[(1+4\alpha_s g_{0,ss}) + \frac{1}{2}\left[(1+e_{ss})\left(1-e_{ss}+2\mu_{fric}\right)\right]\right]$ Good for systems that have more than one solid phase	Ma-ahmadi

.

Radial Distribution Function	
$g_{0,ll} = \left[1 - \left(\frac{\alpha_s}{\alpha_{s,\max}}\right)^{1/3}\right]^{-1} + \frac{1}{2} d_l \sum_{k=1}^{N} \frac{\alpha_k}{\rho_k},\ \alpha_s = \sum_{k=1}^{n} \alpha_k$	Lun et al
$g_{0,ll} = \frac{1}{\left(1-\frac{\alpha_s}{\alpha_{s,\max}}\right)} + \frac{3}{2} d_l \sum_{k=1}^{N} \frac{\alpha_k}{\rho_k},\ \alpha_s = \sum_{k=1}^{n} \alpha_k$	Arastoopour
$g_{0,ll} = \frac{1+2.5\alpha_s+4.59\alpha_s^2+4.52\alpha_s^3}{\left(1-\left(\frac{\alpha_s}{\alpha_{s,\max}}\right)^3\right)^{0.678}} + \frac{1}{2} d_l \sum_{k=1}^{N} \frac{\alpha_k}{\rho_k},\ \alpha_s = \sum_{k=1}^{n} \alpha_k$	Ma-ahmadi
$g_{0,ll} = \frac{1}{(1-\alpha_s)} + \frac{3\left(\sum_{k=1}^{N} \frac{\alpha_k}{\rho_k}\right)}{(1-\alpha_s)^2 (d_j+d_k)} d_k d_l,\ \alpha_s = \sum_{k=1}^{n} \alpha_k$	Syamlal O'Brien

.

Frictional Viscosity	
$\mu_{,fr} = \frac{p_s \sin\phi}{\sqrt[2]{I_{2D}}}$	Schaeffer
$\mu_{,fr} = p_{fr} \sin\phi$	Johnson and Jackson

.

Frictional Pressure	
$p_{,fr} = \frac{\mu_{,fr} * \sqrt[2]{I_{2D}}}{\sin\phi}$	Based-ktgf
$P_{fr} = 0.1\alpha_s \frac{(\alpha_s - \alpha_{s,\min})^n}{(\alpha_{s,\max} - \alpha_s)^p},\quad n=2,\quad p=3$	Johnson and Jackson
$\mu_{s,kin} = \frac{\alpha_s d_s \rho_s \sqrt{\Theta_s \pi}}{6(3-e_{ss})}$ $\left[1 + \frac{2}{5}(1+e_{ss})(3e_{ss}-1)\alpha_s g_{0,ss}\right]$	Syamlal O'Brien

.

.

Granular viscosity	
$\mu_g = \frac{100 d_s \rho_s \sqrt{\Theta_s \pi}}{96 \alpha_s (1+e_{ss}) g_{0,ss}} \left[1 + \frac{4}{5} g_{0,ss} \alpha_s (1+e_{ss})\right]^2 + \mu_{s,\text{col}}$	Gidaspow
$\mu_g = \frac{\alpha_s d_s \rho_s \sqrt{\Theta_s \pi}}{6(3-e_{ss})} \left[1 + \frac{2}{5}(1+e_{ss})(3e_{ss}-1)\alpha_s g_{0,ss}\right] + \mu_{s,\text{col}}$ $\mu_{s,\text{col}} = \frac{4}{5} \alpha_s d_s \rho_s g_{0,ss} (1+e_{ss}) \left(\frac{\Theta_s}{\pi}\right)^{1/2}$	Syamlal O'Brien
Granular Bulk Viscosity	
$\lambda_s = \frac{4}{3} \alpha_s \rho_s d_s g_{0,ss} (1+e_{ss}) \left(\frac{\Theta_s}{\pi}\right)^{1/2}$	Lun et al

.

.

Granular temperature is embodied in some of the models shown above. Granular temperature is dependant on the fluctuation velocity of the particles and it dependant on the type of the particles used. Cody et al [6] studied the dependency of the fluctuation velocity on the particle diameter in gas fluidized beds.

A general equation for Granular temperature is available in FLUENT. The term k_{Θ_s} in the granular temperature model varies depending on the model which is selected for the Granular viscosity. It is possible to set the value as a constant, or set to be found algebraically. An user defined model can also be used. When the option to find granular temperature algebraically is enabled, the convection and diffusion terms are neglected in the general equation.

.

.

Granular Temperature	
$\frac{3}{2}\left[\frac{\partial}{\partial t}\left(\rho_s\alpha_s\Theta_s\right)+\nabla.\left(\alpha_s\rho_s\overrightarrow{v_s}\Theta_s\right)\right]$ $=\left(-p_s\overline{\overline{I}}+\overline{\overline{\tau_s}}\right):\nabla\overrightarrow{v_s}\ +\nabla.\left(k_{\Theta_s}\nabla\Theta_s\right)$ $-\gamma_{\Theta_s}+\phi_{ls},\ \left(-p_s\overline{\overline{I}}+\overline{\overline{\tau_s}}\right)$	General
Here $\nabla\overrightarrow{v_s}$ is the generation of energy by the solid stress tensor. $\nabla.\left(k_{\Theta_s}\nabla\Theta_s\right)$ is the	
diffusion of energy. γ_{Θ_s} is the collisional dissipation of energy. ϕ_{ls} is the energy exchange between the l^{th} liquid or solid phase and the s^{th} solid phase	
When combined with Syamlal O'Brien model as the Granular viscosity model	
$k_{\Theta,s}=\frac{15\rho_s d_s\alpha_s\sqrt{\Theta_s\pi}}{4(41-33\eta)}$ $\left[1+\frac{12}{5}\eta^2\left(4\eta-3\right)\alpha_s g_{0,ss}+\frac{16}{15\pi}\left(41-33\eta\right)\eta\alpha_s g_{0,ss}\right],\ \eta=\frac{1}{2}\left(1+e_{ss}\right)$	Where, $\eta=\frac{1}{2}\left(1+e_{ss}\right)$
When combined with Gidaspow model as the Granular viscosity model	
$k_{\Theta,s}=\frac{150\rho_s d_s\sqrt{\Theta\pi}}{384(1+e_{ss})g_{0,ss}}\left[1+\frac{6}{5}\alpha_s g_{0,ss}\left(1+e_s\right)\right]^2$ $+2\rho_s\alpha_s^2 d_s\left(1+e_{ss}\right)g_{0,ss}\sqrt{\frac{\Theta_s}{\pi}},$	

.

.

Energy Conservation Equation

.

$$\frac{\partial}{\partial t}\left(\alpha_q\rho_q h_q\right)+\nabla.\left(\alpha_q\vec{v}_q\rho_q h_q\right)=-\alpha_q\frac{\partial P_q}{\partial t}+\overline{\overline{\tau_q}}:\nabla\vec{v}_q-\nabla.\vec{q}_q+S_q+\sum_{p=1}^{n}\left(Q_{pq}+\dot{m}_{pq}h_{pq}-\dot{m}_{qp}h_{qp}\right)$$

Here h_q is the specific enthalpy of the q^{th} phase and h_{pq} and h_{qp} are the interphase enthalpies. $\vec{q}_q$ is the heat flux and Q_{pq} is the intensity of heat exchange between the p^{th} and q^{th} phases.

Chapter 3

A CFD Model to Simulate the Bubbling Fluidized Beds in FLUENT

A good combination of the models available in FLUENT for the simulations of Bubbling fluidized beds is to be finalized during this study. The analysis are carried using simulations of a 2-D fluidized bed with an air jet. Results from the analysis are used to finalize a good model (combined model) for simulation of bubbling fluidized beds. The finalized model is used in simulating freely bubbling fluidized beds for further analysis. The results of the simulations are compared with experiments to check the accuracy.

A large number of simulations are done for the purpose of finalizing a good combined model. Most of the models that are available in FLUENT that can be used for this type of simulations (mentioned in Chapter 2) are used in different combinations in the simulations. Different wire frame meshes are used to overcome some of the difficulties raised while running the simulations. Possible effects due to variation of different limit properties of the solid phase are also checked.

Some important findings from those simulations of the fluidized beds with an air jet, comparisons of the results with the experimental results and finalization of a good combination for the model are presented in the subsequent sections of this chapter.

3.1 Dimensions of the Wire Frame Mesh

In order to finalize a good combined model, results of the simulations are compared with the results from one of the previous experiments done by Halvorsen, B. [10] for her Ph.D. A 2-D fluidized bed in a $0.63m$ higher column with a filter at the rear end to avoid escape of particles has used in her experiments. A wire

frame mesh with the same dimensions as the experimental set up is used originally. As reversed flow of solids is noticed in some of the simulations with that column height, a column with $1.0m$ height is used in the rest of the simulations to avoid the reversed flow.

Both wire frame meshes are made using gambit and exported to FLUENT in order to use in the simulations. Dimensions and the boundaries of the wire frame mesh is shown in the Figure 3.1.

3.1.1 Analysis of the Effect of Using Different Bed Heights

As two different column heights are used in the simulations, it is important to check whether there is any effect for the simulated results from that. That helps to conclude whether it is possible to use all the simulations performed so far for the analysis.

A simulation carried with the $1.0m$ column is compared with a simulation carried with the $0.63m$ column. All other conditions are the same for both simulations. Predicted results analyzed for a period of $3\ s$ from both simulations. The residence time of the bubbles, Bed expansion and bubble appearance are compared. The analysis are given in the appendix B. The analysis showed that the use of different column height haven't made a big influence on the simulated results and the simulations with both column heights can be used in the analysis.

3.2 Effect of Different FLUENT Versions on Simulations

There are differences between the options available in the FLUENT versions 6.2 and 6.3. In FLUENT version 6.3 it is possible to give much more details about the solid phase conditions than in FLUENT version 6.2. When the Schaeffer model is selected as the frictional viscosity model, FLUENT allows to define more features, which are not available in the 6.2 version. Those features are the frictional pressure, the frictional modulus and the frictional packing limit. It is possible to define the frictional pressure based on the kinetic theory of granular flow.

The model "Based-ktgf" computes the frictional pressure term depending on the kinetic theory of granular flow. Kinetic theory of granular flow well presents the inelasticity. Lun et al [17] applied the kinetic theories for granular flow for inelastic particles in coutte flow and for slightly inelastic particles in a general flow field.

The model "Based-ktgf" is preferred to use for frictional pressure and the option "derived" is preferred to use for the frictional modulus. It is important to check the effect of using the two versions in simulations as not the both versions have those features. Comparison of two simulations showed that there is no significant effect by using the FLUENT 6.2 version or the FLUENT 6.3 version with frictional pressure and frictional modulus specified as required. The analysis is given in appendix C. Also it is vise to highlight that "Based-ktgf" is

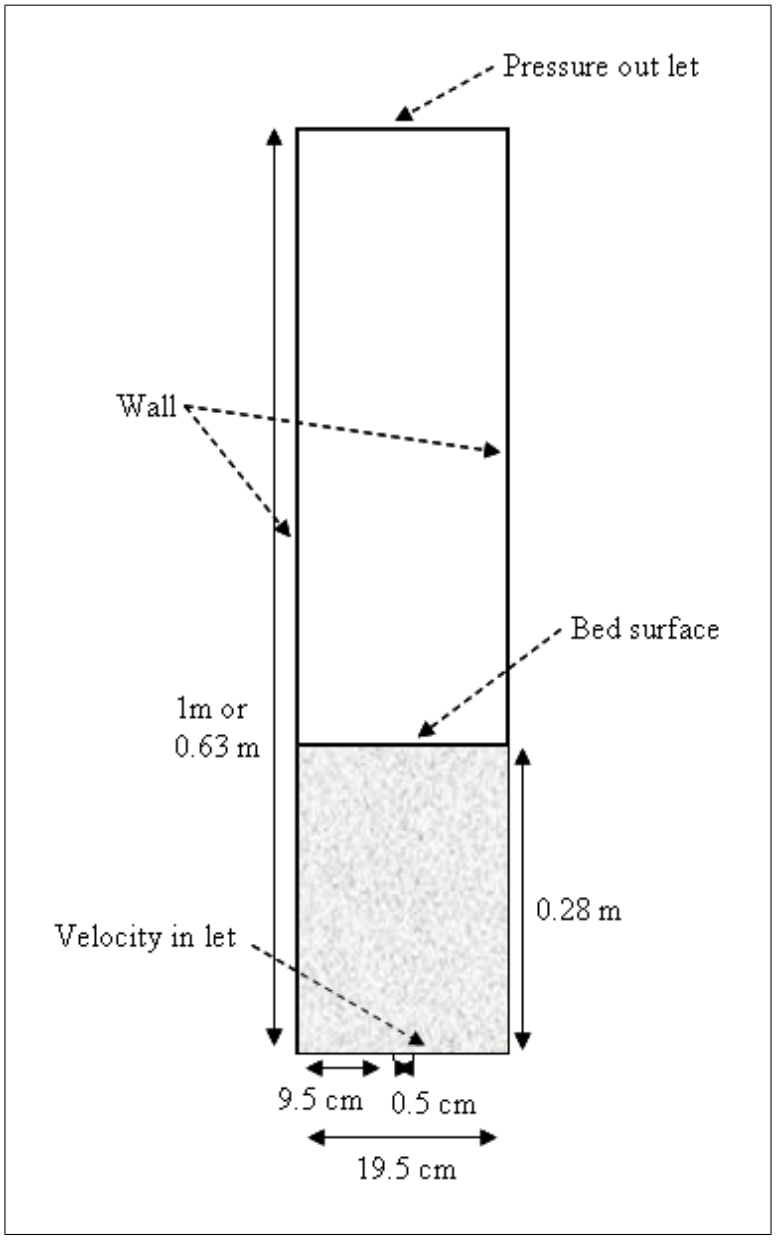

Figure 3.1: Dimensions and the boundaries used for the wire frame mesh

the default model for frictional viscosity and "derived" is the default option for frictional modulus in FLUENT version 6.3. Possibly the same models are used in the FLUENT 6.2 version by default and it is reasonable not to have major differences between the simulations with the two versions, when all the other conditions used are exactly the same.

3.2.1 Effect of the Friction Packing Limit

The possible effects from varying the frictional packing limit from the default value to an other value is studied. Frictional packing limit is the limiting factor of the transition of a granular phase from plastic to elastic region. Gas dynamics have to be faster in the elastic region due to the higher space available for gas in the granular phase than in the plastic region.

In order to check wether a variation in the frictional packing limit will show effects that are in accordance with the previous description, two simulations are done using two different values for the frictional packing limit. The first simulation used the default value (0.61) and the second simulation used a lower value (0.5) as the frictional packing limit. The results of the simulations are compared with each other using solid phase contours and those are presented in Figure 3.2.

Figure 3.2-(a) shows that both simulation had very similar gas dynamics at the beginning. Figure 3.2-(c) shows that the first bubble have had the same size, moved across the bed with the same speed and reached the top of the bed at the same time in both cases.

With the next bubbles, it is noticeable that the bubbles in the simulation with the higher packing limit got bubbles earlier than the simulation with the lower packing limit. But the bubble velocities are in the same region for both simulations. The simulation with higher packing limit have predicted one bubble more than the simulation with the lower packing limit, when the number of bubbles raised are counted for 2 s.

Figure 3.2-(b) compares the time and the position of the bed where the 4^{th} bubble occurs in both simulations. It shows that the simulation with higher packing limit value have got the 4^{th} bubble earlier and also in a higher position in the bed than the simulation with the lower packing limit value. Figures 3.2-(c), 3.2-(d), 3.2-(e), 3.2-(f) show the position of the 4^{th}, 6^{th}, 7^{th} and 12^{th} bubbles at selected time instances. Those figures show that the simulation with higher packing limit value have the bubbles in a higher position in the bed than the simulation with lower packing limit value. In order to compare the bubble velocities, the residence time of the 4^{th}, 6^{th} and 7^{th} bubbles are calculated and presented in the table below. The table shows that the bubbles have had very closer residence times in both simulations.

.

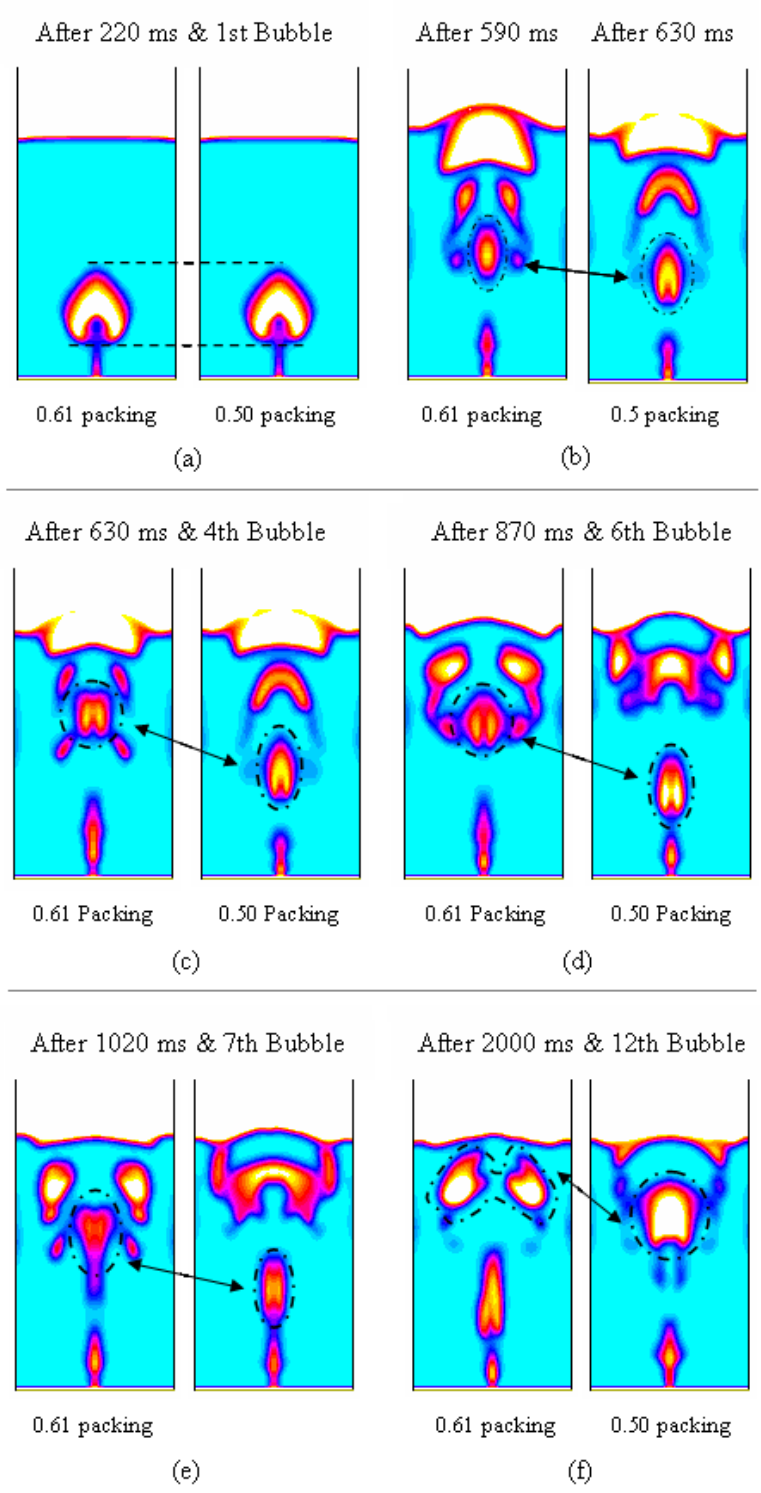

Figure 3.2: Effect form fricional packing limit

Bubble Number	With higher packing limit value	With lower packing limit value
Fourth	0.29 s	0.31 s
Sixth	0.34 s	0.34 s
Seventh	0.32 s	0.31 s

.

.

The analysis helped to conclude that the simulation with the higher packing limit have reached the elastic properties earlier than the simulation with the lower packing limit value. It is reasonable since a higher value for packing can achieve faster than a lower value when a particle bed at the maximum packing limit is being expanded.

3.3 Model Combinations with Unsatisfactory Results

Different combinations of the available models are tried with Eularien multiphase model in order to finalize a good model for simulating bubbling fluidized beds using the commercial CFD software FLUENT. Syamlal O'Brien and Gidaspow are the available and suitable drag models to be used in simulations of bubbling fluidized beds. Those two models are used in combination with the other models for defining solid phase conditions. Some of those model combinations are failed to give satisfactory predictions as they predicted too much variations in the bed. Those results are useful to highlight that some combinations of the available models are not suitable for this kind of simulations. Two of those are shown in the Figure 3.3. Those two simulations are named as simulation F1 and F2 and the conditions used in those simulations are listed in the table given below.

.

	Simulation F1	Simulation F2
No: of phases	One	One
Particle size	491 μm	491 μm
Granular vis:	Syamlal O'Brien	Constant (0)
Granular b: vis:	Constant (0)	Constant (0)
Frictional vis:	Schaeffer	Schaeffer
Angle of int: fri:	Constant (30.00007)	Constant (30.00007)
Granular temp:	Algebraic	Constant (0)
Solids pressure	Syamlal O'Brien	Syamlal O'Brien
Radial distribution	Syamlal O'Brien	Syamlal O'Brien
Elasticity modulus	Derived	Derived
Packing limit	Constant (0.63)	Constant (0.63)
Drag model	Gidaspow	Syamlal O'Brien

.

.

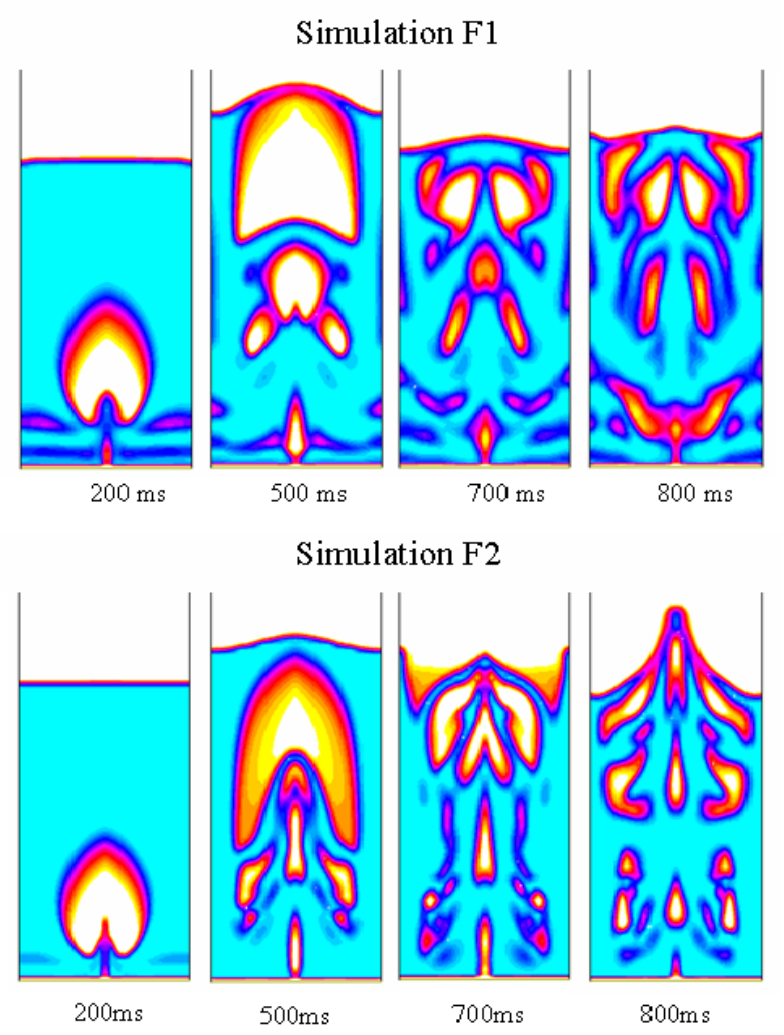

Figure 3.3: Some of the models that failed to give reasonable results

The simulation F1 have predicted more variations in the VOFs than the simulation F2. That can be due to the selection of different conditions for granular viscosity and granular temperature. When considering the behavior of the two simulations it is clear that those doesn't predict bubbles as it is expected when an air jet is implemented in a simulation. The combinations used in the simulations F1 and F2 can be subscribed as not acceptable combinations.

3.4 Comparison of the Simulated and Experimental Results

In addition to the above mentioned combinations, some other combinations of models are used in simulations. All those simulations are performed for a particle bed with spherical glass particles (density $= 2485\ kg/m^3$) of 491μm mean diameter. Different drag models and different models to define the solid phase conditions are used. In all simulations 28 cm is used as the initial height of the particle bed. An air jet is used with y-directional velocity of 4.9 ms^{-1}. The magnitude of the superficial gas velocity used is 0.29 ms^{-1} and it is the same value used in the reference experiment. The maximum possible solid VOF in a gas bubble is taken as 0.2.

3.4.1 Simulations Using Experimental Velocity Values

The drag models "Gidaspow" and "Syamlal O'Brien" are used in combination with the other models, which are available to define the solid phase properties. Six combinations used for simulations are presented in the table below.

.

Models used	**Simulation b1**	**Simulation b2**	**Simulation b3**
Drag	Gidaspow	Gidaspow	Gidaspow
Granular viscosity	Syamlal O'Brien	Syamlal O'Brien	Constant
Granular bulk viscosity	Constant	Constant	Constant
Frictional viscosity	Schaeffer	None	Schaeffer
Solids pressure	Ma ahmadi	Lun et al	Ma ahmadi
Radial Distribution	Ma ahmadi	Lun et al	Ma ahmadi

.

.

Models used	**Simulation b4**	**Simulation b5**	**Simulation b6**
Drag	Syamlal O'Brien	Syamlal O'Brien	Syamlal O'Brien
Granular viscosity	Syamlal O'Brien	Syamlal O'Brien	Gidaspow
Granular bulk viscosity	Constant	Constant	Constant
Frictional viscosity	Schaeffer	None	Schaeffer
Solids pressure	Ma ahmadi	Lun et al	Ma ahmadi
Radial Distribution	Ma ahmadi	Lun et al	Ma ahmadi

.

.

The six simulations are compared with the results of the reference experiment. Comparison is performed using the contours of the solid phase and the

photoes from the reference experiment. Figures 3.4 and 3.5 shows the results of the simulations in comparison with the experimental results at 200 ms and 500 ms from the beginning.

Figure 3.4 shows that all six simulations have predicted higher bed expansions than the experiment. Among those the last three simulations have given closer bed expansion to the experiment while the first three simulations are further away from the experiment. When the bubble size is compared, it is observed that the simulation b5 has the closest prediction. Next important factor to be compared is the bubble velocity. In order to compare the bubble velocity the position of the bubbles in the bed at 200 ms are compared. Light color (light blue) solid and dotted lines shows the top most position of all the bubbles. It is visible that the simulation b3 have predicted the closest bubble position.

Figure 3.5 shows the dynamics in the particle bed after 500 ms from the beginning. The last three simulations have predicted the bubble position better than the rest of the simulations. When the bed height is compared, it is the last three simulations again, which predicted the bed expansion closer to that of the reference experiment. The first simulation has predicted the number of bubbles accurately and also it has predicted the positions of the second and third bubbles very closer to that in the experiment.

When the position of the first bubble is compared at $500ms$, it is noticeable that the first bubble is in a higher position than the experimental bubble. This observations shows that all six simulations have higher values for bubble velocities than those of the experimental bubbles.

From the above comparisons it is noticeable that all six simulations show deviations from the experimental results. Also gives faster bubbles than in the experiment. It is only one simulation that has predicted all three bubbles, which are there in the experiment nicely. Also, there are too much variations of the solid VOF presented in rest of the bed in simulations. Even with those deviations, the simulations with the Syamlal O'Brien drag model gave closer results to the experiment in accordance with the factors considered.

Value of the Superficial Gas Velocity

The value of the superficial gas velocity, which is used in the simulations is checked due to the observation of too many variations of the solid's VOF in the above simulations. The superficial gas velocity used is $0.29\ ms^{-1}$ and it is the same value as in the reference experiment.

The purpose of the gas stream used except the air jet is to fluidize the particle bed. If the superficial gas velocity is higher than the minimum fluidization velocity (U_{mf}) of the particles it can influence the results of the simulations by giving many smaller bubbles in the particle bed.

In order to check the value, which is using for the superficial gas velocity, a simulation is performed with use of uniform distribution of air across the velocity inlet. The value of the fluidization velocity from the experiments (superficial gas velocity) is used as the inlet gas velocity. Results from the simulation is

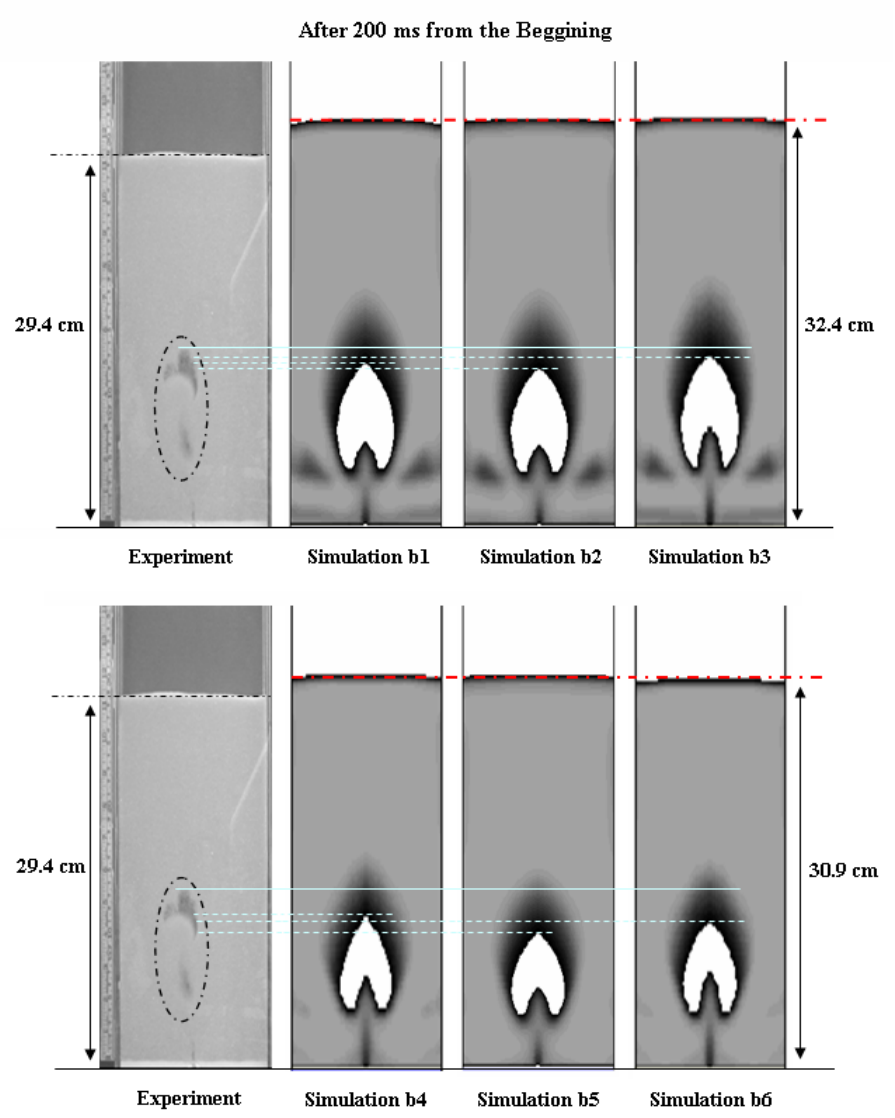

Figure 3.4: Comparison of the simulations with the experimental results at 200 ms from the begining

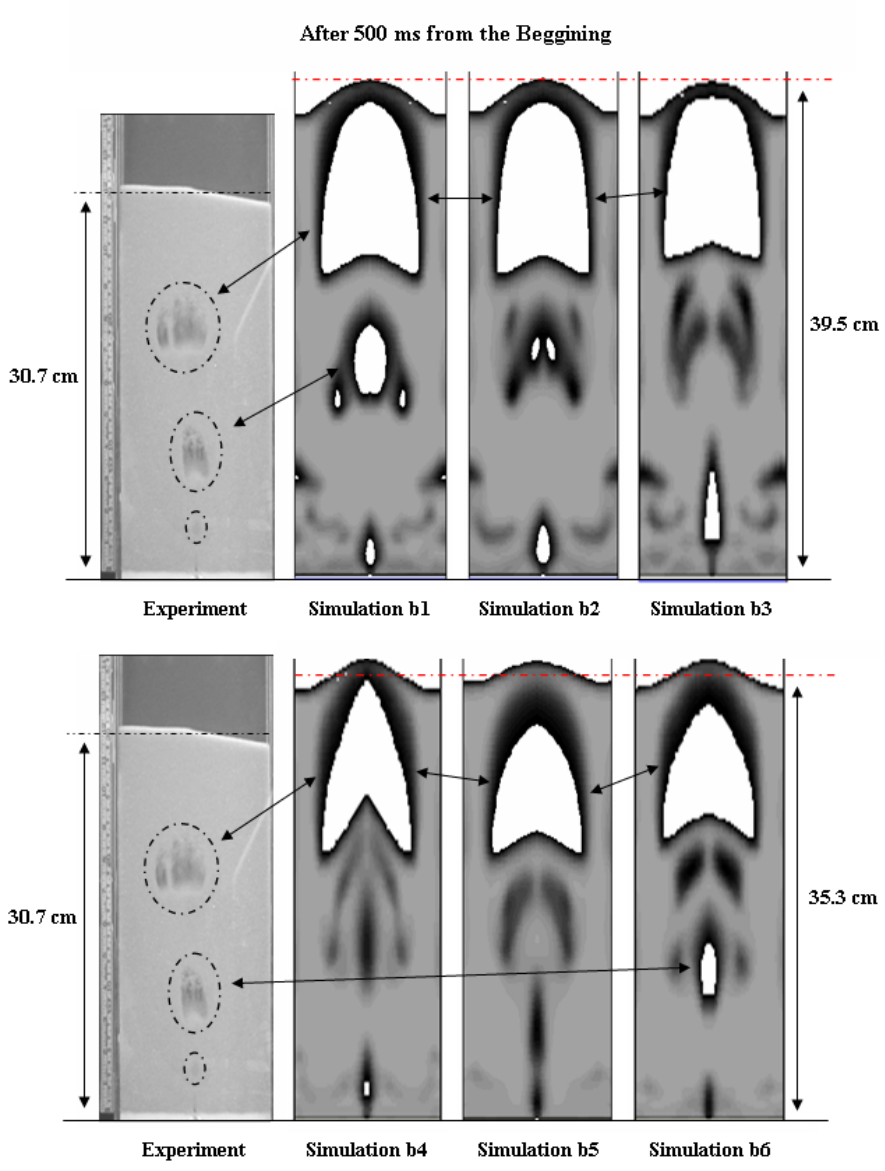

Figure 3.5: Comparison of the simulations with the experimental results at 500 ms from the begining

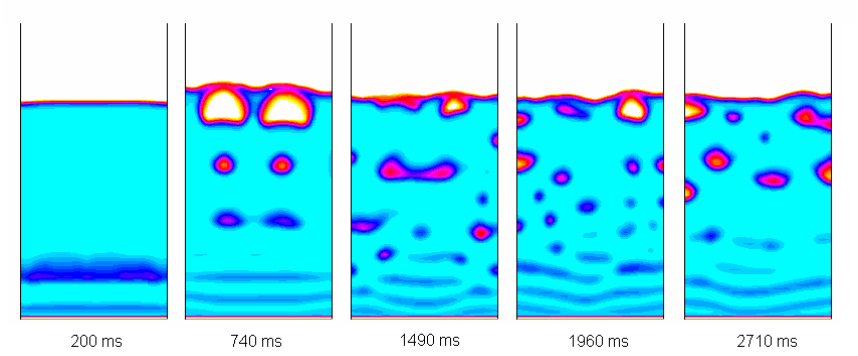

Figure 3.6: Simulation with uniform velocity distribution at the gas inlet

presented in the Figure 3.6. The figure proves that the value of the superficial gas velocity is higher than the U_{mf} as it gave bubbles in the particle bed.

Particles belongs to Geldart B category produce bubbles as soon as the gas velocity exceed that at incipient fluidization [18]. As the particles used in this simulations are belongs to the Geldart B category, the reference experiment shows that the superficial gas velocity used in the experiment is at or lower than the U_{mf}. This observation shows that the experimental and the calculated U_{mf} values could be different from each other. The results of the analysis confirms that the U_{mf} related to the particle size use have to be calculated.

Calculation of the Minimum Fluidization Velocity

The minimum fluidization velocity of the particles, which are used for the experiment as well as for the simulations is calculated. The particle mean diameter is found as 491 μm and that value Is used for the simulations. The U_{mf} of the particles is calculated using the mean particle diameter. Calculation procedure of the mean particle diameter and the U_{mf} is presented in the Appendix D as it is out side of the scope. The U_{mf} of the spherical glass particles of 491 μm mean diameter is found as 0.198 ms^{-1}.

This new value is used in the simulations and the results are compared with the experimental results in the same way the early comparisons are performed.

3.4.2 Simulations Using the New Superficial Gas Velocity

All the simulations presented bellow in this chapter are performed using the superficial gas velocity found above while using the same particle bed used in the early simulations.

The drag models "Gidaspow" and "Syamlal O'Brien" are used in these simulations also in combination with the other models, which are available in FLUENT to define the solid phase properties. Five combinations used for simulations

have presented in the table below.

.

.

models	**Simulation c1**	**Simulation c2**	**Simulation c3**
Drag	Gidaspow	Gidaspow	Gidaspow
Granular viscosity	Syamlal O'Brien	Syamlal O'Brien	Syamlal O'Brien
Granular bulk viscosity	Constant	Constant	Lun et al
Frictional viscosity	Schaeffer	None	Schaeffer
Solids pressure	Ma ahmadi	Lun et al	Lun et al
Radial Distribution	Ma ahmadi	Lun et al	Lun et al

.

.

models	**Simulation c4**	**Simulation c5**
Drag	Syamlal O'Brien	Syamlal O'Brien
Granular viscosity	Syamlal O'Brien	Syamlal O'Brien
Granular bulk viscosity	Constant	Constant
Frictional viscosity	Schaeffer	None
Solids pressure	Ma ahmadi	Lun et al
Radial Distribution	Ma ahmadi	Lun et al

.

.

Figures 3.7 and 3.8 show the comparison of the simulations with the experimental results at 200 ms and 500 ms from the beginning of the simulations. First bubble of the particle bed is presented in the Figure 3.7. The size of the bubbles of computational data are compared with the experimental data and it showed that the the simulation c5 has the best prediction. In order to study the bubble velocity, the bubble position is traced with time. The top most position of the bubbles are marked with light colored solid and dashed lines. The most important factor, the particle bed expansion is also compared. Figure 3.7 shows that last two simulations have predicted the same bed expansion as the experiment had.

Figure 3.8 shows that the simulations c4 and c5 have predicted the size of the first bubble closer to that in the experiment. Analysis of the position of the first bubble verified that the simulations have faster bubbles than the experiment. When the bed expansion is considered, first three simulations give too high values compared to the experiment while the last two simulations give similar magnitude of expansion.

Above comparison proves again that the simulations used Syamlal O'Brien as the drag model gives closer predictions to the reference experiment than the simulations used Gidaspow model as the drag model. The rest of the study for finalizing a good model will only focus on the Syamlal O'Brien drag model.

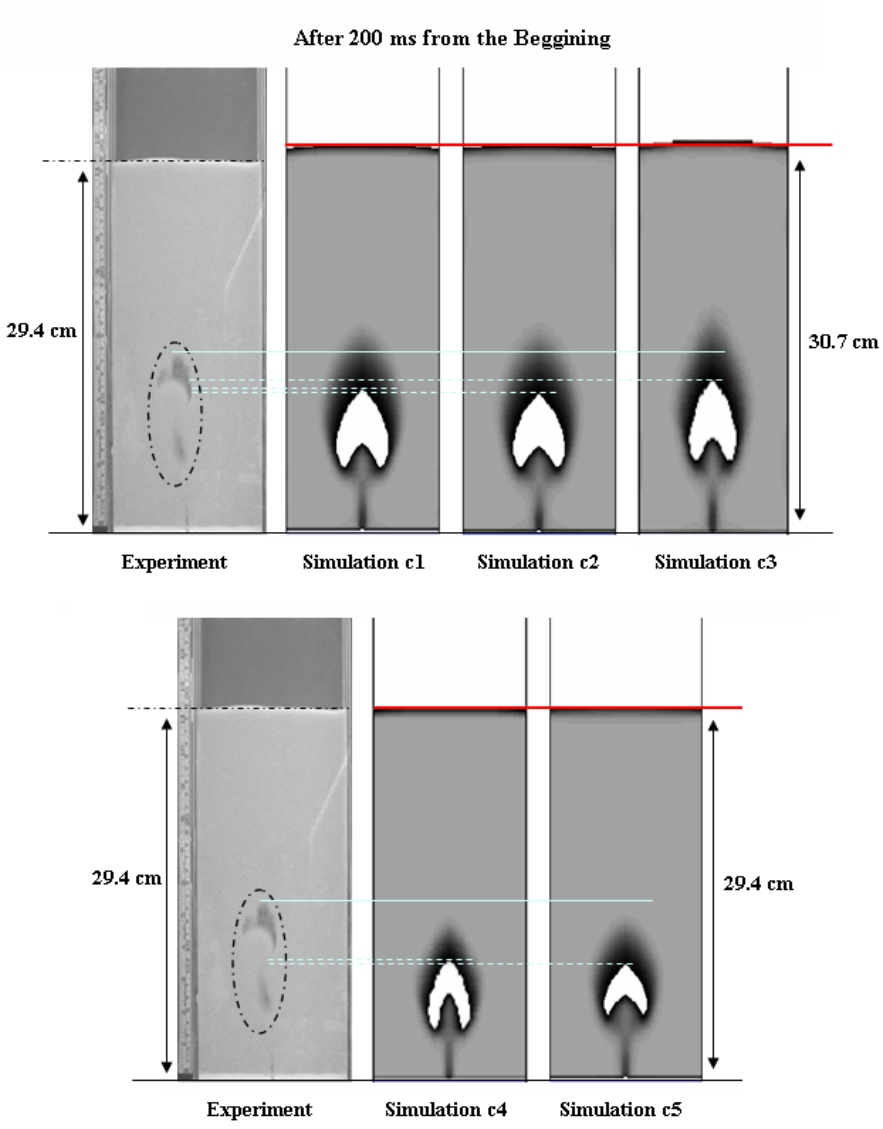

Figure 3.7: Comparison of the simulations with the experimental results at 200 ms from the begining

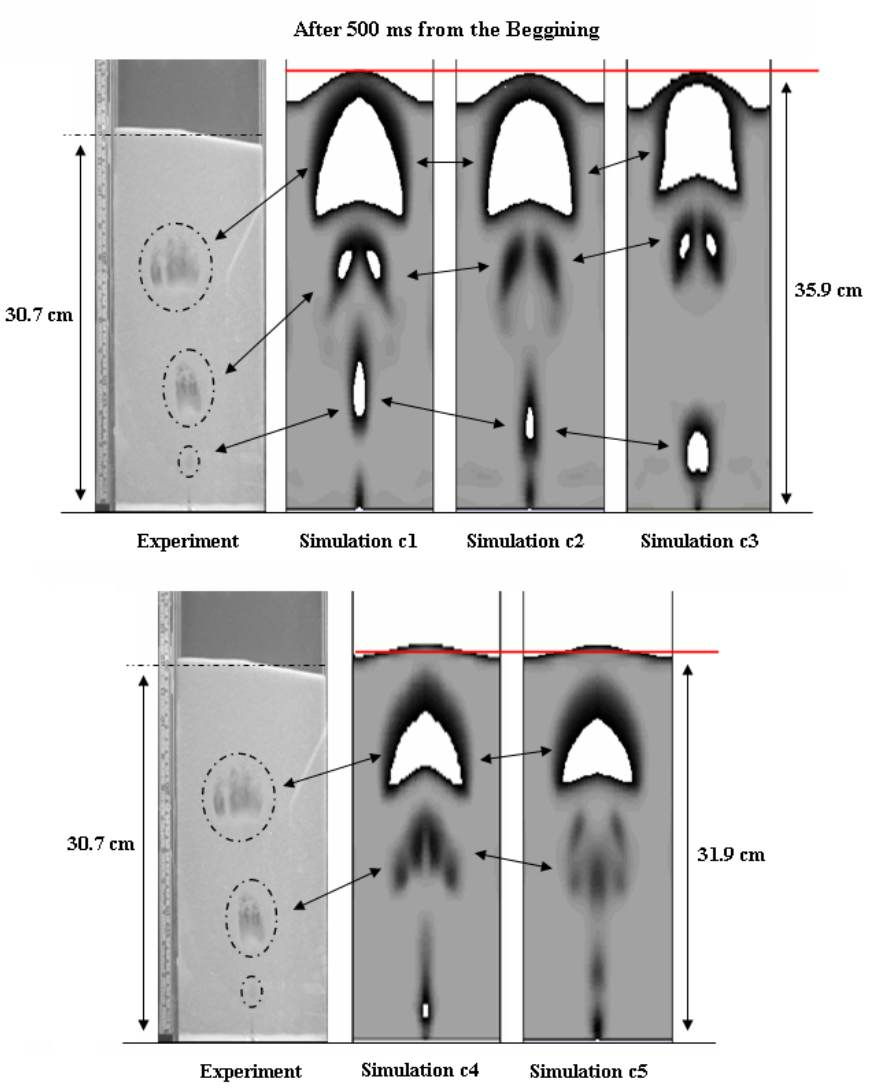

Figure 3.8: Comparison of the simulations with the experimental results at 500 ms from the begining

3.5 More Combinations with Syamlal O'Brien Drag Model

As the simulations with the Syamlal O'Brien drag model gave satisfactory results, few more simulations are performed using the same drag model. The possible combinations of models including Syamlal O'Brien drag model is shown in Figure 3.9. Combinations used in the simulations are marked with a darker color (black) than the rest of the combinations. Respective numbering of the simulations have also displayed in the figure.

The simulations are introduced as the d series in the report for convenience in combination with the same numbering as in the Figure 3.9 . The simulation d5 didn't give reasonable results. Therefore it is not included in the comparison. Figures 3.10 and 3.11 give the comparison of the simulations with the reference experiment at 200 ms and 500 ms from the beginning.

Above comparison shows that the simulations d1, d2, d3, d7 and d8 have predicted reasonable results. Due to the difference in bubble speed between the simulations and the experiment, bubbles are in different positions in the compared frames. That appears to be a negative point in the comparison as the bed height tends to vary with the bubble positions in the bed. It is important to compare the bed expansion of the reference experiment and the simulations with respective to the same bubble positioning in the bed.

3.6 Comparison of Properties while the Bubbles are at the Same Position

Three picture frames, displaying three different positions of the first bubble in the particle bed are selected from the experimental video. The simulations d1, d2, d3, d7 and d8 are presented with respective to the same bubble positions in for the experiment. Comparisons are given in the Figures 3.12, 3.13 and 3.14.

Figure 3.12 shows that the first three simulations (d1, d2 and d3) have predicted the bed expansion closer to the experimental bed expansion. Same figure provides evidence about the difference between the experimental bubble speed and the simulated bubble speeds. To reach the position of the bubble after 200 ms in the experiment, the simulations have taken much longer time.

According to Figure 3.13 simulation d3 has the best bed expansion prediction. The simulations d2, d3 and d7 have good representation of the shape and the size of the first bubble. Those have predicted not only the first bubble but also the rest of the bubbles available in the experimental bed at that particular time instance.

Figure 3.14 shows that the simulation d3 has the best prediction in terms of the bubble position, bubble velocity and the bubble presentation compared to the other simulations.

After considering the three comparisons using figures it is possible to conclude that the combination used in simulation d3 is the best combination from

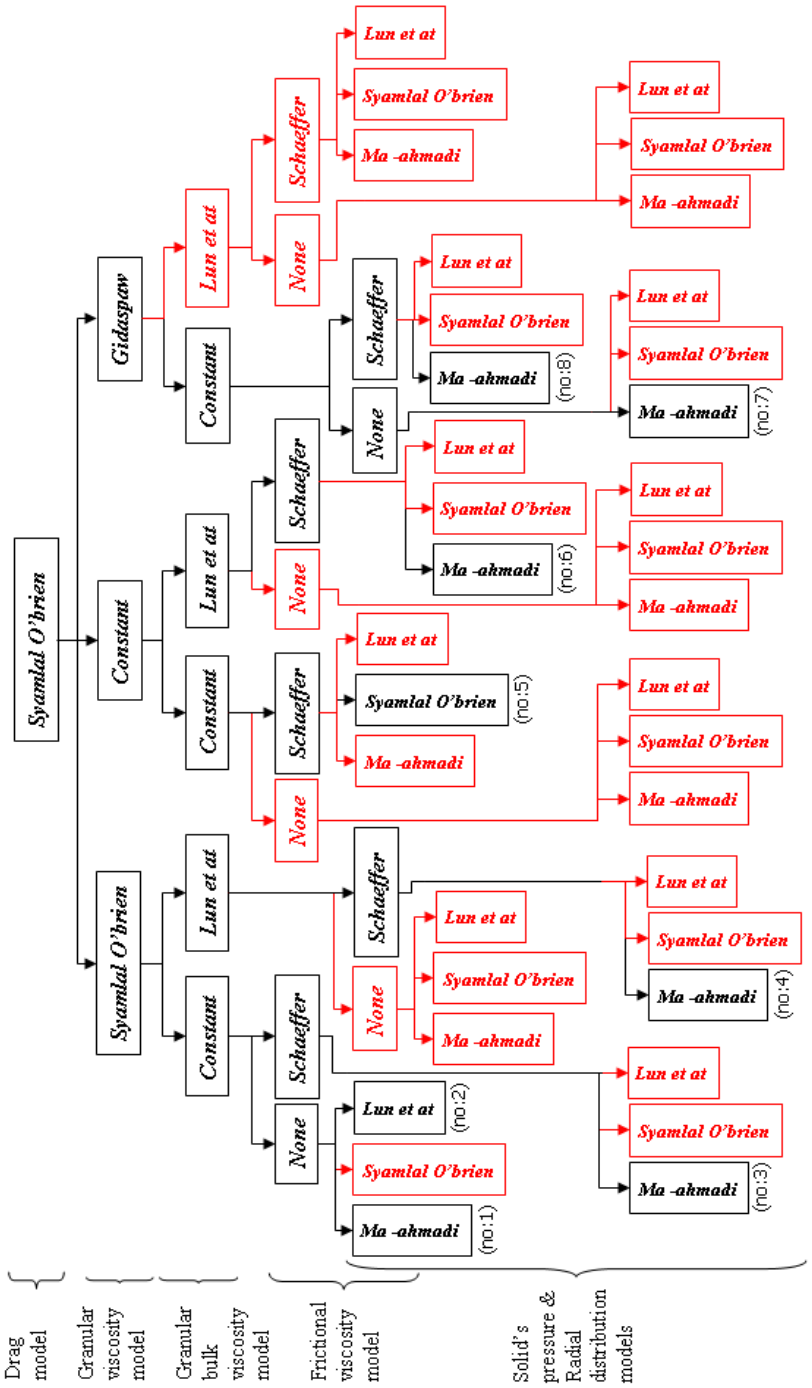

Figure 3.9: All posible combinations of models along with Syamlal O'brien drag model

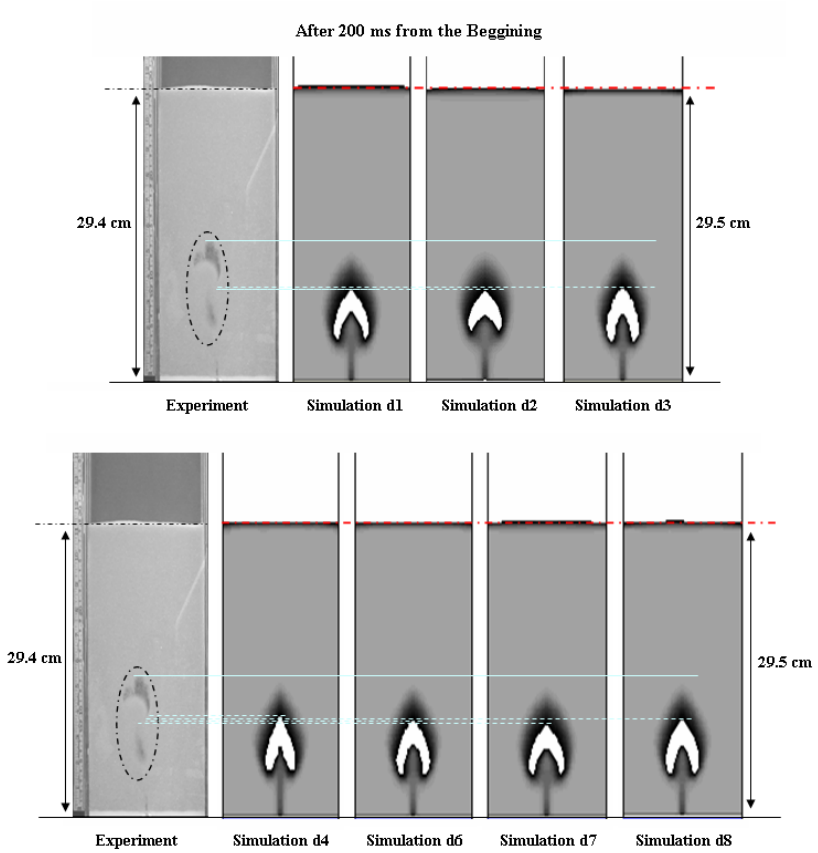

Figure 3.10: Comparison of the simulations with Syamlal O'brien drag model with experiment after 200 ms from the begining

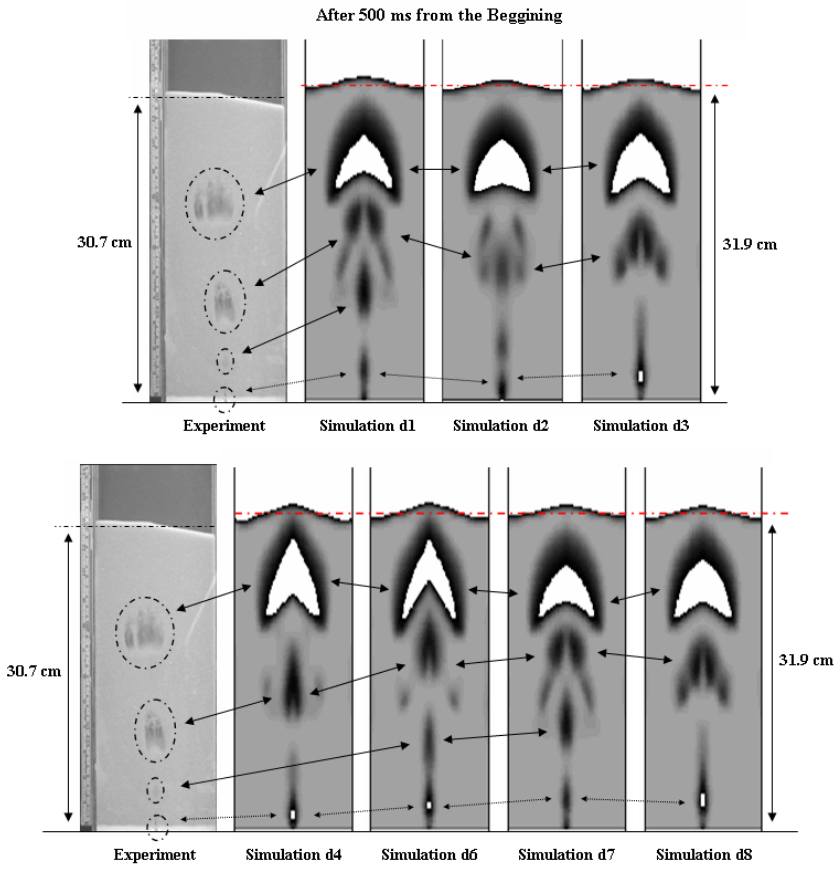

Figure 3.11: Comparison of the simulations with Syamlal O'brien drag model with experiment after 500 ms from the begining

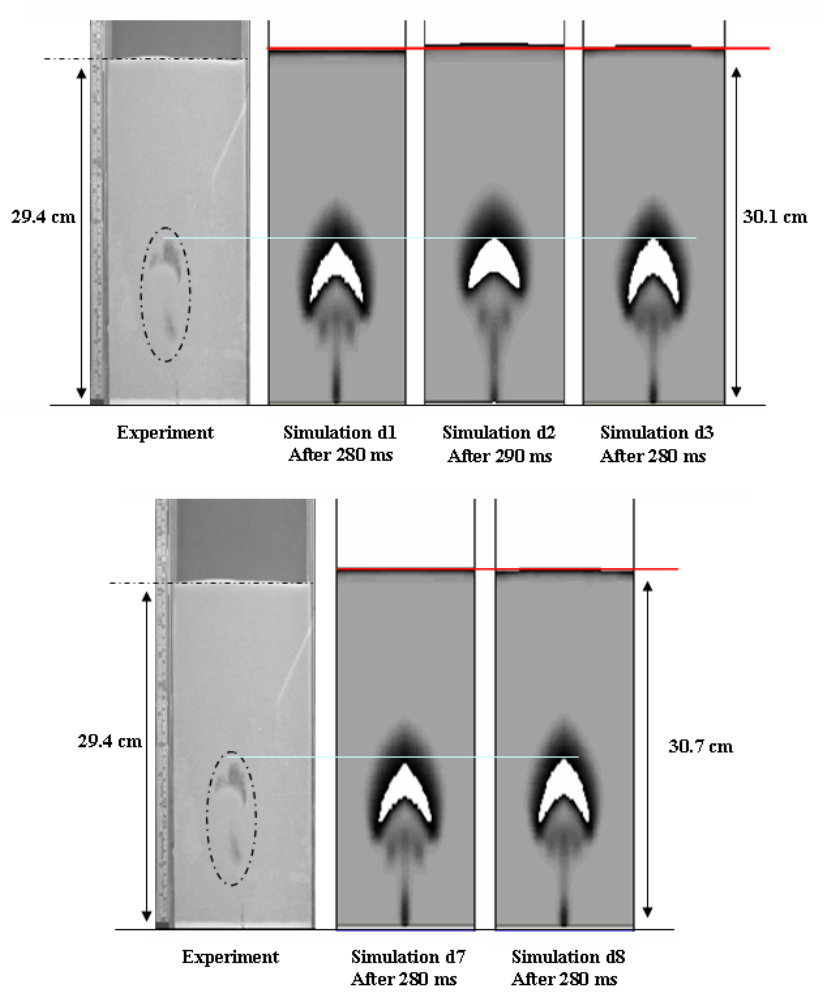

Figure 3.12: Comparison of the bubble position with the experimental bubble position after 200 ms from the beggining of the experiment

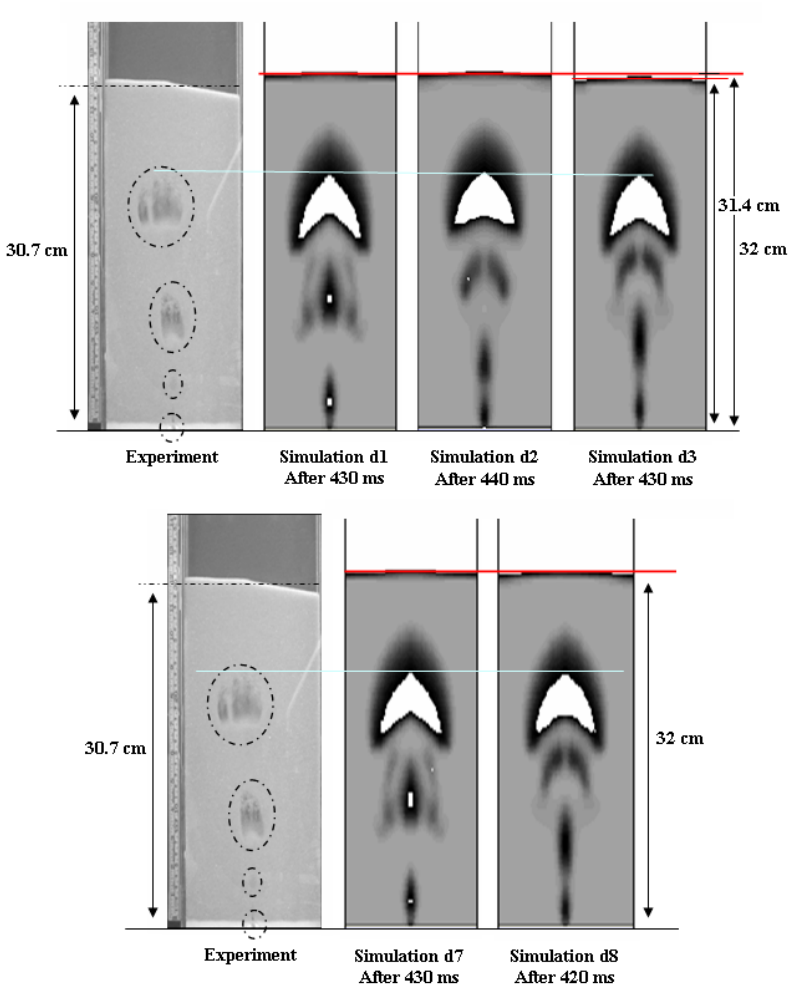

Figure 3.13: Comparison of the bubble position with the experimental bubble position after 500 ms from the beggining of the experiment

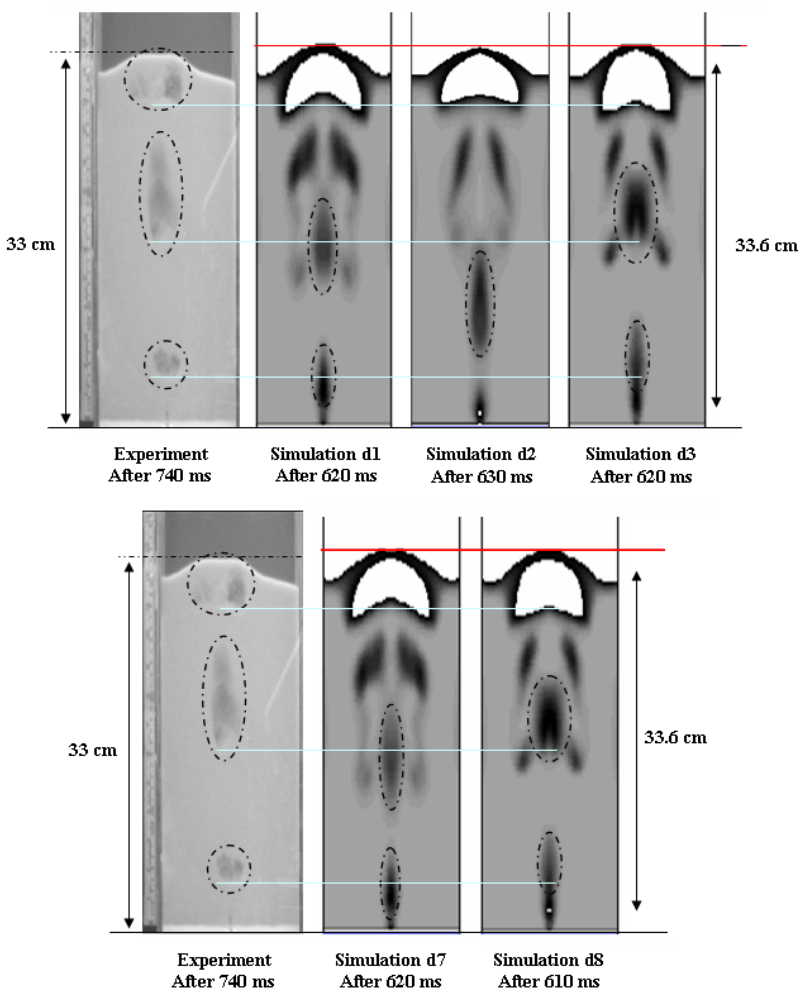

Figure 3.14: Comparison of the bubble position with the experimental bubble position after 740 ms from the beggining of the experiment

all the combinations tried during this study, and it is a good combination to be used for simulating the bubbling fluidized beds.

3.7 Finalized Combination of Models

According to the analysis carried in this part of the project study the following combination has been selected as a good combination of models for simulating the bubbling fluidized beds. The recommended combination consists of the conservation of mass, momentum and energy equations solved in FLUENT facilitated by the following models presented bellow.

.

Drag Model	Syamlal O'Brien
Granular Viscosity	Syamlal O'Brien
Granular Bulk Viscosity	Constant
Frictional Viscosity	Schaeffer
Frictional Pressure	Based-ktgf
Solid Pressure	Ma-ahmadi
Radial Distribution Function	Ma-ahmadi
Rest of the models	use default settings

Drag model

$$K_{ls} = \frac{\alpha_s \rho_s \left(\frac{C_D \operatorname{Re}_s \alpha_l}{24 v_{r,s}^2}\right)}{\tau_s}, \quad C_D = \left(0.63 + \frac{4.8}{\sqrt{\operatorname{Re}_s / v_{r,s}}}\right)^2$$

Here K_{ls}, C_D are the momentum exchange coefficient between the fluid and solid phases and the drag coefficient respectively. Re_s is the relative Reynolds number of the solid phase. α_s and ρ_s are the phasic volume fraction and the physical density of the solid phase. α_l, τ_s and $v_{r,s}$ are the phasic volume fraction of the liquid, the solid phase stress-strain tensor and the terminal velocity for the solid phase respectively.

Granular viscosity

$$\begin{aligned}
\mu_g &= \mu_{s,kin} + \mu_{s,\mathrm{col}} \\
\mu_{s,kin} &= \frac{\alpha_s d_s \rho_s \sqrt{\Theta_s \pi}}{6(3 - e_{ss})} \left[1 + \frac{2}{5}(1 + e_{ss})(3e_{ss} - 1)\alpha_s g_{0,ss}\right] \\
\mu_{s,\mathrm{col}} &= \frac{4}{5}\alpha_s d_s \rho_s g_{0,ss}(1 + e_{ss}) \left(\frac{\Theta_s}{\pi}\right)^{1/2}
\end{aligned}$$

Here μ_g, $\mu_{s,kin}$ and $\mu_{s,\mathrm{col}}$ are granular viscosity, Granular kinetic viscosity and collisional viscosity respectively. d_s is the diameter of the s^{th} solid phase particles.

Frictional viscosity

$$\mu_{,fr} = \frac{p_s \sin\phi}{\sqrt[2]{I_{2D}}}$$

Here $\mu_{,fr}$, ϕ and I_{2D} are the frictional viscosity, the angle of internal friction and the second invariant of the deviatoric stress tensor.

Frictional pressure

$$p_{,fr} = \frac{\mu_{,fr} * \sqrt[2]{I_{2D}}}{\sin\phi}$$

Where p_{fr} is the frictional pressure.

Solids pressure .

$$p_s = \alpha_s \rho_s \Theta_s \left[(1 + 4\alpha_s g_{0,ss}) + \frac{1}{2} \left[(1 + e_{ss}) \left(1 - e_{ss} + 2\mu_{fric} \right) \right] \right]$$

Here p_s is the solids pressure and Θ_s is the granular temperature. $g_{0,ss}$, e_{ss} and μ_{fric} is the radial distribution function, the coefficient of restitution for particle collisions and frictional viscosity respectively.

Radial distribution function

$$g_{0,ss} = \frac{1 + 2.5\alpha_s + 4.59\alpha_s^2 + 4.52\alpha_s^3}{\left(1 - \left(\frac{\alpha_s}{\alpha_{s,\max}} \right)^3 \right)^{0.678}} + \frac{1}{2} d_l \sum_{k=1}^{N} \frac{\alpha_k}{\rho_k}, \ \alpha_s = \sum_{k=1}^{n} \alpha_k$$

Here d_l is the diameter of the l^{th} solid phase particles. α_k and ρ_k are the phasic volume fraction and physical density of each phase if more than one solid phase exists.

Part III

Influence of Particle Size Distribution

Chapter 4

Background Information

Particles used in industrial operations are usually consist of a wide range of particle sizes (distribution of particle sizes). Simulations are used to collect information about those operations. Common practice is to use the mean diameter of the particles to represent powders in simulations. As the fluid dynamics should be dependant on the particle size distribution, above mentioned practice can lead to loss of valuable information. It is important to check the influence from introducing particle size distributions in simulations.

Research have been done in this study area and those have shown that there is an effect on the simulated results by using particle size distributions in the simulations. Huilin et al [12] has used multi fluid Eulerian CFD model with closure relationships according to the kinetic theory of granular flow to study the motion of particles in a gas bubbling fluidized bed with the binary mixtures. They have concluded that in order to obtain realistic bed dynamics from fundamental hydrodynamic models, it is important to correctly take the effect of particle size distribution and energy dissipation due to non-ideal particle-particle interactions into account.

Different solid phases can be used to represent different particle sizes of a distribution in a simulation. As found from the literature survey, most of the simulations of bubbling fluidized beds have used only one or two solid phases and it is interesting to use more than two particle phases in simulations and check the influence.

Five simulations are performed using different number of particle phases,

- One with one particle phase
- Two with two particle phases
- One with three particle phases
- One with four particle phases

to study the influence of introducing particle size distributions. Simulated data are analyzed and compared with each other with respect to the bubble behavior, the bed expansion and the particle segregation. Also the simulations are compared with an experiment, which is performed using the same conditions as the simulations and the same mean particle diameter by Mr. Wu W.J. at

Telemark University College, Norway. Results from the analysis are presented in the following chapters.

4.1 Conditions Used in the Simulations and the Experiment

The simulations for this study are performed using the model finalized in the early part of this study while keeping the same conditions in all the simulations except the number of particle phases. A wire frame mesh similar to the mesh shown in Figure 3.1 with 0.2 m and 1.5 m as the column width and the height, is used. The mean diameter used in the simulations is 487.97 μm. When the number of solid phases are increasing the compositions of the particle phases are computed as the same mean particle diameter is provided in every mixture. The mean diameter of the particle phases are selected using the particle size distribution of the powders used in the reference experiment.

The reference experiment is performed using a mixture of three type of powders. Those powders have their own particle size distributions for each. A sieve analysis is performed to find the particle size distribution of those powders. Mean diameter of each powder is calculated using the results of the sieve analysis. The calculating procedure is presented in the appendix D.

Mean particle diameters and the compositions of the particle phases used in the simulations are presented in the table below.

.

	Phase 1	Phase 2	Phase 3	Phase 4
Mean diameter (μm)				
Simulation P1	487.97			
Simulation P2	153	624.79		
Simulation P3	153	960		
Simulation P4	153	487.97	960	
Simulation P5	153	424.6	577.78	960
Composition (%)				
Simulation P1	100			
Simulation P2	29	71		
Simulation P3	58.5	41.5		
Simulation P4	29	50	21	
Simulation P5	29	30.5	10.5	21

The superficial gas velocity of 0.134 ms^{-1} is used both in the simulations and the reference experiment. Each simulation represents 30 seconds from the flow time.

The simulation P1 is a special case as it didn't give any changes in the VOF and also there are no bubbles in the particle bed. Figure 4.1 shows the behavior in the particle bed in the simulation P1 with time at the used superficial gas velocity. The U_{mf} for the corresponding particle size is calculated and the

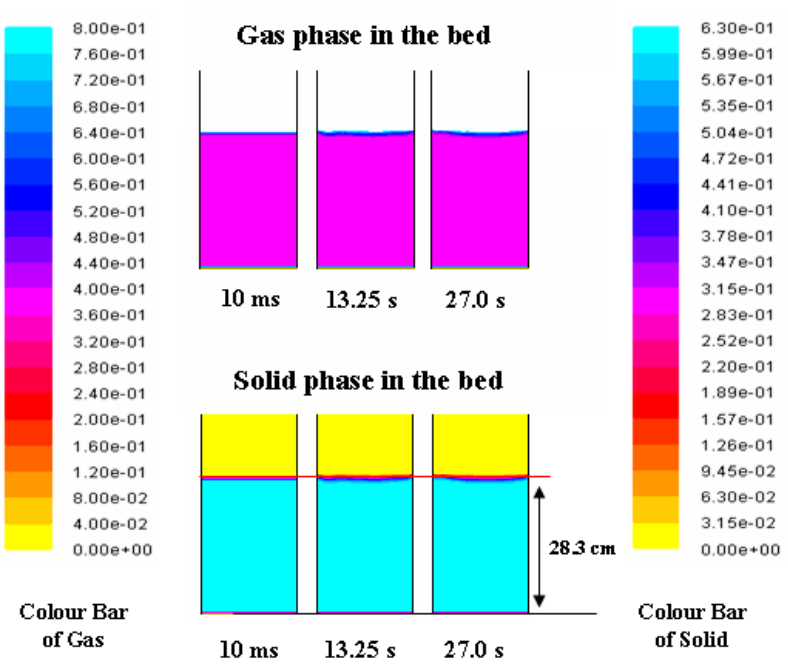

Figure 4.1: Solid and gas volume fractions with time in the particle bed

calculation is presented in the appendix D. The calculated value is 0.19535 ms^{-1} and it is higher than the superficial gas velocity used in the simulations. That is the reason for not having any bubbles and no variations in the particle VOF in the particle bed.

Chapter 5

Particle Segregation

Particle segregation is a common phenomena when a mixture of particles is used in a fluidized bed. Particle segregation exists and appears very clearly in the reference experiment. Figure 5.1 shows the bubble distribution and the approximate height where the segregation occur in the experimental particle bed. The light color (red) line in the picture shows the lowest position of bubble occurrence in the bed approximately and that information will be used in analysis later in this study.

The simulations with multiple particle phases, P2, P3, P4 and P5 are analyzed to check the ability of predicting the particle segregation. The contours of solid phases are compared and presented in this chapter for evidence.

5.1 Comparison of Contours of Particle Phases

Figure no: 5.2 presents the prediction of particle segregation in the simulation P2. It shows that the simulation has predicted particle segregation up to a certain level. The same figure presents clearly that the small particles tends to concentrate at the top of the bed while the larger particles tends to concentrate close to the bottom of the bed. The prediction of the position where the segregation is clear has a big deviation from the reference experiment.

Contours from the simulation P3 are presented in Figure 5.3 and 5.4 to demonstrate the prediction of particle segregation. Particle segregation is clear close to the bottom of the particle bed, and it is very much different from the experimental observation.

Particle segregation predicted by the simulation P4 is presented in the Figure 5.5 with respect to the three particle phases available in the simulation. It shows that either small or large particle phase can be used for the analysis of particle segregation. It is not possible to use the medium sized particles as those are more distributed all over the bed. Prospective boundaries are marked with white in all the frames belongs to small and large particles. The large particles

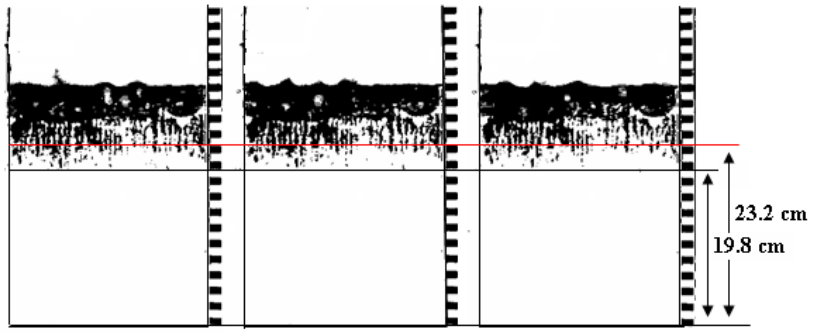

Figure 5.1: Bubble appearence in the reference experiment

always tends settle down to the bottom and they are unable to present the bed surface clearly. The small particle phase is the best selection to be compared with the reference experiment as the bed surface is also well presented with this phase.

Five frames are selected from the simulated movie of the small particles, which represent a time range approximately from 1 s to 30 s. Those frames are presented in the Figure 5.6 along with a picture frame from the reference experiment. Areas where the small particle volume fraction is high are marked using white lines in the figure. A black line is used to mark the areas where the particle separation is clear in the experiment.

Also, the Figure 5.6 presents the progress of the particle segregation with time in the particle bed. The first frame (time: 1.02 s) shows that the small particles are more or less distributed all over the bed while a very few has cumulated at the top. The denser areas of small particles increased with time while giving very low concentrations of small particles in some areas close to the bottom of the bed. When it is in the last two frames (time: 25.5 s and 28.93 s) most of the small particles has accumulated in the top of the bed and very few left in the rest of the bed. The next most important factor is that only the small particle phase has shown in the simulated frames but not in the experimental frame. There are other sizes of particles also in the top area of the bed even in the experiment but not visible as it is not possible to see phase by phase. That is the reason for not having the segregation as clear as in the case of experiments when it come to the simulations. But the observations are clear enough to say that there is particle segregation predicted in the simulation and the margin is close to that of the experiment.

The Figure 5.7 represents the results from the simulation P5 and the reference experiment. It shows a good agreement between the simulations and the experiment. In the experiment it is possible to identify two boundaries with regard to particle segregation. The simulation P5 has predicted the second margin also. The first margin is marked in white and the second margin which is closer

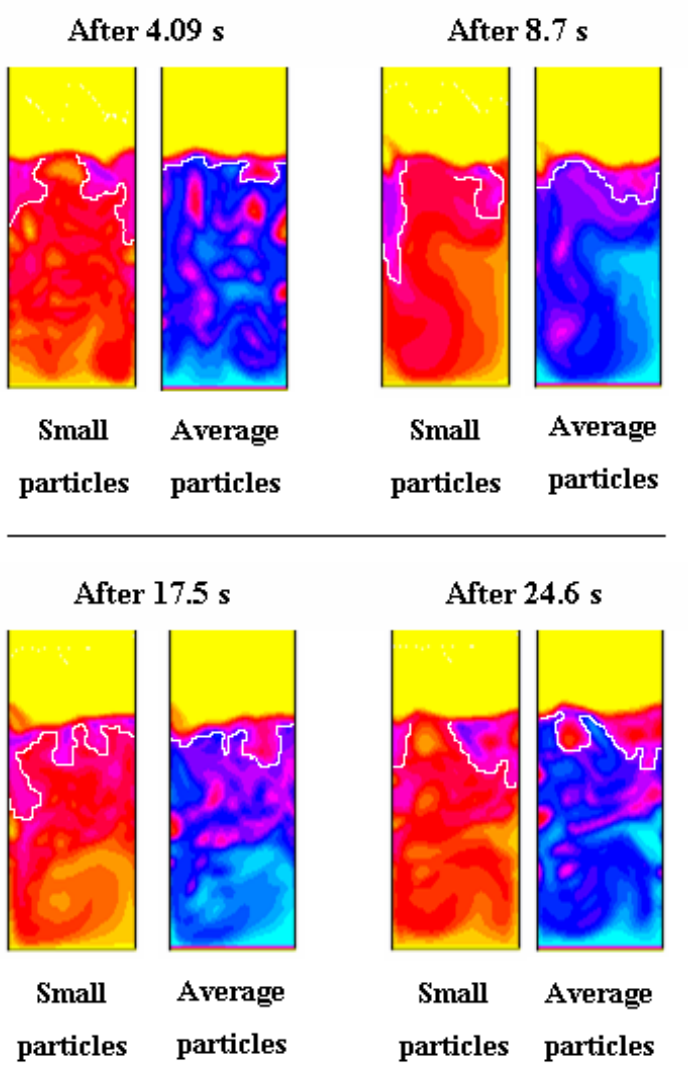

Figure 5.2: Particle segregation in the simulation P2 with respect to the small and average particle phases

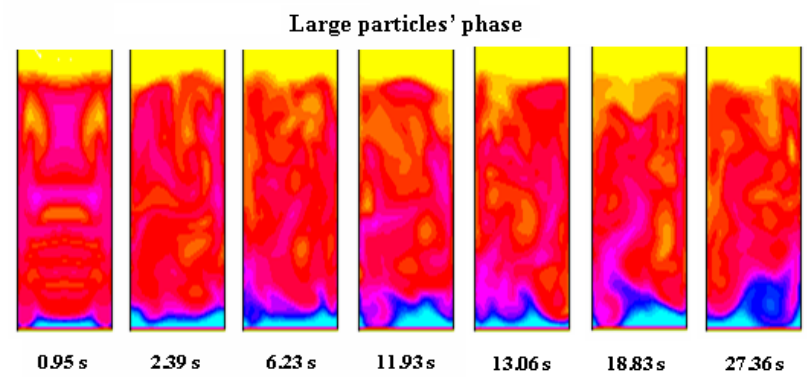

Figure 5.3: Particle segregation in the simulation P3 with respect to the large particle phase

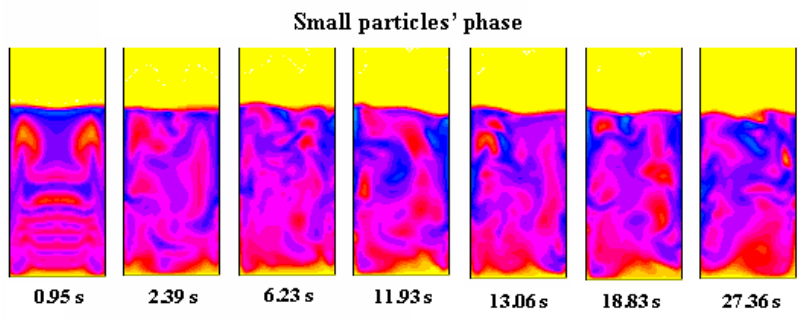

Figure 5.4: Particle segregation in the simulation P3 with respect to the small particle phase

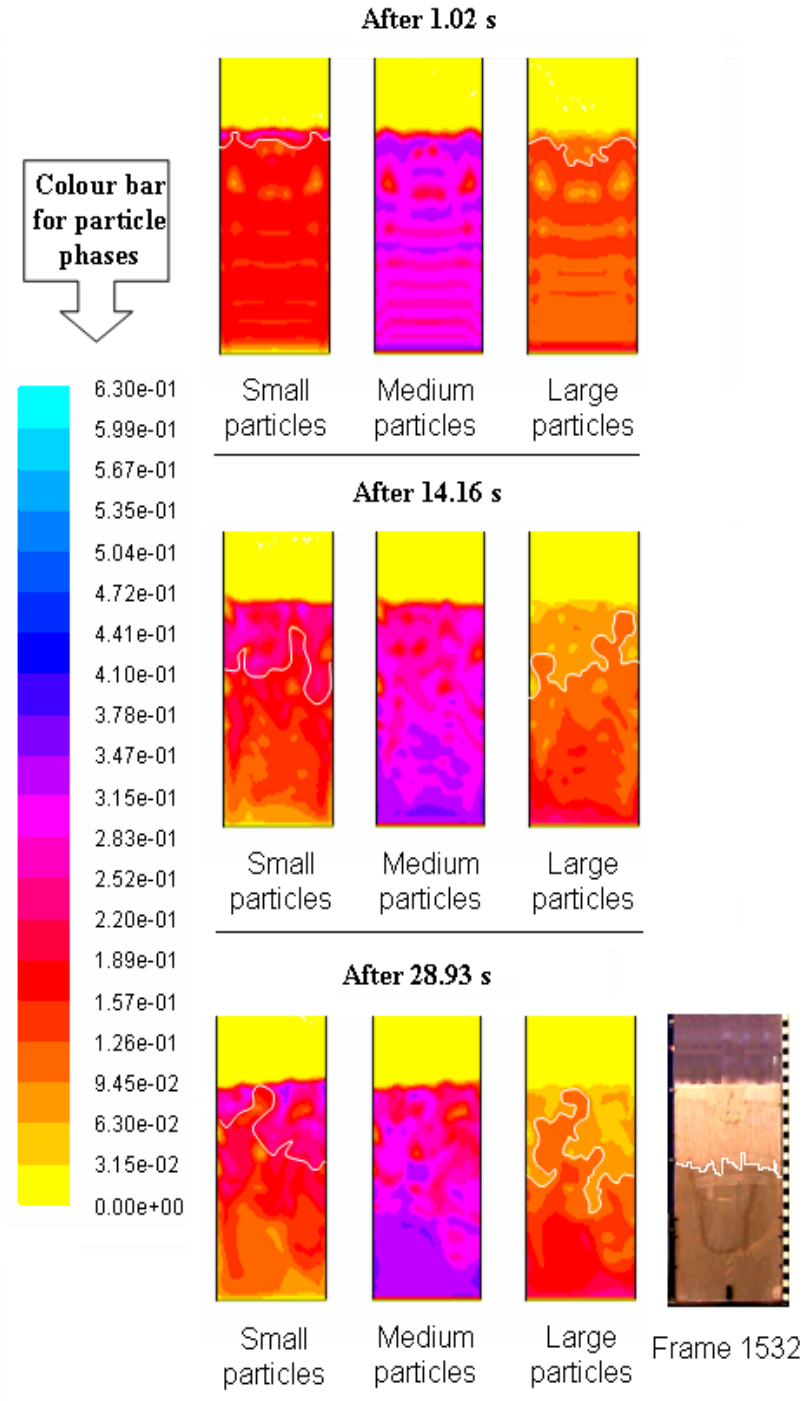

Figure 5.5: Comparison of particle segregation in the simulation P4 and the reference experiment

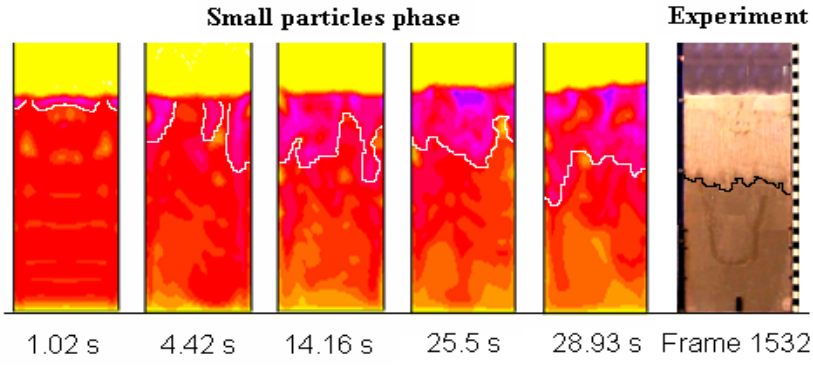

Figure 5.6: Comparison of particle segregation in the simulation P4 and the reference experiment with respective the small particle's phase in the simulation

to the bed surface is marked with a black line in the simulation frames. In the frame from the experiment the first margin is marked with black and the second margin is marked with a lighter color.

Figure 5.8 gives a comparison of the simulation P5 with the reference experiment using the small particle phase alone. Reason for selecting only the small particle phase is the same as with the previous simulation. The comparison proves that the prediction of particle segregation agrees well with the reference experiment.

Above analysis shows that the simulations with three and four particle phases are in good agreement with the reference experiment with respect to the particle segregation. That observation provides evidence about the tendency to predict particle segregation better with the increasing number of particle phases.

5.2 VOF of Particles in the Particle Bed

In addition to the contours, simulated data of VOF of particle phases itself can be plotted and used for analyze the particle segregation. This quantitative analysis is suitable to get further information about the particle segregation once the tendency is identified with use of the contours. VOF of different phases are presented along the width of the bed at different bed heights for each simulation. The VOF values of the particle phases are averaged at the last 25 s of the simulation and used for plotting.

Figure **??** and 5.9 present the averaged VOF of the small and average particle phases of the simulation P2. The curves of small particles show that the small particles have the highest VOF at the highest level analyzed in the bed and have the lowest at the lowest analyzed level of the bed. The averaged particles shows the highest VOF at the lowest analyzed level and the lowest VOF at the highest analyzed level. Corresponding plots for the simulations P3, P4 and P5

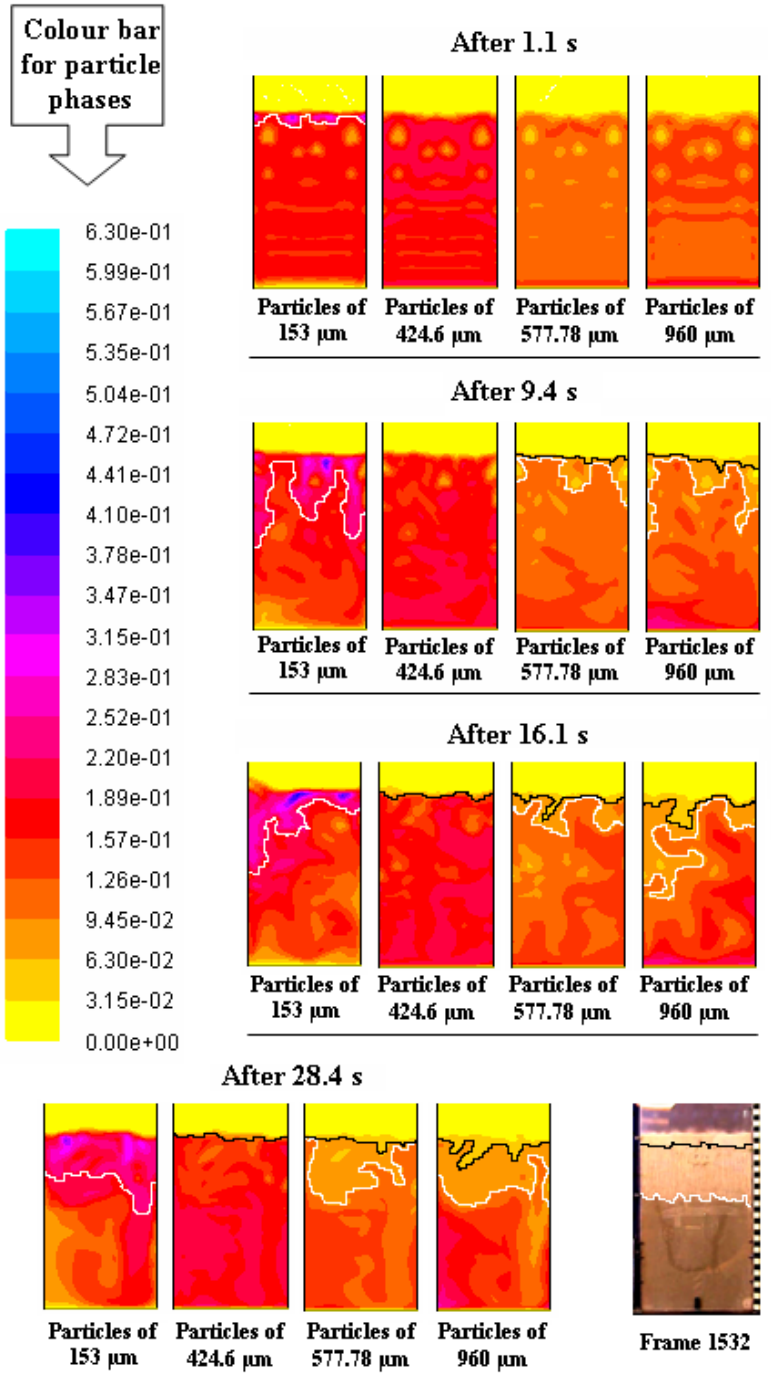

Figure 5.7: Comparison of particle segregation in the simulation P5 and the reference experiment with respective the small particle's phase in the simulation

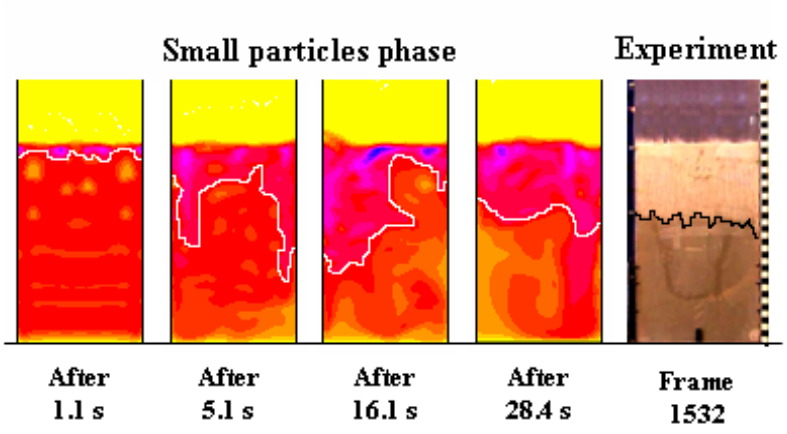

Figure 5.8: Comparison of particle segregation in the simulation P5 and the reference experiment with respective the small particle's phase in the simulation

are included in appendix E.

All the simulations have shown similar results with small particle phase to that of the simulation P2 and other particle phases are predicted similar to the average particle phase in the simulation P2.

The plots from all four simulations show that the small particles accumulate closer to the top and all other particle phases tends to accumulate closer to the bottom. The reason for this observation could be the big difference in the mean particle size between the small and all other particle types.

The importance of this analysis is that the VOF values can read out from the plots easily at each position of the particle bed. Those readings are used for further analysis. In the simulation P2 the small particles VOF is around 0.11, 0.14 and 0.18 at the heights of $0.055m$, $0.155m$ and $0.255m$ respectively. In the simulation P3 it is around 0.27 and 0.31 at the heights of $0.055m$ and $0.255m$ respectively. At the height of 0.155 m the VOF of small particles has reached to a very high value, which is around 0.5 close to the left wall of the column. But the rest of the bed at the same level is having a value about 0.305. The deviation can be due to the formation of bubbles in the rest of the bed. In simulation P4 the small particles VOF is around 0.14, 0.175 and 0.215 at $0.055m$, $0.155m$ and $0.255m$ of the bed respectively. In simulation P5 also there is a sudden variation in the pattern of VOF of small particles at the area about 0.05 m away from the left wall at a height of 0.055 m in the bed. When that is ignored the small particles VOF is around 0.13, 0.172 and 0.215 at $0.055m$, $0.155m$ and $0.255m$ of the bed respectively. Comparison of the VOF data from the plots provide that the simulations P4 and P5 are having the highest difference between the VOF of small particles at their highest and lowest positions analyzed in the bed. This observation confirms that the simulations P4

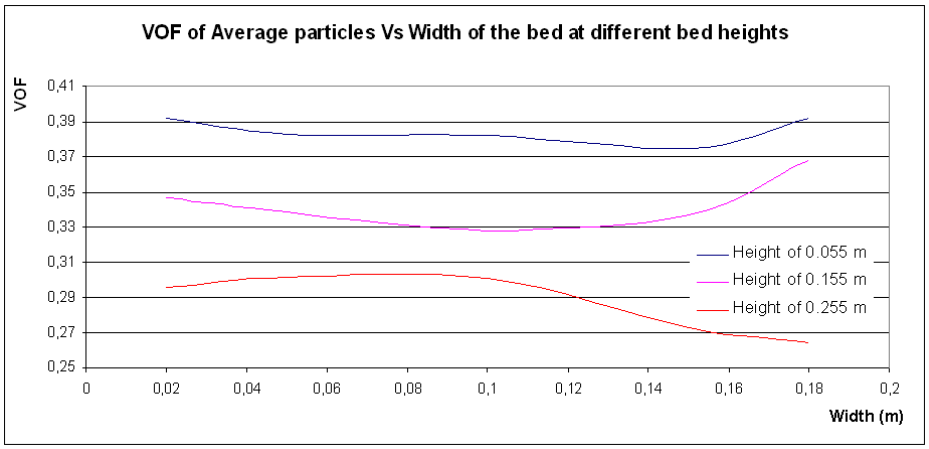

Figure 5.9: VOF of average particles as a fuction of the width of the bed at different levels in the particle bed, predicted by the simulation P2

and P5 predicted particle segregations better than the rest of the simulations.

Readings from the plots of the simulation P4 shows that the large particle VOF is around 0.142, 0.123 and 0.09 at $0.055m$, $0.155m$ and $0.255m$ of the bed respectively. It is around 0.15, 0.115 and 0.085 at $0.055m$, $0.155m$ and $0.255m$ respectively for the simulation P5. Those readings confirm that the simulation P5 has slightly better prediction of particle segregation than the simulation P4.

5.2.1 VOF of Particles Along the Bed Height

Plots showing the VOF of particles along the bed height gives better picture of segregation. VOF are averaged for the last 25 s of the simulation time. Two radial positions are selected and the averaged VOF data are plotted along the height of the particle bed at those positions. One position is close to a wall (0.05 away from a wall) and the other in the center of the column. It is assumed that the analysis of only one side of the bed cross section is enough even though the behavior of both sides are not exactly the same all the time.

Figure 5.10 and 5.11 present the plots from the simulation P5 and the plots from the rest of the simulations are presented in the appendix F. These plots provide evidence about the contribution of different particle types for particle segregation. Gradient of each plot shows how strong the separation at each particle phase.

5.2.2 Variation of VOF with Time

The analysis so far have confirmed that the better the representation of particle size distribution, the better the prediction of particle segregation in the simu-

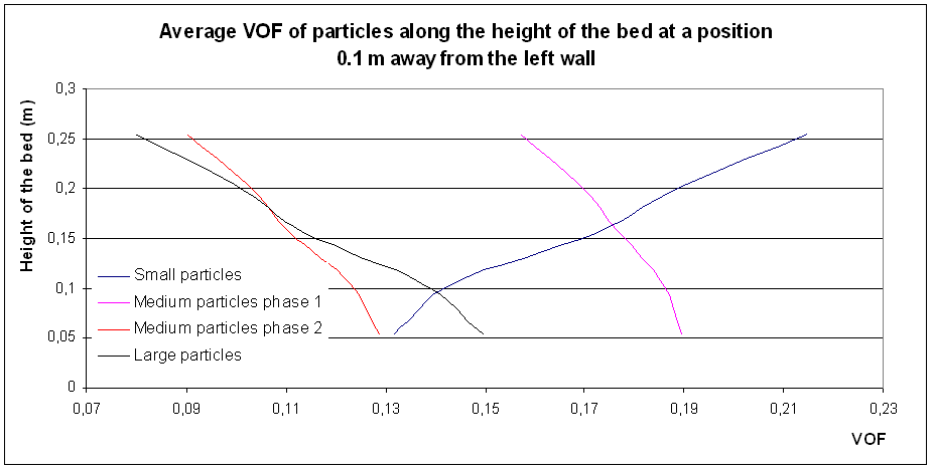

Figure 5.10: VOF of the particles phases along the height of the bed at a position 0.05 m away from the wall predicted by the simulation P5

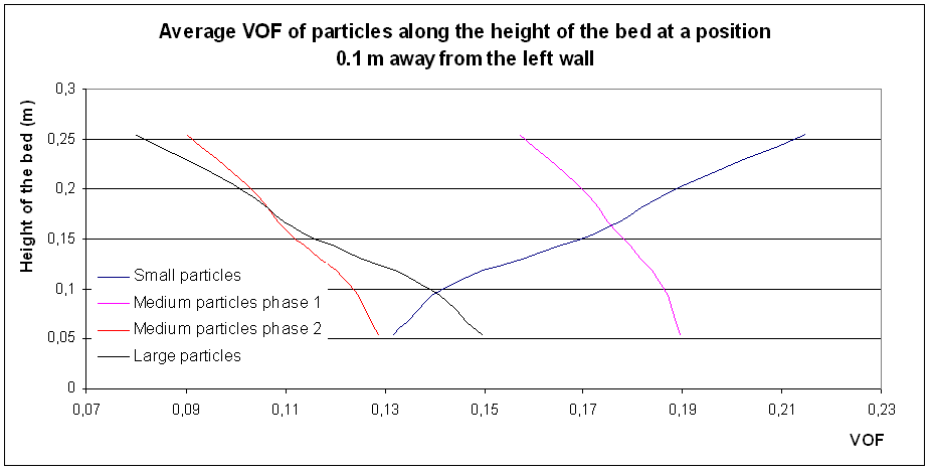

Figure 5.11: VOF of the particles phases along the height of the bed at a position 0.1 m away from the wall predicted by the simulation P5

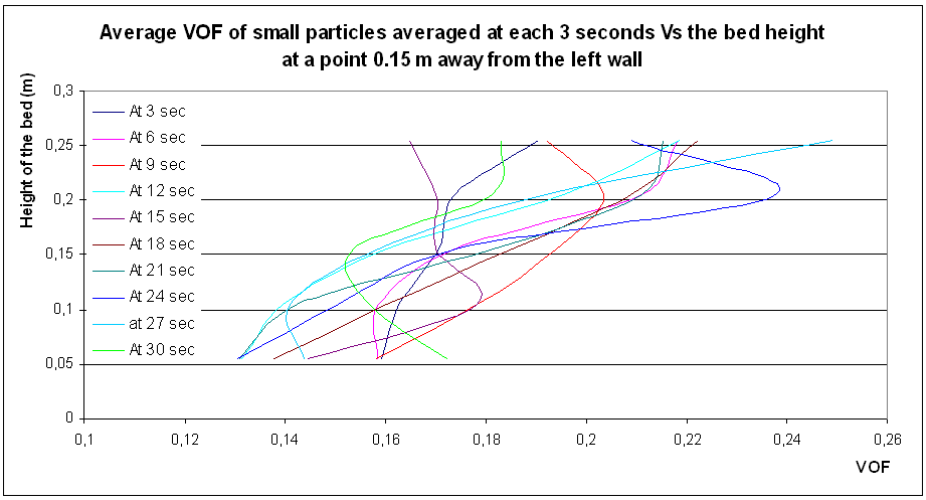

Figure 5.12: Averaged VOF of small particles as a function of the height of the bed, at each 3 s from the beginning of the simulation P2

lations. The progress of particle segregation with time will be studied next in all four simulations. Progress will be checked at the same two radial positions used in the above analysis and two selected points (one close to the top and one close to the bottom) in the particle bed. VOF data of all particles phases are averaged at each 3 seconds of the simulation time.

Progress of Particle Segregation at the Radial Positions

The averaged VOF data at each 3 seconds from the beginning of the simulation are plotted along the bed height. Figure 5.12 provides curves representing all ten time intervals, which show the progress of particle segregation in small particle phase. It presents a redial position 0.05 m away from a wall in of the simulation P2. Assumption of symmetry has used, and the analysis have done either at 0.05 m or 0.15 m away from the left wall and at the center of the particle bed.

Figure 5.12 shows that all curves together doesn't provide a smooth pattern. The reason can be the appearance of bubbles in the bed. Few curves are selected from the that figure and presented in Figure 5.13 as a separate plot to present the progress clearly. Same procedure is followed to present the progress of segregation at the selected positions for all particle types available in all simulations. Those Plots are available in appendix G.

Analysis of all the plots show that small particles VOF value is increased with time close to the top of the particle bed and is decreased with time close to the bottom of the bed. All the other particles behave in an opposite way to the small particles. Reason for this behavior can be the considerable difference in

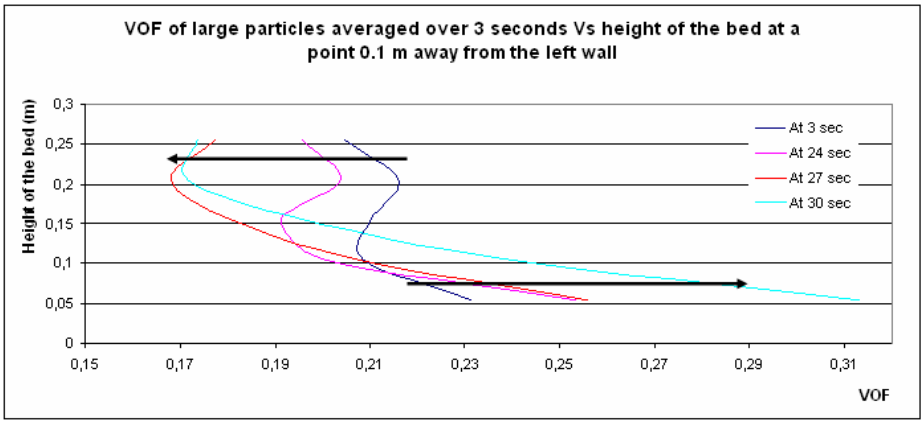

Figure 5.13: Progree of particle segregation along the height of the bed at a radial position 0.05 m away from a wall with respect to the small particles in the simulation P2

the mean particle size between the small particles and all other types of particles used in the simulations.

Progress of Segregation at a Point

Two points are selected from the particle bed of each simulation for this analysis. Those two points represent a higher and a lower position in the bed. Change of VOF of each particle phase with time at those points are analyzed. Simulated time domain is divided in to 10 intervals and took the averaged VOF of each interval. Averaged VOF are presented in plots along with the flow time. Figure 5.14 shows the change of particle phases in simulation P5 with time in a point at 0.255 m from the bottom in the particle bed. Dashed lines marked with 1 and 2 have presented the tendency of the small and the medium particles (only the small portion of medium particles) after studying their curves. It is reasonable to use the same tendency as given by dashed line 2 for the large particles and the large portion of the medium particles.

Figure 5.15 shows the behavior of the particle phases in the simulation P5 with time in a point at 0.055 m from the bottom of the bed. Dashed lines 3 and 4 shows the tendency small and large particles VOF at this point. The two phases, which represent the small and large portions of the medium particles have similar tendencies as the line 4.

Similar figures have used to analyze all four simulations, and the rest of the plots are presented in the appendix G.2. The simulations P2, P4 and P5 have predicted increase of small particles VOF in the point closer to the top and decrease in the point closer to the bottom. All other particle phases present in the simulations have shown an opposite behavior to the small particles.

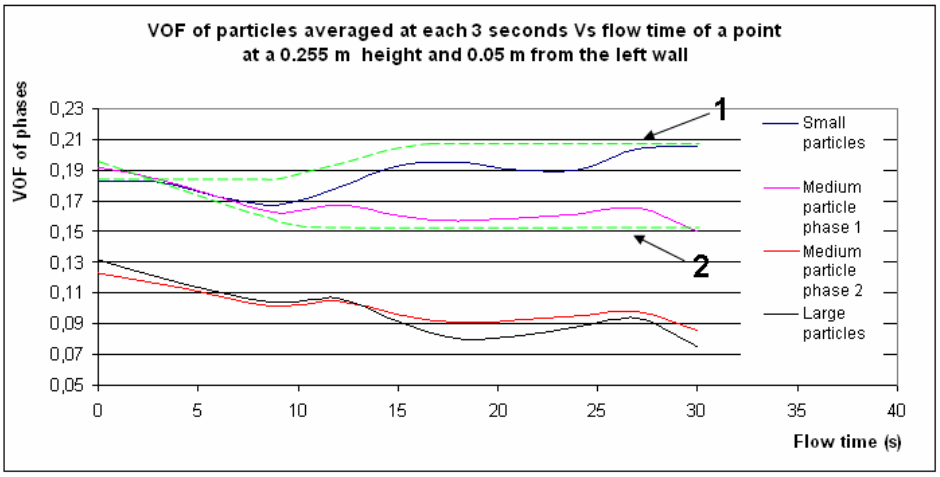

Figure 5.14: VOF of particles as a function of time at a point close to the top of the bed in the simulation P5

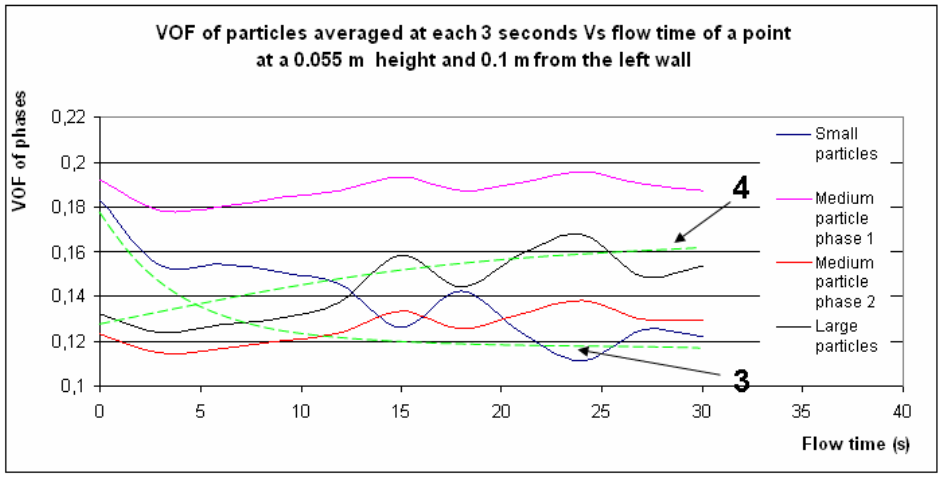

Figure 5.15: VOF of particles as a function of time at a point close to the bottom of the bed in the simulation P5

All the analysis done so far have confirmed that simulations with more than one particle phase have predicted particle segregation. The prediction is better with the increasing number of particle phases used in the simulations. Also, it is important to include the correct distribution as present in the experiment. A different distribution will give results with higher deviations from the experimental results. That is observed with the results from the simulation P3.

Chapter 6

Bubble Behavior in the Particle Bed

Bubble characteristics are very important in the design of fluidized beds as they govern hydrodynamics and efficiency of the operation for which the bed is used [3]. In order to check whether the simulations have predicted the bubble characteristics similar to the experiments, bubble behavior in the particle bed is analyzed. Bubble velocity, Bubble distribution and bubble frequency have been analyzed in the simulations P2, P3, P4 and P5. As the simulation P1 didn't predict any bubbles, it is not included in the analysis. Those simulations are compared with each other and also with the reference experiment with respect to the bubble behavior.

6.1 Bubble Distribution

Bubble distribution in the particle bed of each simulation is compared using the contours of the VOF of gas phase. The contours selected for the analysis are well distributed in the whole time domain of the simulations. Some frames from the movie of the reference experiments are used to present the bubble appearance in the experiment and those are presented in Figure 5.1. It provides that the lowest position of bubble appearance in the experiment is 23.2 cm approximately.

Figure 6.1 shows the bubble distribution in the particle bed at different time instances of the simulation P2. Eventhough most of the bubbles are appeared close to the walls there are some bubbles appeared in the middle area of the bed also, when the radial positions are considered. In addition, the simulation P2 has predicted bubbles even in lower positions about 7.4 cm in the bed. Bubble distribution predicted by this simulation with two particle phases shows that there is a major effect by introducing particle size distribution to CFD simulations. That is because there is no bubble prediction in the simulation with only one particle phase.

Bubble distribution predicted in the simulation P3 is presented in the Figure

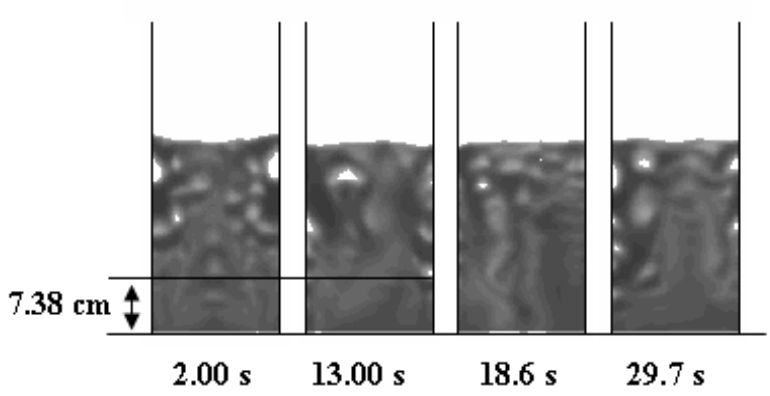

Figure 6.1: Bubble distribution in the particles bed of the simulation P2

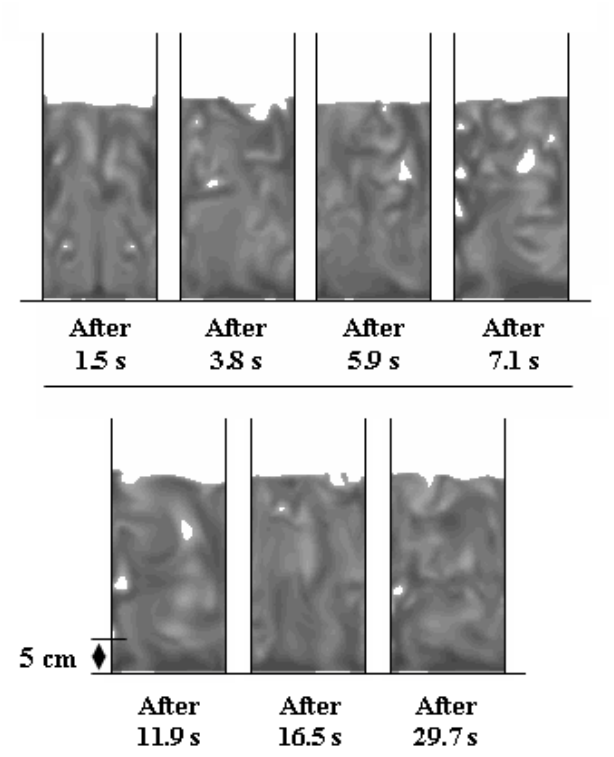

Figure 6.2: Bubble distribution in the particles bed of the simulation P3

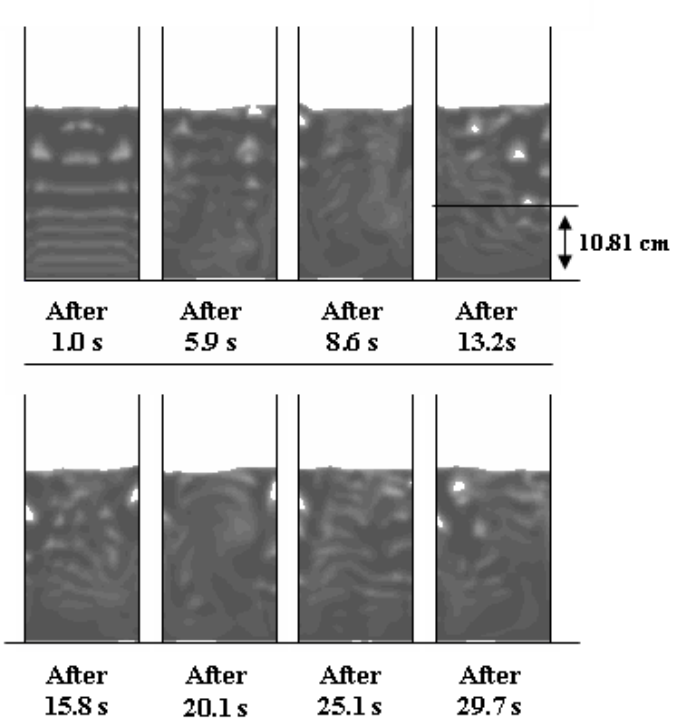

Figure 6.3: Bubble distribution in the particles bed of the simulation P4

6.2. It provides that there are bubbles well distributed in the upper section of the bed. Lowest position of bubble appearance is about 5 *cm*, which is far bellow than the reference experiment. The reason can be the large amount of small particles in the mixture, which have resulted a particle distribution far away from the distribution used in the reference experiment.

Figures 6.3 and 6.4 present the bubble distribution in the particle bed of the simulations P4 and P5. Both figures provides that there are not many bubbles at the central area as well as on the walls of the bed when the upper section of the bed is considered. Also the lowest level of bubble appearance is not as low as the previous simulations. Among the simulations P4 and P5, P5 has better prediction as the lowest position predicted is more closer to the reference experiment than any other simulation analyzed.

6.2 Bubble Frequency in the Bed

Bubble frequency is also an important factor to comment on the prediction of bubble behaviors by simulations. The bubble frequency is calculated for

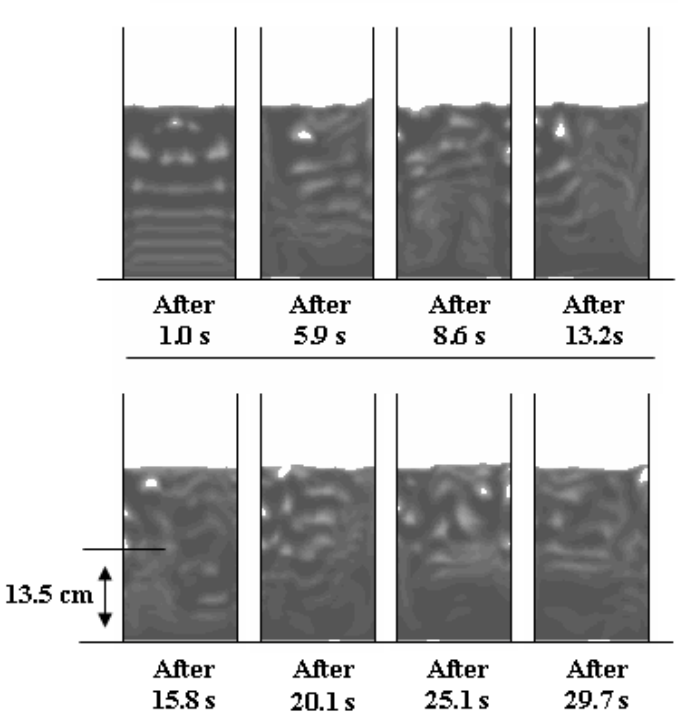

Figure 6.4: Bubble distribution in the particles bed of the simulation P5

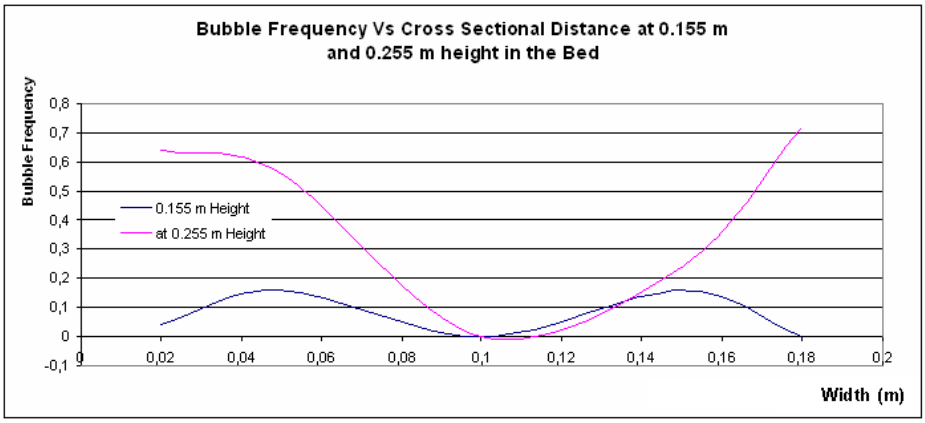

Figure 6.5: Bubble frequency in the bed as a function of the width of the bed at two different heights predicted by the simulation P2

all four simulations used for analysis. Figures 6.5, 6.6, 6.7 and 6.8 shows the bubble frequency data of all four simulations from P2 to P5. Those figures confirm the observation made earlier about higher bubble appearance in the area between the center of the bed and the walls. Increased frequency of bubbles have predicted with the increased position (height) in the bed.

The assumption of solid free bubbles is an oversimplification of what actually happens in the particle bed [5]. To accept some solid particles in side the bubbles, the limit VOF value of gas to accept as a bubble is chosen as 0.7 of gas VOF. Figure 6.8 haven't provided the frequency at the level of 0.155 m in the bed as there is very few (1 or 2) bubbles appeared at that level. Also, even at 0.205 m height, the simulation P5 has predicted lower frequency of bubbles. That observation confirms that simulation P5 have predicted the lowest position of bubble occurrence better than the other simulations.

6.3 Rise Velocity of Bubbles

Rise velocity is the velocity of a bubble that rises upwards on a bubbling bed. In literature it has been shown that the bubbles in a fluidized bed behaves similar to the bubbles in a liquid. According to theories, bubbles in a fluidized bed have a shape close to spherical when small, flatterned and distorted when large. Those bubbles rise slowly when small and rise faster when large. Normally a train of bubbles may coalesce to give larger bubbles and interaction of a train gives a different rise velocity.

Bubbles in a fluidized bed can be distinguished in to two groups depending on whether the bubble rises faster or slower than the emulsion gas. Those are the cloudless (slow bubbles, $u_{br} < u_f$) or the clouded (fast bubbles, $u_{br} > u_f$)

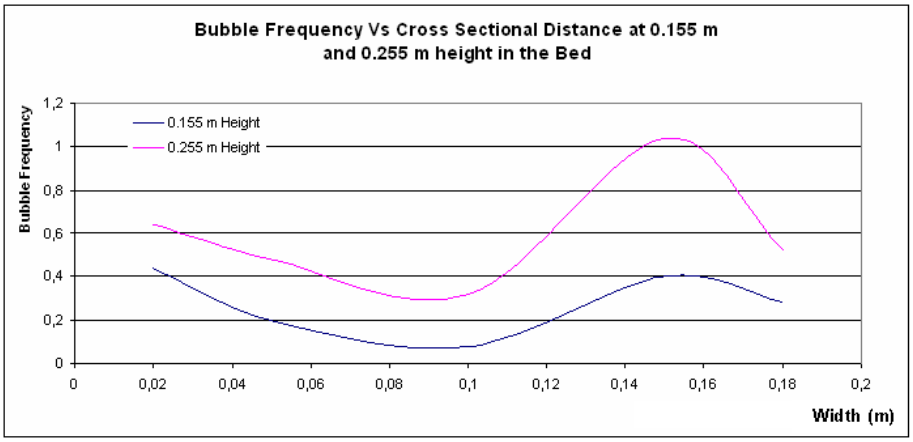

Figure 6.6: Bubble frequency in the bed as a function of the width of the bed at two different heights predicted by the simulation P3

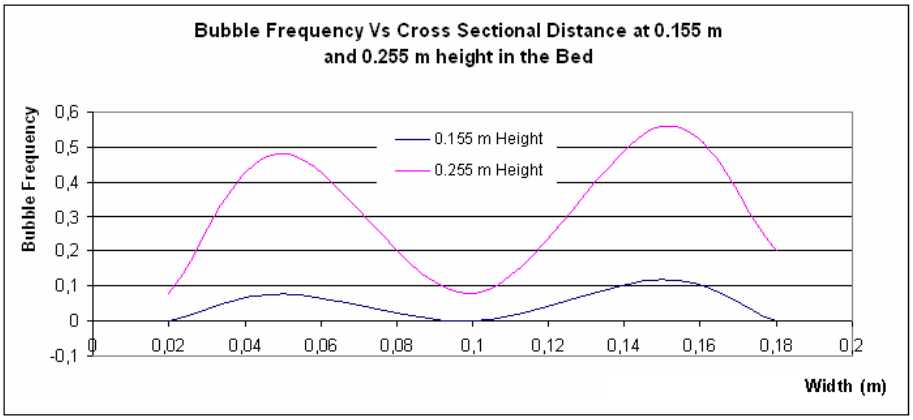

Figure 6.7: Bubble frequency in the bed as a function of the width of the bed at two different heights predicted by the simulation P4

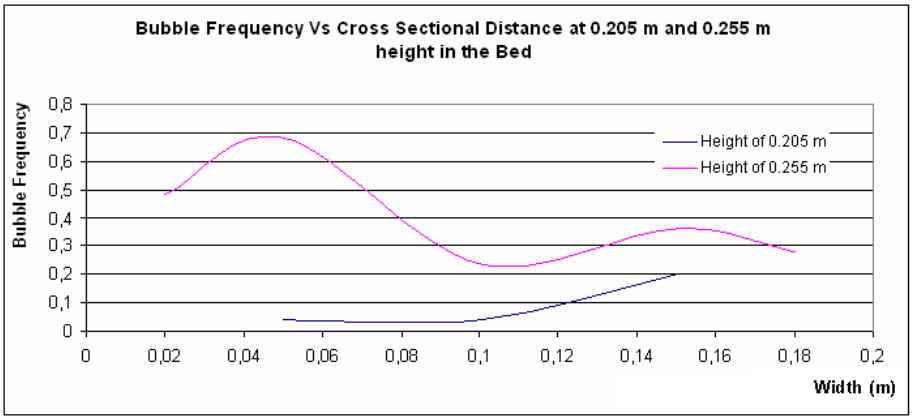

Figure 6.8: Bubble frequency in the bed as a function of the width of the bed at two different heights predicted by the simulation P5

bubbles [16]. In the case of cloudless bubbles the emulsion gas rises faster than the bubble, hence it uses the bubble as a convenient shortcut on its way through the bed. Gas enters the bubble at it's bottom and leaves at the top, while an annular ring of gas does circulate within the bubble, moving upward with it. The amount of gas in the bubble increases as the bubble velocity slows to the rise velocity of emulsion gas.

In the case of clouded bubbles also the emulsion gas enters the lower part of the bubble and leaves at the top. But as the bubble is rising faster than the emulsion gas, the gas leaving the top of the bubble is swept around and returns to the base of the bubble. The region around the bubble, where the gas is circulating is called the cloud. The rest of the gas in the bed move aside as the fast bubble and it's cloud passes by instead of mixing with the recirculating gas .

6.3.1 Rise Velocity of Bubbles Predicted in Simulations

Calculation of the rise velocities is an important step to be carried out when analyzing simulated results. Rise velocities can use to study the dynamics in the particle bed and also to compare the prediction of the simulations with the reference experiment to evaluate how close the simulations are to the experiment. Figure 6.9 presents the change of the position of a selected bubble with time in the experimental bed. Frame rate of 30 fps have used for filming the experiment, and that rate is used to calculate the bubble velocity. The bubble have a velocity of 0.174 ms^{-1} at the first interval and a velocity of 0.321 ms^{-1} at the second time interval, which gives an average velocity of 0.223 ms^{-1}.

Rise velocities of the bubbles in the simulations are calculated using some of the bubbles raised in the particle bed at each simulation. It is performed using

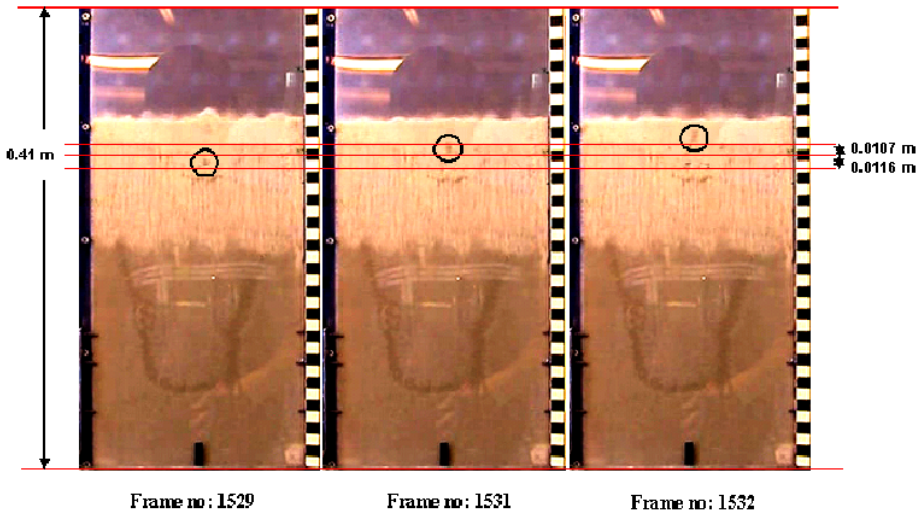

Figure 6.9: Bubble position with time in the reference experiment

contours of VOF of the gas phase. To calculate the rise velocity, one or more bubbles are selected and the change of the position of the bubble with time is measured. Figure 6.10 presents the change of the position of two bubbles with time in the simulation P2. Firstly analyzed bubble have an average velocity of 0.357 ms^{-1} and the secondly analyzed bubble have 0.219 ms^{-1}.

Three bubbles from the simulation P3 are analyzed to check the bubble velocity, and those are presented in the Figure 6.11. The firstly analyzed bubble has 0.206 ms^{-1}, 0.399 ms^{-1} and 0.556 ms^{-1} respectively as the rise velocity in the selected time intervals. The secondly and thirdly analyzed bubbles have 0.333 ms^{-1}, 0.484 ms^{-1} and 0.257 ms^{-1}, 0.24 ms^{-1}, 0.454 ms^{-1}respectively for the rise velocity. It is easily observable that the bubble in this simulation grows faster and reaches higher velocities as they grow.

Four bubbles at different time intervals are selected from the simulation P4 for analysis. Change of the bubble position with time is shown in the Figure 6.12. According to the figure the bubbles appeared at about 700 ms has 0.363 m/s and 0.423 m/s during the selected time intervals. The secondly selected bubble has 0.48 m/s and 0.45 m/s respectively at the two time intervals as the rise velocity. The thirdly analyzed bubble has more uniform velocity (0.23m/s) in the first two intervals and has moved with a higher velocity (0.31m/s) at the third time interval. This bubble has an average velocity of about 0.26m/s. Fourth bubble analysis shows that the bubble shrinks during the first 100ms and grows during the second 100ms, and also has a value of 0.285 m/s and 0.24 m/s for the velocity at the first and second time intervals respectively.

Bubble position variation of two selected bubbles with time from the simu-

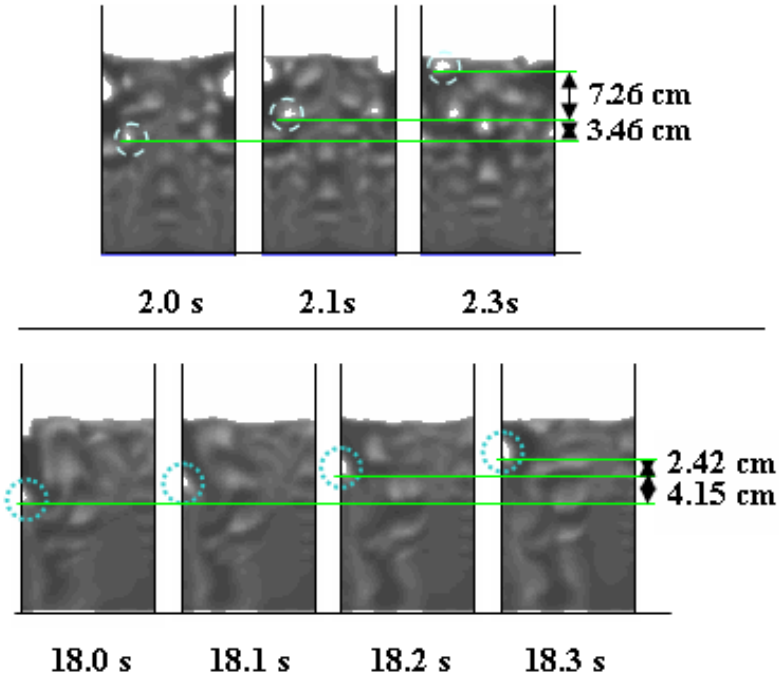

Figure 6.10: Bubble position with time in the simulation P2

velocity$_s l$

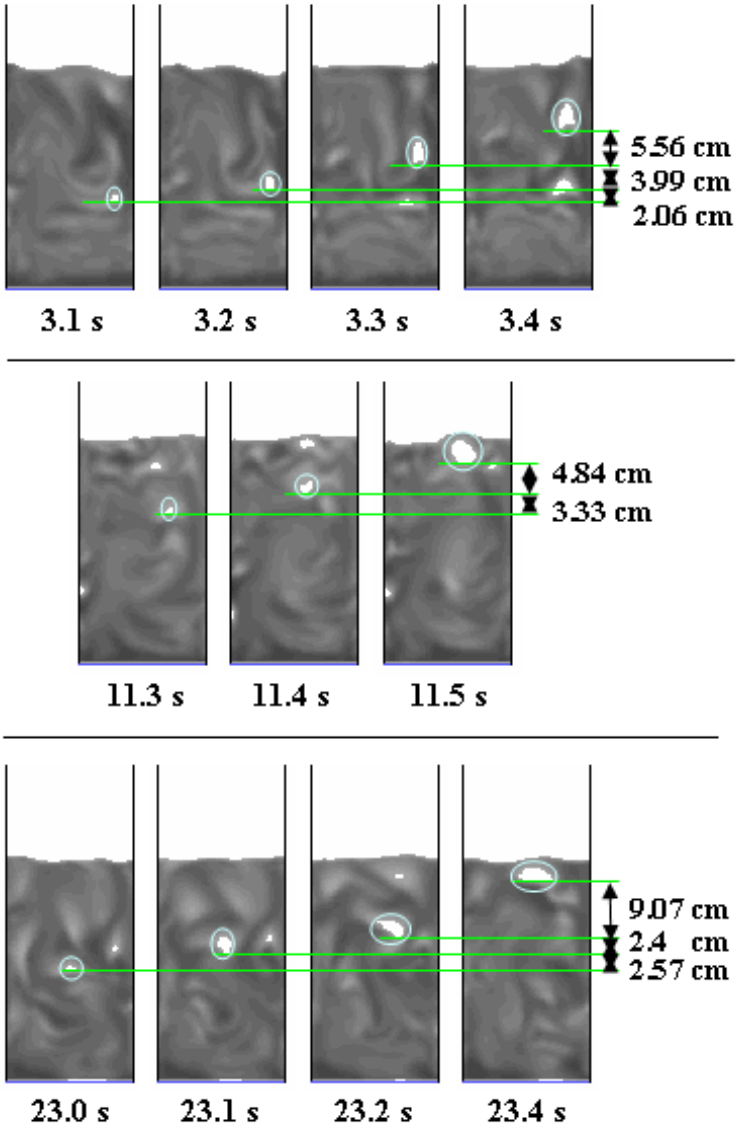

$_4$3.*pdf*

Figure 6.11: Bubble position with time in the simulation P3

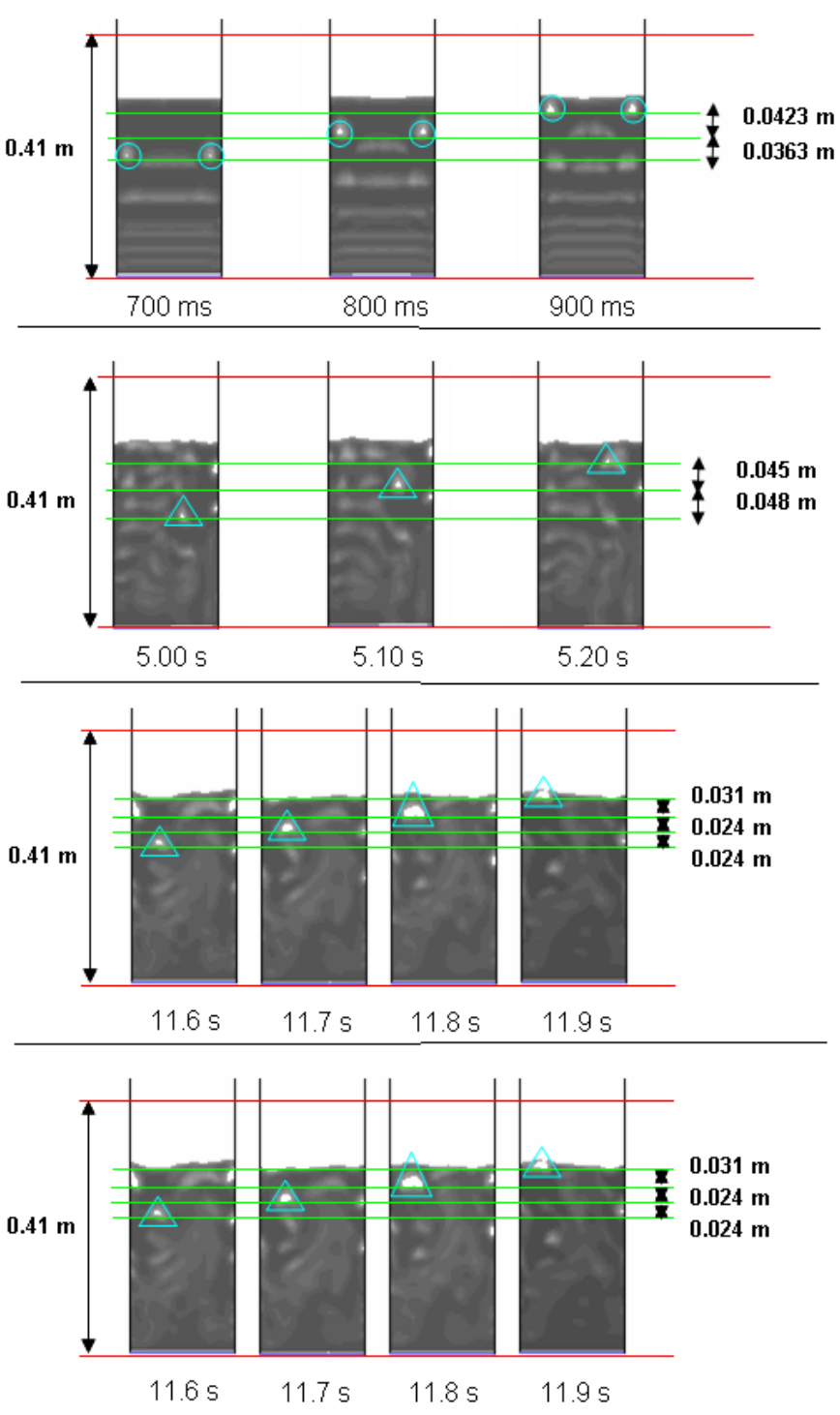

Figure 6.12: Bubble position with time in the simulation P4

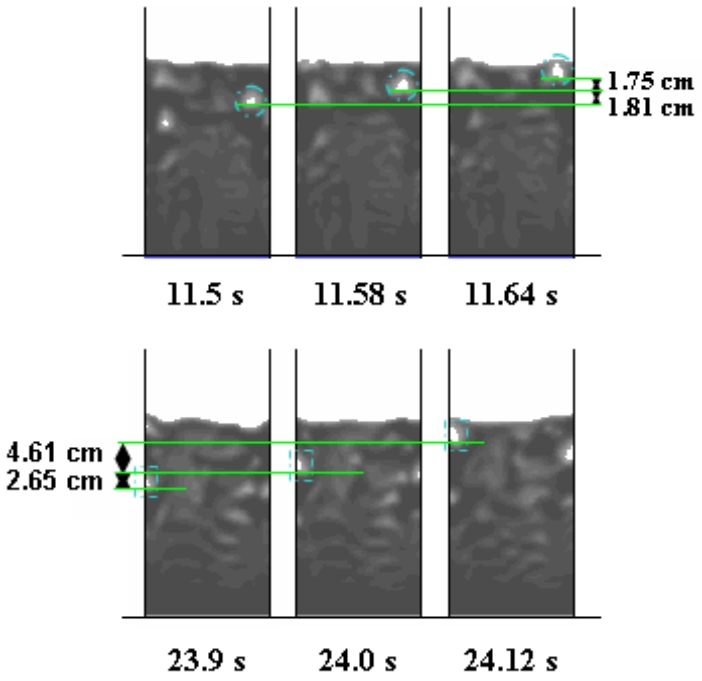

Figure 6.13: Bubble position with time in the simulation P5

lation P5 is presented in the Figure 6.13. Those two bubbles have 0.254 ms^{-1} and 0.33 ms^{-1} respectively as their average rise velocities.

Above analysis showed that all three simulations except the simulation P3 have predicted bubbles those have rise velocities in the same range as the reference experiment. In addition, it is clear that the bubbles are growing larger with time and speeds up as the bubbles grow. This observation supports the statements done at the beginning of this chapter about the bubbles in a fluidized bed. Also, when the rise velocities are compared with the emulsion gas velocity, it is clear that all of the analyzed bubbles are fast moving bubbles.

Chapter 7

Particle Bed Height

Expansion of the particle bed is one of the most important factors to check whether a simulation gives reasonable results. If a simulation gives similar bed expansion to that of the reference experiment, the results of the simulation are accepted as a good prediction. To check the reliability of the simulated results of the four simulations analyzed so far, a bed height analysis is performed and it is presented in this chapter. As small particle phase can present the bed height accurately than any other particle phase, the small particle phase has used for the bed height comparisons.

The results from the previous analysis showed that the simulations P4 and P5 are the closest prediction to the reference experiment. Only those two simulations are used for the bed height analysis. Figures 7.1 and 7.2 provide the comparison of the predicted bed height by the simulations P4 and P5 with the reference experiment. Analysis of the figures show that both simulation have predicted the bed expansion similar to the experiment. The simulation P5 has the best prediction.

Observations of the bed height analysis show that the higher the number of particle phases used to represent the particle size distribution, the better the prediction of bed expansion.

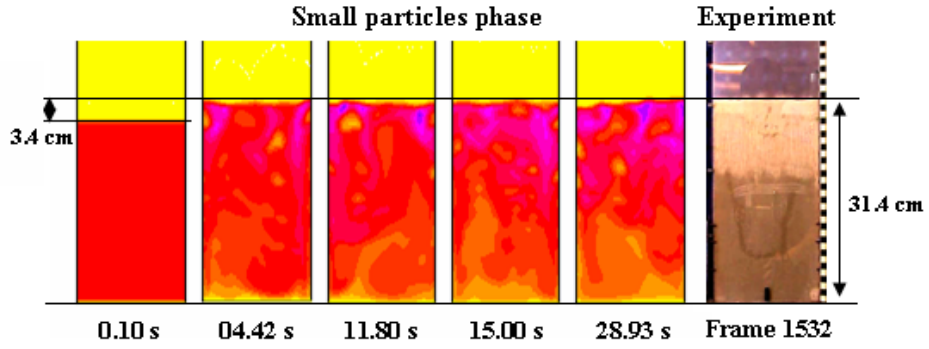

Figure 7.1: Expansion of the particle bed predicted by the simulation P4

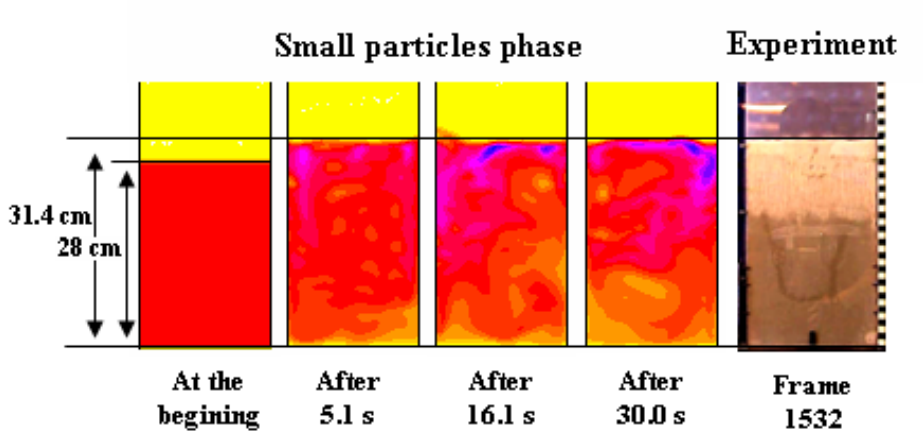

Figure 7.2: Expansion of the particle bed predicted by the simulation P5

Chapter 8

For Future Work

1. The fictional viscosity term is defined in the simulations performed to analyze the influence of particle size distribution on the simulations by using the Shaeffer model available in FLUENT. The influence of Shaeffer model on the results can study in more details and it is possible to try to make a UDF to specify the frictional viscosity

2. The "Syamlal O'Brien" drag model is used to introduce the drag force between the particles and the fluid and the "Syamlal O'Brien Symmetric" drag model is used to introduce the drag force between the particle phases. It is possible to analyze the equations used in those two models in details and try to introduce a better drag model, and check the prediction of the simulations with multiple particle phases.

3. The prediction of the bubble frequency in the simulations couldn't compare with the reference experiment as the movie of the experiment is not very clear. It is possible to make a good movie of a experiment with the same conditions and compare the bubble frequencies as well, to check the prediction of bubble appearance in the particle bed.

4. Can increase the number of particle phases even further than used in this study and try to check an optimum number of particle phases to be used to represent a powder or a powder mixture in a simulation.

5. Eventhough this study showed some results providing that there is an influence from introducing particle size distributions in the simulations, the results are far beyond the reality as the simulations and the experiments are performed using 2-D particle bed. Making an ideal 2-D bed is not possible and the experimental beds used are just approximations of the 2-D beds. It is important to do a similar study using 3-D simulations to check the influence from introducing the particle size distributions in the simulations.

Part IV

Conclusions

A computational study of the influence of particle size distribution on bubbling fluidized beds is performed. Several simulations are performed using Eulerian multiphase model for a two dimensional fluidized bed with an air jet as preliminary work. The commercial software FLUENT is used to perform the simulations. The results of the simulations are compared with a reference experiment. The simulations used the same dimensions for the particle bed as in the reference experiment. Particles with the mean particle diameter of 491 μm is used in the analysis.

Effects from using different FLUENT versions, different column heights in the mesh and different packing limits are analyzed. The bubble prediction, bubble velocity and the bed expansion predicted in the simulations are compared with the reference experiment. Using the results of the comparisons of the simulations with the experiments, a combination of the models available in FLUENT is finalized as a good combination to be used in the main work.

The finalized combination of models is used to simulate a two dimensional fluidized bed with uniform distribution of air in order to check the influence of particle size distribution on simulations. The "Syamlal O'Brien Symmetric" drag model is used to introduce the solid-solid drag forces and the "Syamlal O'Brien" drag model to introduce the solid-fluid drag forces. Five simulations, P1,P2,P3,P4 and P5 are performed with increasing number of particle phases in the bed, such as, the simulation P1 with one particle phase, the simulations P2 and P3 with two particle phases and the simulations P4 and P5 with three and four particles phases in each. The five simulations are compared with each other and with a reference experiment.

Representation of the particle size distribution in the simulations is arranged according to the particle distributions of the particle mixture used in the reference experiment except in the simulation P3. Each particle phase is represented by the corresponding mean particle diameter. The same mean particle diameter persists in all five simulations.

As the simulation with only the single particle phase didn't predict variations in VOF of particles or bubbles in the particle bed it is not used in the analysis. The reason is found as the superficial gas velocity used in the simulations, which is well bellow the minimum fluidization velocity of the particles used in the bed. The comparison of the multiphase simulations with the reference experiment is conducted in terms of the particle segregation, expansion of the particle bed and the bubble characteristics in the particle bed.

Prediction of particle segregation in simulations is analyzed and compared with each other and the reference experiment using the contours of the particle phases as well as the plots of volume fraction (VOF) data it self. The progress of the particle segregation also analyzed using VOF data of particle phases at along the height of the bed and at selected points of the bed. Comparison showed that the higher the number of particle phases the better the prediction of particle segregation. Also, the analysis showed that if the particle distribution is not in accordance with that of the reference experiment, the simulated results tends to show high deviations from the experiment.

Bubble behavior prediction is analyzed in terms of bubble velocity, bubble

frequency, bubble distribution in the bed and the lowest position of bubble occurrence in the bed. The bubble velocity, bubble appearance and the lowest position of bubble occurrence are analyzed and compared using the contours of the particle phases. The bubble frequency data are calculated after analyzing the VOF data of the gas phase and plotted as a function of the width of the bed. Plots of the bubble frequency are used to check the observations from the contours used to present the bubble appearance in the particle bed. The analysis and the comparisons with the reference experiment confirmed that there is an influence on the simulated data from introducing the particle size distributions in the simulations.

The bed expansion in the simulations is presented using the contours of the small particle phase and compared with the reference experiment using a photo frame from the movie of the reference experiment. The comparison showed that the simulation with four particle phases has predicted the bed expansion very close to that of the reference experiment and the prediction is better than all other multiphase simulations performed under this study.

The total comparison of the simulated results with the reference experiment showed that the higher the number of particle phases the better the prediction of particle segregation, bubble behavior and the bed expansion in the simulations. Also it is observed that, the closer the presentation of the particle size distribution in the simulation to the mixture used in the experiment the better the prediction of the dynamics of the particle bed.

Two abstracts have been sent to the AICHE – 2008 annual meeting and SIMS 2008 conference using some of the work performed related to this study. The abstracts are given in the appendix H and I.

Part V

References

1. Ahmadi, G. & Ma, D. (1990). A THERMODYNAMICAL FORMULATION FOR DISPERSED MULTIPHASE TURBULENT FLOWS–1. *Multiphase Flow,* 16 (2) pp. 232 - 340

2. Arastoopour, H. (2001). Numerical simulation and experimental analysis of gas / solid flow systems: 1999 Flour-Daniel Plenary lecture. *Powder Technology,* 119 pp. 59-67

3. Busciglio, A., Vella, G., Micale, G. & Rizzuti, L. (2008). Analysis of the bubbling behavior of 2D gas solid fluidized beds, Part I. Digital image analysis technique. *Chemical Engineering Journal.* [Online]. Available from: http://www.elsevier.com [15^{th} March 2008].

4. Boemer, A., Qi, H. & Renz, U. (1998). Verification of Eulerian simulation of spontaneous bubble formation in a fluidized bed. *Chemical Engineering Science,* 53 (10) pp. 1835-1846

5. Cui, H., Mostoufi, N & Chaoki, J. (2000). Characterization of dynamic gas-solid distribution in fluidized beds.*Chemical Engineering Journal 79.* [Online]. Available from: http://www.elsevier.com [8^{th} March 2008].

6. Cody, G. D., Johri, J. & Goldfarb, D. (2008). Dependence of particle fluctuation velocity on gas flow, and particle diameter in gas fluidized beds for monodispersed spheares spheres in the Geldart B and A fluidization regimes. *Powder Technology 182.* [Online]. Available from: http://www.elsevier.com [2^{th} February 2008].

7. Enwald, H., Peirano, E. & Almstedt, A.E. (1996). EULERIAN TWO-PHASE FLOW THEORY APPLIED TO FLUIDIZATION. *Multiphase Flow,* 22 pp. 21-66

8. Fluent (2006). Modeling Multiphase Flows. **In** *Fluent 6.3 User's Guide,* pp 37-71.

9. Gidaspow, D. (1994 (a)). The Fluidized State. **In** *Multiphase Flow and Fluidization, Continuum and Kinetic Theory Descriptions,* pp. 97-114. California: Academic press,Inc.

10. Halvorsen. B. M. (2005). An Experimental and Computaional Study of Flow Behavior in Bubbling Fluidized Beds. **In** *Thesis for the degree of Dr. Ing,* pp. 32-45.

11. Huilin, L., Yunhua, Z., Ding, J., Gidaspow, D. & Wei, L. (2007). Investigation of mixing / segregation of mixture particles in gas-solid fluidized beds. *Chemical engineering science 62.* [Online]. Available from: http://www.elsevier.com [15^{th} February 2008].

12. Huilin, L., Yurong, H. & Gidaspow, D. (2003). Hydrodynamic modelling of binary mixture in a bas bubbling fluidized bed using the kinetic theory of granular flow. *Chemical Engineering Science 58.* [Online]. Available from: http://www.elsevier.com [5^{th} March 2008].

13. Kunii, L & Levenspiel, O. (1991). Introduction. **In** *Fluidization Engineering, 2^{nd} edition,* pp 1-13. Newton: Butterworth-Heinemann, a devision of reed publishing (USA) Inc.

14. Kunii, L & Levenspiel, O. (1991). Industrial Applications of Fluidized Beds. **In** *Fluidization Engineering, 2^{nd} edition,* pp. 15-59. Newton: Butterworth-Heinemann, a devision of reed publishing (USA) Inc.

15. Kunii, L & Levenspiel, O. (1991). Fluidization and Mapping of Regims. **In** *Fluidization Engineering, 2^{nd} edition,* pp. 61-94. Newton: Butterworth-Heinemann, a devision of reed publishing (USA) Inc.

16. Kunii, L & Levenspiel, O. (1991). Bubbles in Dense Beds. **In** *Fluidization Engineering, 2^{nd} edition,* pp. 115-135. Newton: Butterworth-Heinemann, a devision of reed publishing (USA) Inc.

17. Lun, C.K.K., Savage, S.B., Jeffrey, D.J. & Chepurniy, N. (1984). Kinetic theories for granular flow: inelastic particles in couette flow and slightly inelastic particles in a general flowfield. *Fluid Mechanics, 140* pp. 223-256

18. Rietema, K. (1991). General Introduction. **In** R**.** Clift, ed. *The dynamics of fine powders*, pp. 1-18. England: Elsevier science publishers Ltd.

19. Massah, H. & Oshinowo, L. (2000). Advanced Gas-Solid Multiphase Flow Models Offer Significant Process Improvements: JA112. *JOURNAL ARTICLES BY FLUENT SOFTWARE USERS,* p. 2. Fluent .Inc

20. Patil, D.J., Annaland, M.V.S. & Kuipers, J.A.M. (2005 (b)). Ctritical comparison of hydrodynamic models for gas-solid fluidized beds–Part II: freely bubbling gas-solid fluidized beds. *Chemical engineering science 60.* [Online]. Available from: http://www.elsevier.com [10^{th} February 2008].

21. Patil, D.J., Annaland, M.V.S. & Kuipers, J.A.M. (2005 (a)). Ctritical comparison of hydrodynamic models for gas-solid fluidized beds–Part I: bubbling gas-solid fluidized beds operated with a jet. *Chemical engineering science 60.* [Online]. Available from: http://www.elsevier.com [10^{th} February 2008].

22. Wong, A.C.Y. (2002). Use of angle of repose and bulk densities for powder characterization and the prediction of minimum fluidization and minimum bubbling velocities. *Chemical engineering science 57.* [Online]. Available from: http://www.elsevier.com [5^{th} March 2008].

Part VI

Appendixes

Appendix A

Comparison of Types of Contacting for Reacting Gas-Solid Systems

TABLE 1 Comparison of Types of Contacting for Reacting Gas-Solid Systems.

	Solid-Catalyzed Gas-Phase Reaction	Gas-Solid Reaction	Temperature Distribution in the Bed	Particles	Pressure Drop	Heat Exchange and Heat Transport	Conversion
Fixed Bed	Only for very slow or nondeactivating catalyst. Serious temperature control problems limit the size of units.	Unsuited for continuous operations, while batch operations yield nonuniform product.	Where much heat is involved large temperature gradients occur.	Must be fairly large and uniform. With poor temperature control these may sinter and clog the reactor.	Because of large particle size pressure drop is not a serious problem.	Inefficient exchange, hence large exchanger surface needed. This is often the limiting factor in scale-up.	With plug flow of gas and proper temperature control (which is difficult) close to 100% of the theoretical conversion is possible.
Moving Bed	For large granular rapidly deactivated catalyst. Fairly large-scale operations possible.	For fairly uniform sized feed with little or no fines. Large-scale operations possible.	Temperature gradients can be controlled by proper gas flow or can be minimized with sufficiently large solid circulation.	Fairly large and uniform; top size fixed by the velocities of the solid recirculation system, bottom size by the fluidizing velocity in reactor.	Intermediate between fixed and fluidized beds	Inefficient exchange but because of high heat capacity of solids, the heat transported by circulating solids can be fairly large.	Flexible and close to ideal countercurrent and cocurrent contacting allows close to 100% of the theoretical conversion.
Bubbling and Turbulent Fluidized Bed	For small granular or powdery nonfriable catalyst. Can handle rapid deactivation of solids. Excellent temperature control allows large-scale operations.	Can use wide range of solids with much fines. Large-scale operations at uniform temperature possible. Excellent for continuous operations, yielding a uniform product.	Temperature is almost constant throughout. This is controlled by heat exchange or by proper continuous feed and removal of solids.	Wide size distribution and much fines possible. Erosion of vessel and pipelines, attrition of particles and their entrainment may be serious.	For deep beds pressure drop is high, resulting in large power consumption.	Efficient heat exchange and large heat transport by circulating solids so that heat problems are seldom limiting in scale-up.	For continuous operations, mixing of solids and gas bypassing result in poorer performance than other reactor types. For high conversion, staging or other special design is necessary.
Fast Fluidized Bed and Cocurrent Pneumatic Transport	Suitable for rapid reactions. Attrition of catalyst is serious.	Suitable for rapid reactions. Recirculation of fines is crucial.	Temperature gradients in direction of solids flow can be minimized by sufficient circulation of solid.	Fine solids top size governed by minimum transport velocity. Severe equipment erosion and particle attrition.	Low for fine particles, but can be considerable for larger particles.	Intermediate between fluidized and moving bed.	Flow of gas and solid both close to cocurrent plug flow, hence high conversion possible.
Rotary Cylinder (Kiln)	Not used	Widely used, suitable for solids which may sinter or agglomerate.	Temperature gradients in direction of solids flow may be severe and difficult to control.	Any size, from fines to large lumps	Very low	Poor exchange, hence very long cylinders often needed.	Close to countercurrent plug flows, hence conversions can be high.
Flat Hearth	Not used	Suitable for solids liable to sinter or melt.	Temperature gradients are severe and difficult to control.	Both big and small	Very low	Poor exchange	Fair, scrapers or agitators are needed.

Figure A.1: comparison of types of contacting for reaction gas-solid systems [13]

Appendix B

Effect of Using Different Column Heights

The effect Is analyzed by comparing two simulations, which are performed with the 0.63 m long column and the 1.0 m long column. The residence time of the bubbles, the expansion of the particle bed and the bubble appearance are compared.

B.1 Residence Time Analysis

Residence time (time taken by the bubbles to reach to the top) data extracted from the two simulations are presented in the table below. Eleven bubbles are appeared in the bed for a period of 2 s and ten of those are managed to reach to the top of the particle bed in both cases. Only the second bubble dispersed in to the bed without reaching the top.

.

Bubble Number	Time taken for reach to the top (s)	
	With old height	With new height
1	6.9	6.9
2	-	-
3	8.7	8.7
4	1.02	1.02
5	1.2	1.2
6	1.4	1.38
7	1.48	1.46
8	1.64	1.64
9	1.75	1.75
10	1.95	1.95
11	2.0	1.97

.

.

From the residence time it is noticeable that most of the bubbles have the same residence time in both simulations. Even if there are deviations between two simulations those are negligible.

B.2 Bed Height and Bubble Position Comparison

At the residence time comparison the 6^{th}, 7^{th} and 11^{th} bubbles showed higher residence times in the simulation with $0.63m$ column. That can be due to the reversed flow. Which means that the dynamics of the bed may slows down when the reversed flow is present, and achieves normal conditions after the forward flow established again. The reason would be the backward force acting on the solids and air due to the reversed flow. But still the difference between the residence times are very small ($\approx 20 - 30\ ms$) and can be neglected.

The purpose of this analysis is to compare the position of a common bubble at a specified time instance among the two simulations. This can be used to confirm the findings from the residence time analysis. In addition to that the bed height is also compared. That is because the bed height is an important factor when simulating the fluidized beds. Contours of the solid phase were compared at the time instances 630, 870 and 2000 ms. Contours are presented in the Figure B.1.

Figure B.1 shows that the two simulations give all most the same results at the time instances 630 ms and 870 ms. Some difference is visible at 2 s. It shows that the simulation with higher column has faster dynamics when it is about $2s$. As both simulations have given all most the same bed height the result of both simulations are acceptable as the bed height is more important than the bubble velocity.

The residence time, bed expansion and bubble position analysis show that there is a slight effect from the reversed flow to the results of a simulation. But the results from a simulation which experienced reversed flow is acceptable as the effect is not too high. That means the simulations used 0.63 m high column can also used in the analysis of finalizing the combined model for simulating the bubbling fluidized beds.

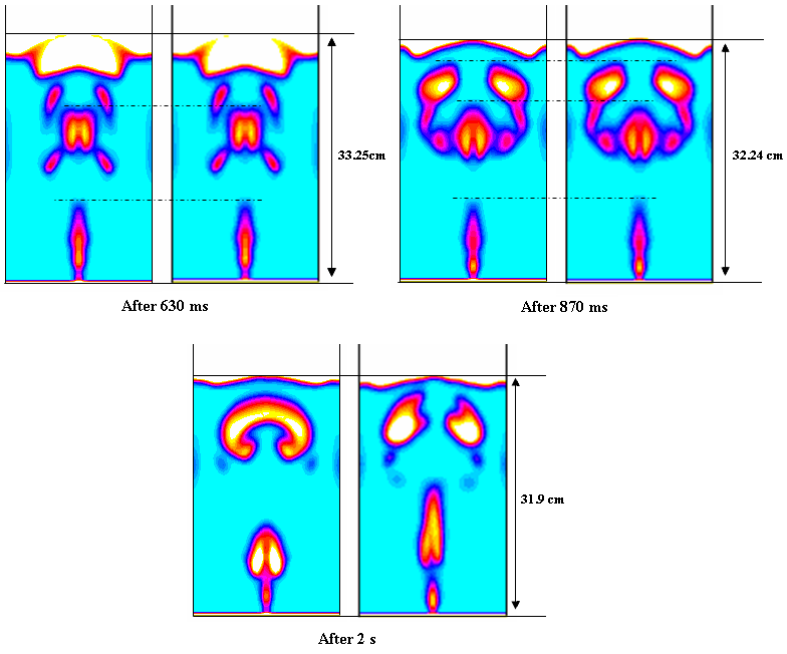

Figure B.1: Comparison of contours from the simulations with different column heights

Appendix C

Effect of Using Different FLUENT Versions

A simulation used FLUENT 6.3 version has used the model "Based-ktgf" for the frictional pressure and "derived" option for frictional modulus. Results from the simulation are compared with another simulation that was done with the FLUENT 6.2 version. All other conditions were the same for both simulations. Simulation with 6.2 version is named as "simulation a1" and the simulation with 6.3 version is named as "simulation a2". Some contours are extracted from the simulations and presented in the Figure C.1 as an aid for the comparison.

Bubbles to be compared are marked in the figure using dotted lined shapes. Common bubbles have joined using double ended arrows. From the Figures C.1-(a) and C.1-(b) it is possible to see that both simulations have given similar number of bubbles and similar bed heights. Also from the Figures C.1-(c) it is possible to see that even though the bubble position is not the same, both simulations give similar bed heights in all time instances. Simulation a2 has given better shaped bubbles compared to simulation a1.

For further evidence, the number of clear bubbles raised within 2 s in the particle bed of both simulations were counted. The simulation a1 has got 13 bubbles and the simulation a2 has got 12 bubbles. But still it is possible to conclude that the results with the 6.2 version is also fair enough to use as it has given similar bed heights and almost the same bubble prediction.

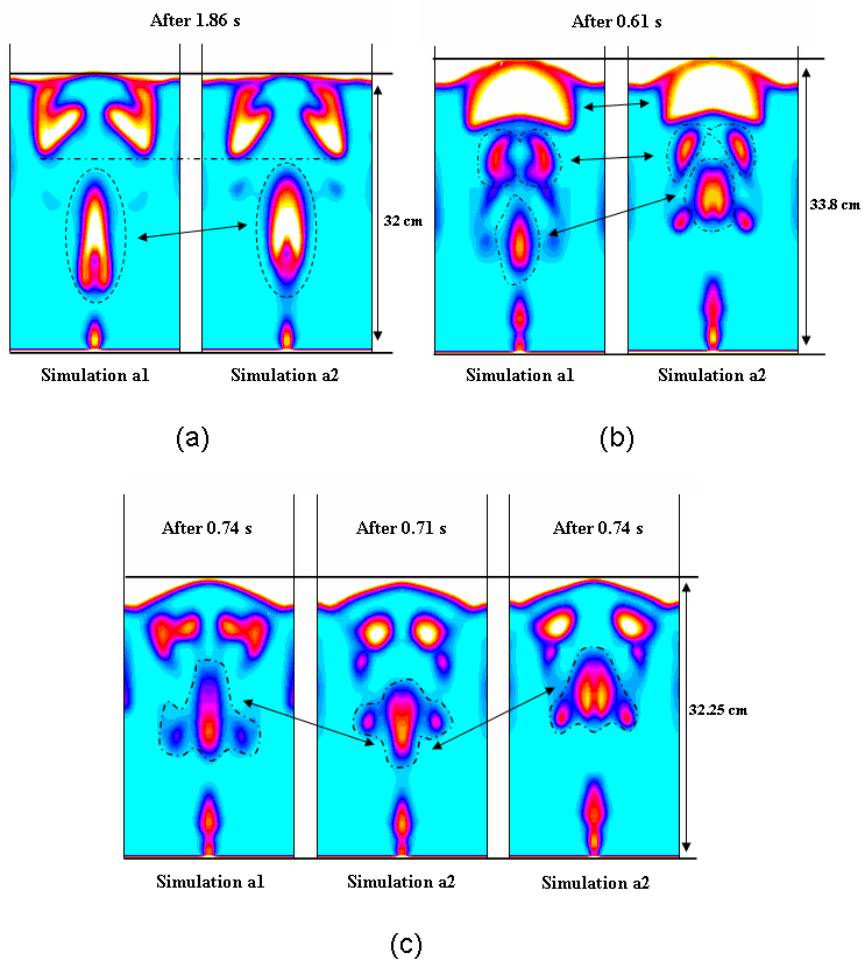

Figure C.1: Comparison of the simulated results using the FLUNT version 6.3 and FLUNT version 6.2

Appendix D

Particle Sampling for the Analysis

It is important to get an idea about the mean particle diameters, and particle distributions of the particle types used in the reference experiment. The mean particle diameter is used in simulations to present the particle phase. The particle are measured and the range of particle diameters and the mean particle diameters are calculated.

D.1 Particle Size Calculation

The shape of the particles are very much of importance when the diameter is to be calculated. It is easier with the spherical particles but a little more work with non spherical particles. When the particles are non spherical, a parameter called sphericity can be used to find the correct size of the particles when the equivalent diameters such as "equivalent spherical diameter" is known.

The parameter sphericity is defined as follow,

$$sphericity = \phi_s = \left(\frac{\text{surface of sphere}}{\text{surface of particle}} \right)_{\text{of the same volume}}$$

According to the above definition, $\phi_s = 1$ for spheres and $0 < \phi_s < 1$ for any other particle shape. Sphericity values for different particle shapes can normally be found in literature.

If the particle size can be measured at least by a representative spherical diameter, d_{sph}, that means a sphere which has the same volume as the required particle, then a bed of required, non spherical particles can be represented with an effective particle size, d_{eff}.

$$d_{eff} = \phi_s * d_{sph} \tag{D.1}$$

In that method a bed of non spherical particles can be represented by a bed of spherical particles which have the effective diameter of the required diameter of the particles such as both beds have the same total surface area and same frictional voidage. The challenge is to measure the particle size and the measuring method can also vary with the particle size range, that means, whether those are large particles ($> 1\ \mu m$), intermediate particles and small particles.

D.1.1 Large Particles

The particle size of the larger particles can be measured using calipers or micrometers if the particles are regular in shape. If not the volume can find by weighing a sample of the particles if the density is known. Also, can use the displacement of fluid by a sample of particles and find the volume of the particles to calculate the diameter if the particles are non-porous. With use of the above mentioned methods the equivalent spherical diameter can be calculated and then the eq. D.1 can be used to calculate the effective particle diameter.

D.1.2 Intermediate Particles

The most convenient method to measure the particle sizes of the intermediate particles is to use calibrated sieves. Numerous number of calibrated sieves are available. Size of a particle which goes through one sieve and stays on the next sieve can find as an average of the sizes of the sieves.

Example 1

Mesh no:	*Aperture (μm)*
1	*104*
2	*74*

The particle size of the particle which passes trough the sieve no:1and stays on the sieve no:2 can be calculated as shown below,

$$d_p = \frac{104 + 74}{2} = 89 \mu m \tag{D.2}$$

The results from a sieve analysis can plot (normally gives a standard deviation) with the average diameters of the particles stays on each sieve. The mean particle diameter can read from the plot.

D.1.3 Very Small Particles

For the particles smaller than 40 μm sieve analysis cannot be used. In order to find the particle sizes of those, some other methods can be used, like scanning a magnified photograph of the required particles. Also there is an other bit complex method too. In that method, the equivalent spherical diameter can be found with use of the terminal settling velocity of the particles by using the sedimentation of particles in a known fluid.

D.2 Mean Particle Diameters of the Particles Used in the Experiment

The particle types used in the reference experiment are in the range of medium size particles. Three different particle size ranges are included in the interested particle types. Those are spherical particles in the size range of 750-1000 μm, 400-600 μm and 100-200 μm. A sieve analysis is performed to find the mean particle diameters of the particle types which are to be analyzed by the simulations. The results of the screen analysis has given below,

.

.

Sieve no:	Mass on the screens		
(μm)	(g)		
-	750-1000	400-600	100-200
< 63	-	-	0,09
63	-	-	9,44
106	-	-	42,17
150	-	-	46,16
200	-	-	2,12
250	-	-	0,01
< 300	-	0,35	-
300	-	2,45	-
355	-	22,56	-
425	-	47,68	-
< 500	0.03	-	-
500	0.02	26,77	-
630	0.04	0,31	-
710	24.12	-	-
850	64.3	-	-
1000	11.58	-	-

.

.

(- = not applicable)

The analysis is carried out using the mean diameters calculated according to the mean size calculation for sieves using the eq. D.2.

D.2.1 For the Particles in the Range of 100-200 μm

The mean sizes of the particles for each sieve and the weight of the particles on each sieve are analyzed in order to get the mean particle diameter of the particle group.

.

.

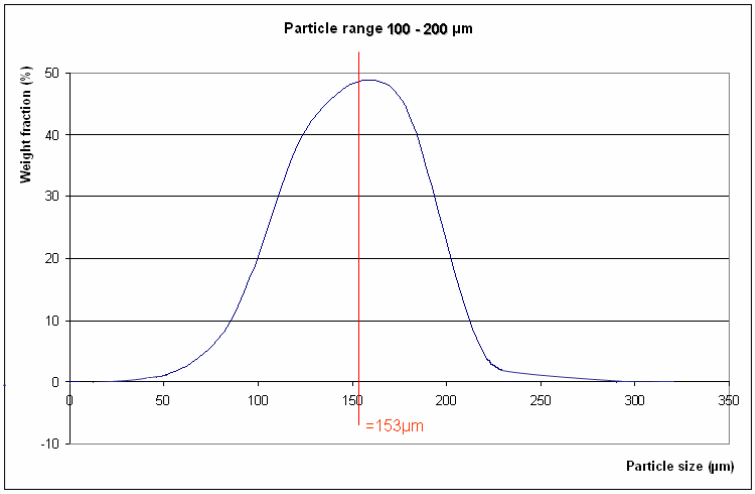

Figure D.1: Extraction of the mean diameter from the particle size distribution of the sample of particles which is in the range 100 - 200 μm

Average Screen size (μm)	Mass on the screens (g)
40	0,09
84.5	9,44
128	42,17
175	46,16
225	2,12
300	0,01

.

.

The deviation of the particle diameter is presented in the Figure D.1 and the mean diameter is extracted. The line in the center of the plot represents the mean diameter.

D.2.2 For the Particles in the Range of 400-600 μm

Same steps as in the above mean diameter calculation are used.

.

.

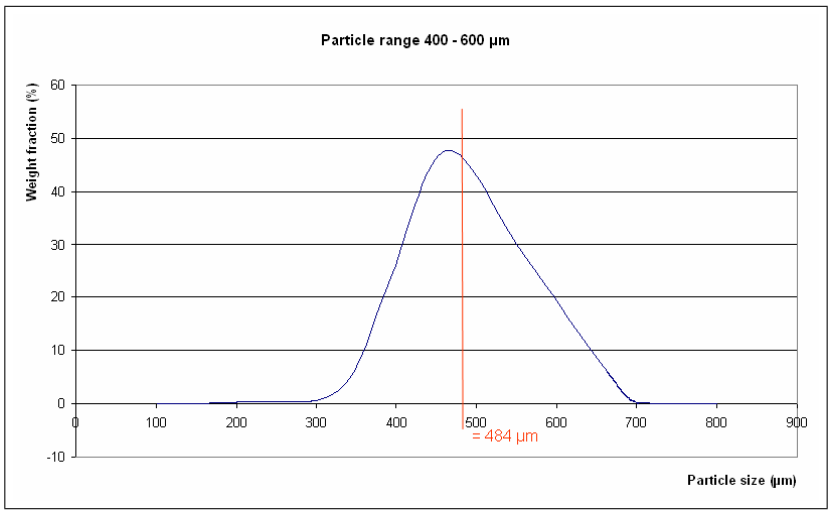

Figure D.2: Extraction of the mean diameter from the particle size distribution of the sample of particles which is in the range 400 - 600 μm

Average Screen size	Mass on the screens
(μm)	(g)
200	0.35
327.5	2.45
390	22.56
462.5	47.68
565	26.77
700	0.31

.

.

Mean Diameter is found by doing the same as mentioned above and presented in the Figure D.2.

D.2.3 For the Particles in the Range of 750 - 1000 μm

Same method as above subsections is followed.

.

.

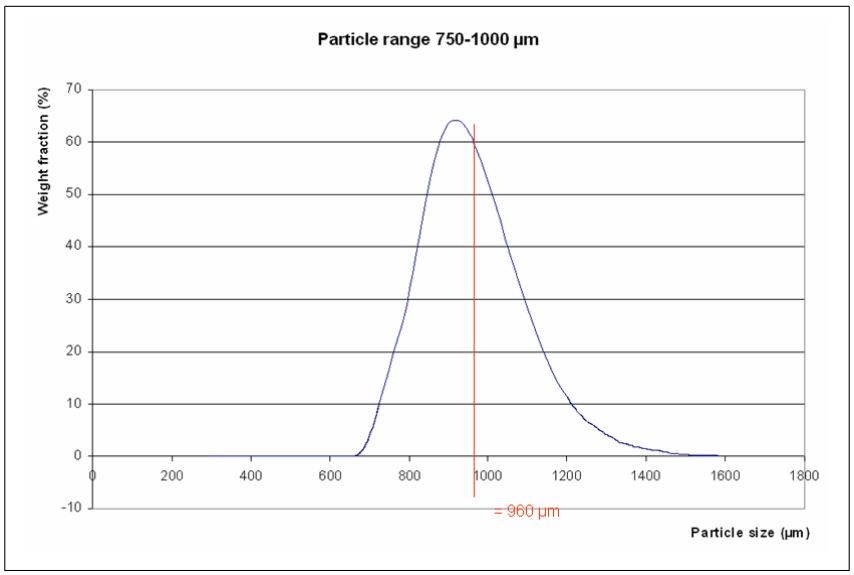

Figure D.3: Extraction of the mean diameter from the particle size distribution of the sample of particles which is in the range 750 - 1000 μm

Average Screen size (μm)	Mass on the screens (g)
400	0.03
565	0.02
670	0.04
780	24.10
925	64.24
1200	11.57

.

.

Mean Diameter is found by doing the same as mentioned above and presented in the Figure D.3.

The summery of the above analysis is given below.

.

Particle size range	100 - 200 μm	400 - 600 μm	750 - 1000 μm
Mean diameter	153 μm	484 μm	960 μm

.

After reading out all the values for mean particle diameters the theoretical values for the minimum fluidization velocity can be calculated using the those diameter values.

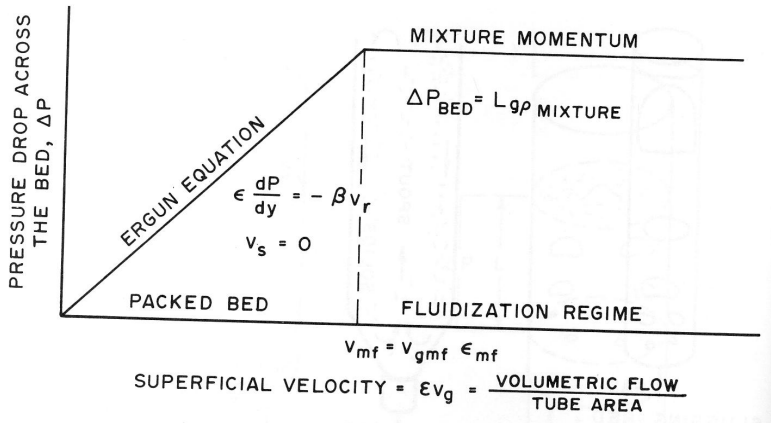

Figure D.4: Diagram for determination of minimum fluidization velocity [9]

D.3 Calculation of U_{mf} Theoretically

Calculation of the U_{mf} theoretically could be done either using a graphical method or numerical calculation. U_{mf} can be found from the intersection of the pressure drop versus the spherical velocity curve and the pressure drop equals the weight of the bed line [9], see Figure D.4.

Wong A.C.Y [22] shows that it is more realistic to predict the minimum fluidization velocities depending on the angle of repose. But in this study the minimum fluidization velocity is calculated numerically by using some extensions of the conservation equations. In those equations the gas-wall friction and solid stress transmitted by the particles have neglected so that the buoyancy equals the drag at the minimum fluidization conditions. Also it has taken in to consideration the fact that the velocity of solids is zero at the minimum fluidization.

In general, for isotropic-shaped solids the following relation gives a quadratic in U_{mf} [15].

$$\frac{1.75}{\varepsilon_{mf}^3 \phi_s}\left(\frac{d_p U_{mf}\rho_g}{\mu}\right)^2 + \frac{150\,(1-\varepsilon_{mf})}{\varepsilon_{mf}^3 \phi_s^2}\left(\frac{d_p U_{mf}\rho_g}{\mu}\right) = \frac{d_p^3 \rho_g\left(\rho_s - \rho_g\right) g}{\mu^2} \quad \text{(D.3)}$$

In spherical case for small particles, eq. D.3 can be re-written as,

$$U_{mf} = \varepsilon_{mf} * v_{mf} = \frac{d_p^2 * \Delta\rho * g}{150 * \mu_g}\left(\frac{\phi_s^2 * \varepsilon_{mf}^3}{1-\varepsilon_{mf}}\right) \quad \text{(D.4)}$$

For spherical particles of uniform size it is not unreasonable to expect the porosity at the minimum fluidization to be close to the porosity of a bed packed with spheres in a cubic mode, with $\varepsilon_{mf} = 1 - \frac{\pi}{6} = 0.476$ [9]

Eq. D.4 can be further simplified for small particles [9],

$$\left(\frac{\phi_s^2 * \varepsilon_{mf}^3}{1-\varepsilon_{mf}}\right) \cong \frac{1}{11}$$

$$\therefore \quad U_{mf} = \frac{d_p^2 * \left(\rho_s - \rho_g\right) * g}{1650 * \mu_g}, \ \mathrm{Re}_{mf} < 20 \tag{D.5}$$

In this study the analytical method has used in order to calculate the minimum fluidization velocities of the above mentioned particle groups. Those tree groups are introduced as small. medium and large accordingly from the smallest to largest particle size respectively. Densities of the glass particles and gas are known as $2485 kg/m^3$ and $1.2 kg/m^3$ respectively. The viscosity of gas is known as $1.8 * 10^{-5} Pa.s$

D.3.1 U_{mf} for Small Particles

Particle mean diameter = 153 μm

Using the eq. D.5 ;

$$U_{mf} = \frac{\left(153 * 10^{-6}\right)^2 * (2485 - 1.2) * 9.81}{1650 * 1.8 * 10^{-5}} = 1.920\,5 \times 10^{-2} ms^{-1}$$

Have to check whether the Reynolds number of the flow is in the required value region in order to be able to use eq. D.5 for calculating the minimum fluidization velocity.

$$\mathrm{Re} = \frac{\rho * U * d}{\mu} = \frac{1.2 * 1.920\,5 \times 10^{-2} * 153 * 10^{-6}}{1.8 * 10^{-5}} = 0.195\,89$$

Re number has a value which is well bellow the limit.

$\therefore$ The theoretical $U_{mf} = 1.920\,5 \times 10^{-2} ms^{-1}$

D.3.2 U_{mf} for Medium Size Particles

Particle mean diameter = 484 μm

Using the eq. D.5 ;

$$U_{mf} = \frac{\left(484 * 10^{-6}\right)^2 * (2485 - 1.2) * 9.81}{1650 * 1.8 * 10^{-5}} = 0.192\,19 ms^{-1}$$

Have to check whether the Reynolds number of the flow is in the required value region in order to be able to use eq. D.5 for calculating the minimum fluidization velocity.

$$\mathrm{Re} = \frac{\rho * U * d}{\mu} = \frac{1.2 * 0.192\,19 * 484 * 10^{-6}}{1.8 * 10^{-5}} = 6.201\,3$$

Re number has a value which is well bellow the limit.

$\therefore$ The theoretical $U_{mf} = 0.192\,19 ms^{-1}$

For the Simulation Used in the Part 1

The simulation in part 1 used particles with 491 μm of mean particle size. The U_{mf} of the glass particles with 491 μm mean particle diameter is also calculated.

Particle mean diameter = 491 μm

Using the eq. D.5 ;

$$U_{mf} = \frac{\left(491 * 10^{-6}\right)^2 * (2485 - 1.2) * 9.81}{1650 * 1.8 * 10^{-5}} = 0.197\,78 ms^{-1}$$

Have to check whether the Reynolds number of the flow is in the required value region in order to be able to use eq. D.5 for calculating the minimum fluidization velocity.

$$\mathrm{Re} = \frac{\rho * U * d}{\mu} = \frac{1.2 * 0.197\,78 * 153 * 10^{-6}}{1.8 * 10^{-5}} = 2.\,017\,4$$

Re number has a value which is well bellow the limit.

$\therefore$ The theoretical $U_{mf} = 0.197\,78\ ms^{-1}$

D.3.3 Large Particles

Particle mean diameter = 960 μm

Using the following relation for U_{mf};

$$U_{mf} = \frac{\left(960 * 10^{-6}\right)^2 * (2485 - 1.2) * 9.81}{1650 * 1.8 * 10^{-5}} = 0.756\,09 ms^{-1}$$

Have to check whether the Reynolds number of the flow is in the required value region in order to be able to use eq. D.5 for calculating the minimum fluidization velocity.

$$\mathrm{Re} = \frac{\rho * U * d}{\mu} = \frac{1.2 * 0.756\,09 * 960 * 10^{-6}}{1.8 * 10^{-5}} = 48.\,390$$

Re number has a value which is out of range, so have to do the calculation using an other suitable equation. Eq. D.3 is used for the calculation of U_{mf} for this particle group.

$$\begin{aligned} & \frac{1.75}{0.476^3}\left(\frac{960 * 10^{-6} * U_{mf} * 1.2}{1.8 * 10^{-5}}\right)^2 + \frac{150 * (1 - 0.476)}{0.476^3}\left(\frac{960 * 10^{-6} * U_{mf} * 1.2}{1.8 * 10^{-5}}\right) \\ = & \frac{\left(960 * 10^{-6}\right)^3 * 1.2 * (2485 - 1.2) * 9.81}{\left(1.8 * 10^{-5}\right)^2} \\ & 46642.U_{fm} + 66463.U_{fm}^2 = 79843 \end{aligned}$$

Solution for the above quadratic equation has two values, $-1.\,501\,7,\ 0.799\,95$. As the negative value can not be accepted as the minimum fluidization velocity of the particles, the positive value is selected as the U_{mf} value.

$\therefore$ The theoretical $U_{mf} = 0.799\,95 ms^{-1}$

D.4 Mixture Properties

U_{mf} of the particle mixture used in the simulations performed to check the influence of particle size distribution is to be calculated. The mixture consists of the following compositions of small, medium and large particles.

mixture = 100 - 200 : 29%
400 - 600 : 50%
750 - 1000 : 21%

Using the mixture composition data the mean particle diameters and the corresponding minimum fluidization velocities for the mixture can be calculated as shown below.

D.4.1 Mean Particle Diameter

$D_{m1} = (153 * 0.29) + (484 * 0.5) + (960 * 0.21) = 487.97\ \mu m$

D.4.2 U_{mf} Theoretical

Particle mean diameter = 487.97 μm (Geldart B)
shape = Spherical , $\phi = 1$ and $\varepsilon_{mf} = (1 - \pi/6) = 0.476$
Using the following relation for U_{mf};

$$U_{mf} = \varepsilon_f * V_{mf} = \frac{d_p^2 * \Delta\rho * g}{150 * \mu} \left(\frac{\phi_s^2 * \varepsilon_{mf}^3}{1 - \varepsilon_{mf}} \right),$$

$$where \quad \left(\frac{\phi_s^2 * \varepsilon_{mf}^3}{1 - \varepsilon_{mf}} \right) = \frac{1}{11}$$

$$\therefore \quad U_{mf} = \frac{\left(487.97 * 10^{-6}\right)^2 * (2485 - 1.2) * 9.81}{150 * 1.8 * 10^{-5}} * \frac{1}{11} = 0.195\,35$$

Have to check whether the Reynolds number of the flow is in the required value region in order to be able to use the above equation to calculate the minimum fluidization velocity.

$$\mathrm{Re} = \frac{\rho * U * d}{\mu} = \frac{1.2 * 0.195\,35 * 489.01 * 10^{-6}}{1.8 * 10^{-5}} = 6.368\,5$$

This value is well beyond the limit. $\therefore$ The theoretical $U_{mf} = 0.195\,35 ms^{-1}$

Appendix E

Average VOF Values at Different Heights of the Bed

VOF of each particle phase are plotted at three height levels of the bed. All VOF values are averaged for the last 25 seconds of the simulation and the plots are presented below for the simulations P3, P4 and P5.

E.1 Simulation P3

Figures E.1 and E.2 provides the VOF behavior of small and large particle phases with the height of the particle bed.

E.2 Simulation P4

Figures E.3, E.4 and E.5 present the behavior of VOF of the small, medium and large particle phases with the height of the particle bed.

E.3 Simulation P5

Figures E.6, E.7, E.8 and E.9 present the VOF behavior of the four particle phases (small, medium phase 1, medium phase 2, large) used in the simulation along with the height of the particle bed.

Figure E.1 and E.2, the plots of VOF of small and large particle phases from the simulation P3, the small particle phase have higher VOF at higher positions and large particle phase have higher VOF at lower positions. Figure E.3, E.4 and E.5, the plots of medium and large particle phases of the simulation P4, show that the small and large particle phases have the same tendency as in the above cases. The plots of medium particles show that the medium size particles also behaves in a similar way to the large particles and give highest VOF at the lowest position. That behavior is predictable as the medium particles are very

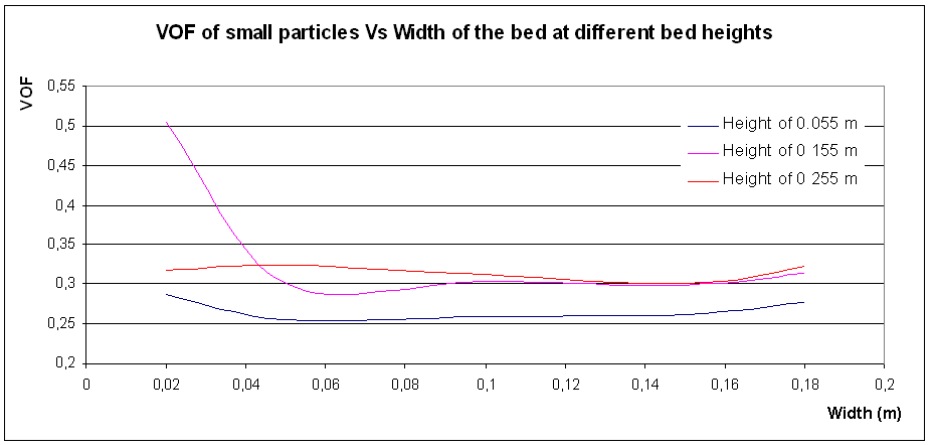

Figure E.1: VOF of small particles as a fuction of the width of the bed at different levels in the particle bed, predicted by the simulation P3

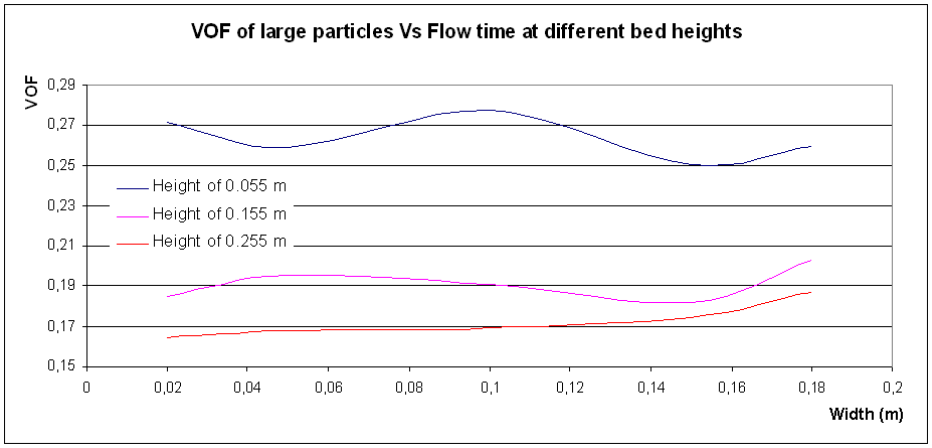

Figure E.2: VOF of large particles as a fuction of the width of the bed at different levels in the particle bed, predicted by the simulation P3

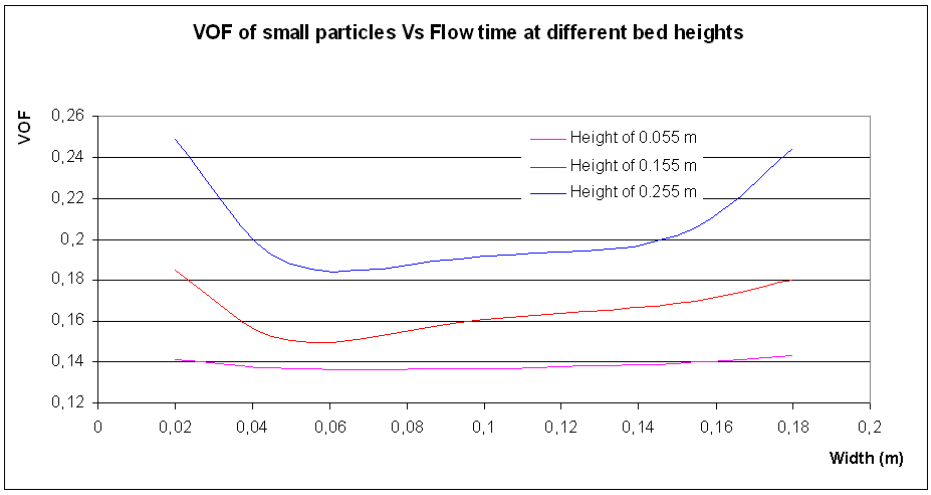

Figure E.3: VOF of small particles as a fuction of the width of the bed at different levels in the particle bed, predicted by the simulation P4

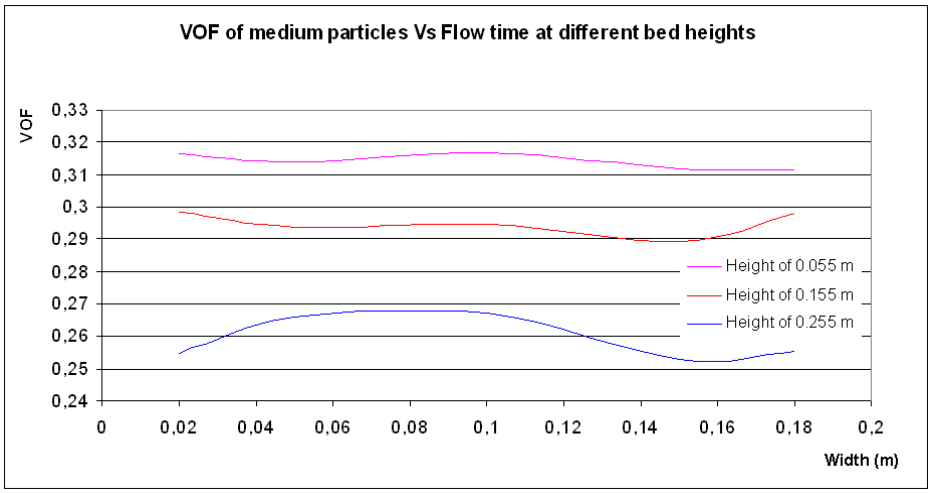

Figure E.4: VOF of medium particles as a fuction of the width of the bed at different levels in the particle bed, predicted by the simulation P4

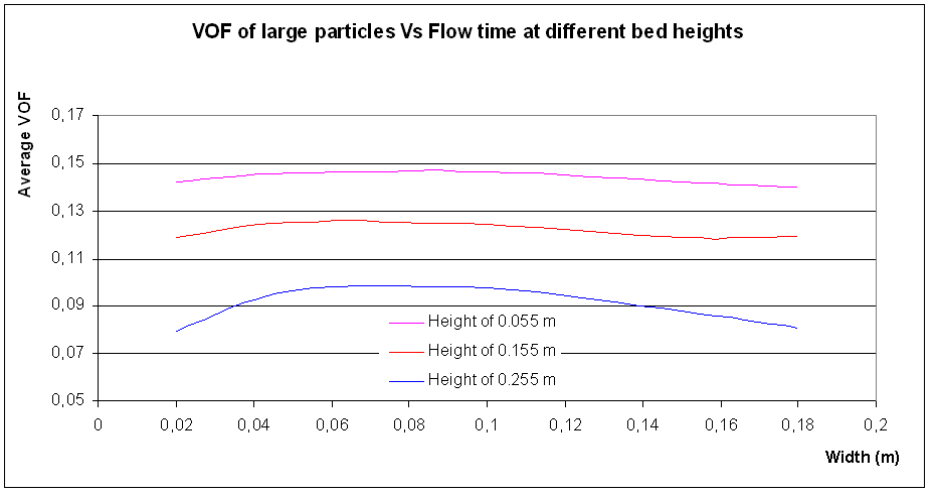

Figure E.5: VOF of large particles as a fuction of the width of the bed at different levels in the particle bed, predicted by the simulation P4

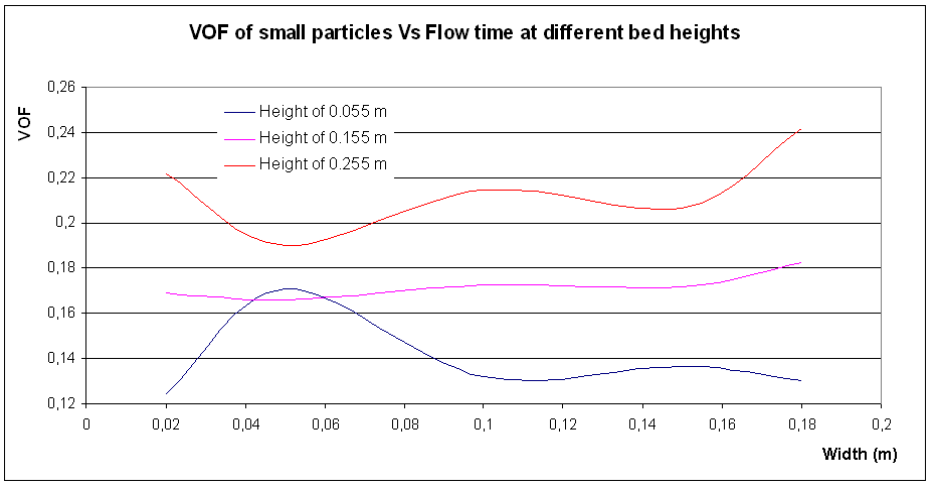

Figure E.6: VOF of small particles as a fuction of the width of the bed at different levels in the particle bed, predicted by the simulation P5

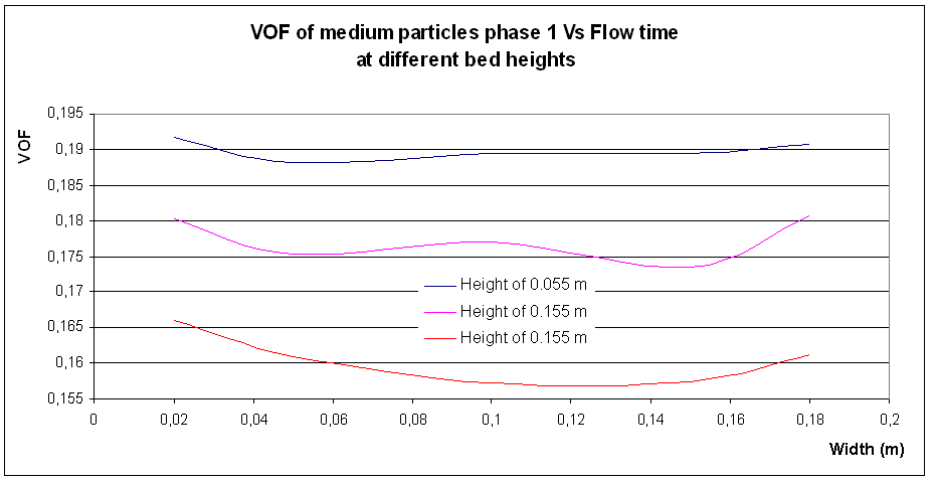

Figure E.7: VOF of small portion of the medium particles as a fuction of the width of the bed at different levels in the particle bed, predicted by the simulation P5

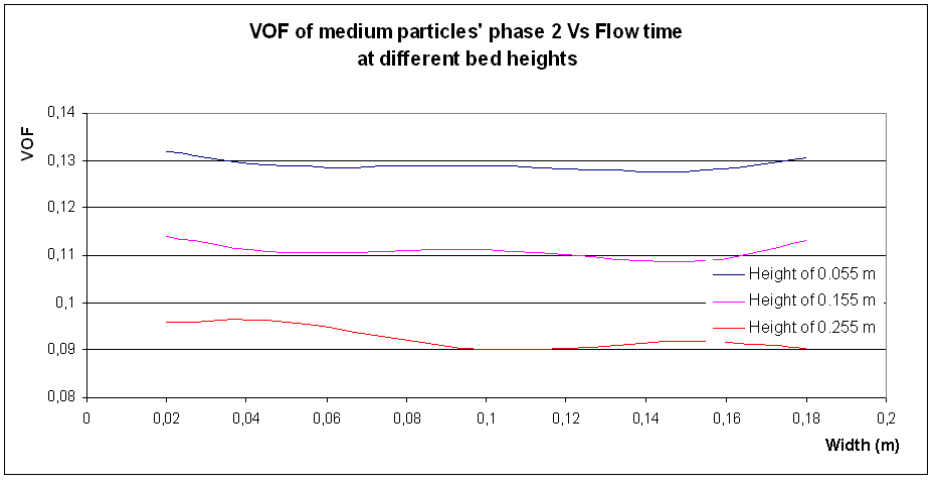

Figure E.8: VOF of large portion of the medium particles as a fuction of the width of the bed at different levels in the particle bed, predicted by the simulation P5

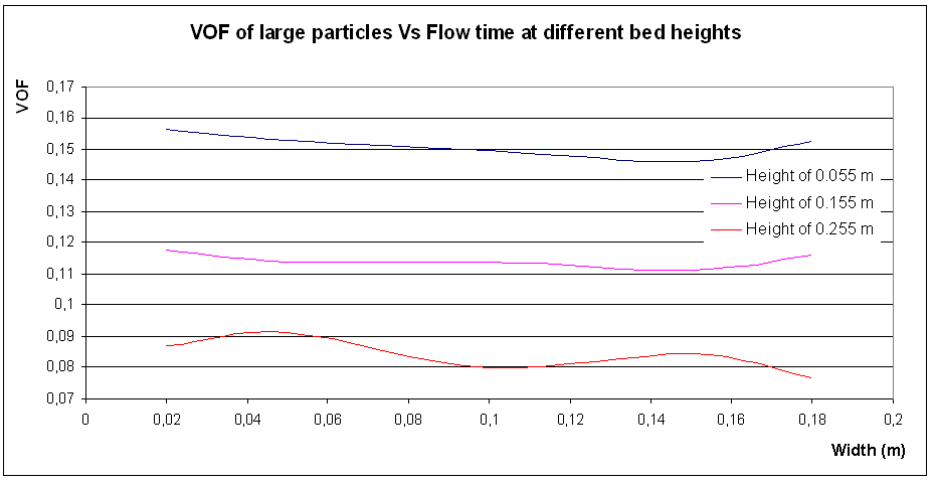

Figure E.9: VOF of large particles as a fuction of the width of the bed at different levels in the particle bed, predicted by the simulation P5

much larger in size than the smaller particles in the mixture when the mean particle diameter is considered. Figure E.6, E.7, E.8 and E.9, plots of the four particle phases available with the simulation P5, shows the tendency of small particles to accumulate at the top of the bed and the tendency of the other particle phases to accumulate closer to the bottom of the bed.

Appendix F

VOF of Particles Along the Bed Height

VOF of each particle phase are plotted at two radial distance levels from the column walls. One position is close to a wall (0.05 away a wall) and the other position is in the center of the column. It is assumed that analysis of only one side of the bed cross section is enough eventhough the behavior of both sides are not exactly the same all the time. VOF values are averaged for the last 25 seconds of the simulations and the plots are presented below for the simulations P2 and P4.

F.1 Positions Close to the Walls

Depending on the assumption of symmetry of the bed only one side has analyzed. Simulation P2 has used a vertical line 0.05 m away from the left wall and the simulation P4 had used a vertical line 0.15 m away from the left wall for the analysis. Those plots are presented in the Figures F.1 and no: F.2.

F.2 Positions at the Middle of the Bed

A vertical line, 0.1 m away from the walls has analyzed in both simulations P2 and P4 and presented in the following Figures F.3 and no: F.4.

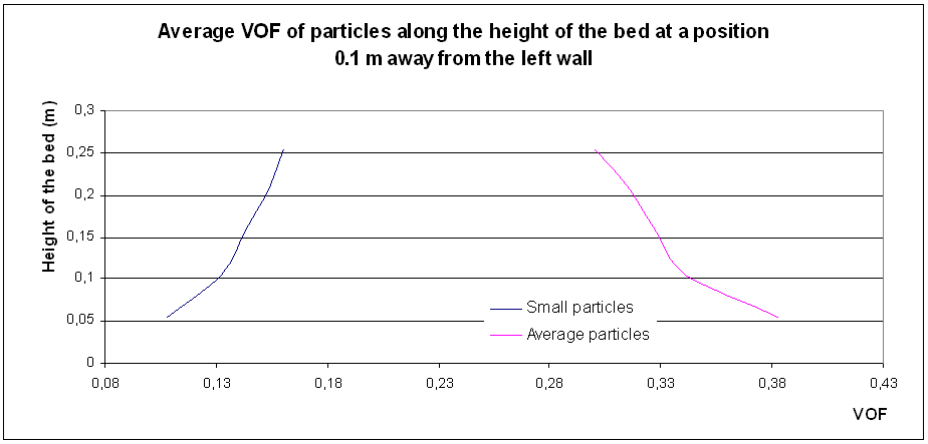

Figure F.1: VOF of the particles phases along the height of the bed at a position 0.05 m away from the wall predicted by the simulation P2

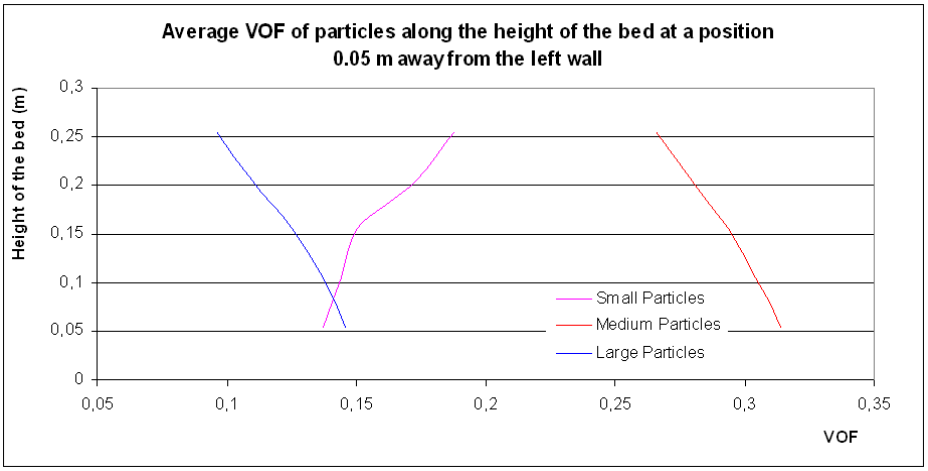

Figure F.2: VOF of the particles phases along the height of the bed at a position 0.05 m away from the wall predicted by the simulation P4

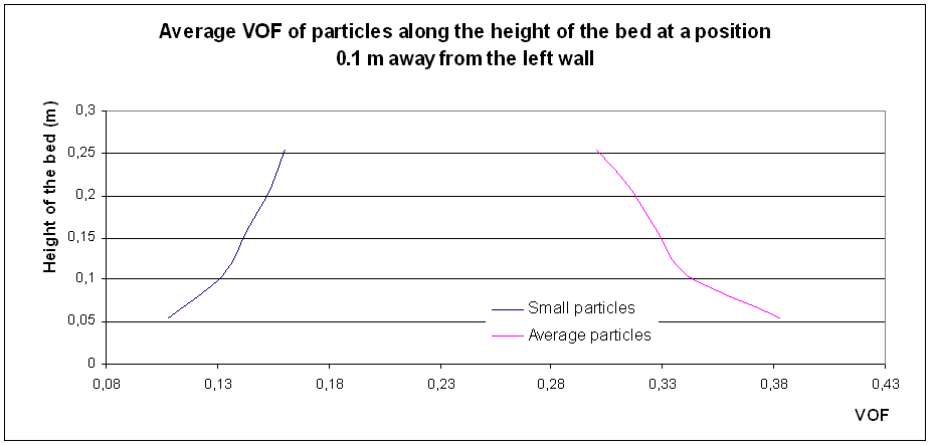

Figure F.3: VOF of the particles phases along the height of the bed at a position 0.1 m away from the wall predicted by the simulation P2

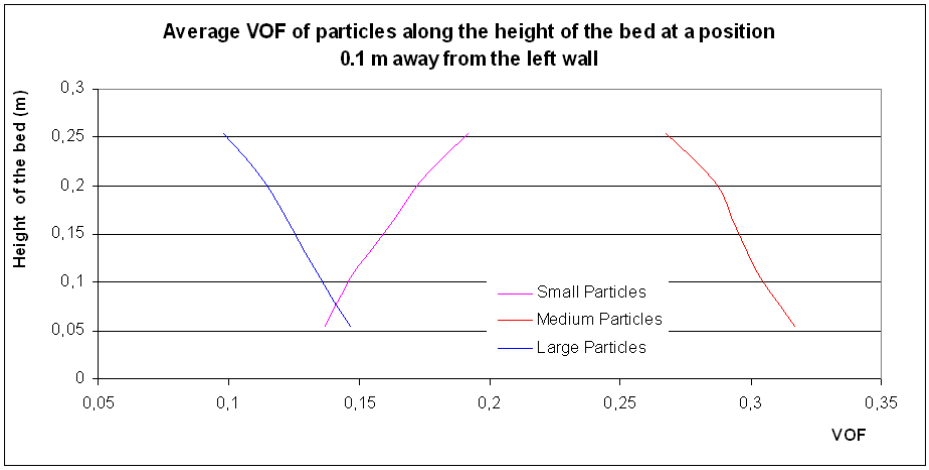

Figure F.4: VOF of the particles phases along the height of the bed at a position 0.1 m away from the wall predicted by the simulation P4

Appendix G

Progress of Particle Segregation

The progress of particle segregation in the four simulations are analyzed. Progress is tracked at two selected radial positions (one close to the wall and one in the center) and two selected points (one close to the top and one close to the bottom) of the particle bed. VOF data of all particle phases are averaged at each 3 seconds of the simulation.

G.1 Progress at Radial Positions

Progress of particle segregation in the simulations with time has analyzed. The simulation time domain is has divided in to 10 intervals and the averaged VOF at each interval for each phase is plotted. It is clear that not all the curves in the plots are smooth, and because of that few curves have selected from the original plots and those curves are presented in a separate plot to exhibit the particle segregation with time. Plots from each simulation has presented separately.

G.1.1 Simulation P2

Figures G.1, G.2 and G.3 shows the selected curves to present the progress of particle segregation.

G.1.2 Simulation P3

Figures G.4, G.5 and G.6 shows the selected curves to present the progress of particle segregation. Small particles at central area couldn't presented as a clear plot as the curves were not showing a pattern at all.

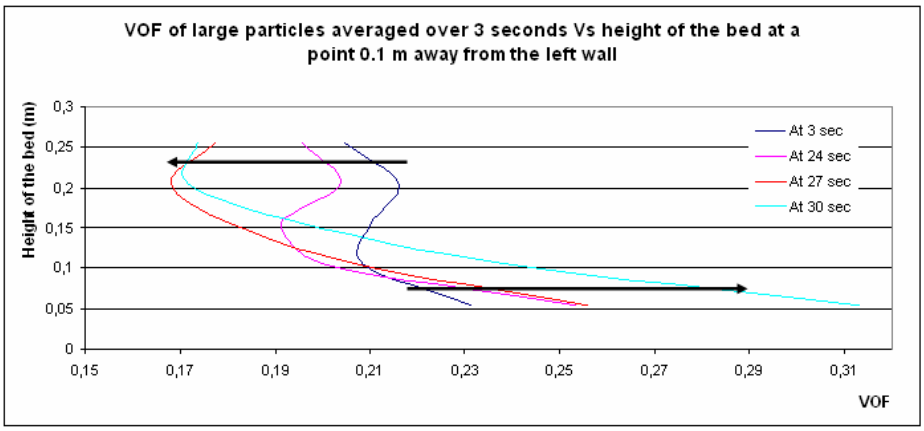

Figure G.1: Progree of particle segregation along the height of the bed at a radial position 0.1 m away from a wall with respect to the small particles in the simulation P2

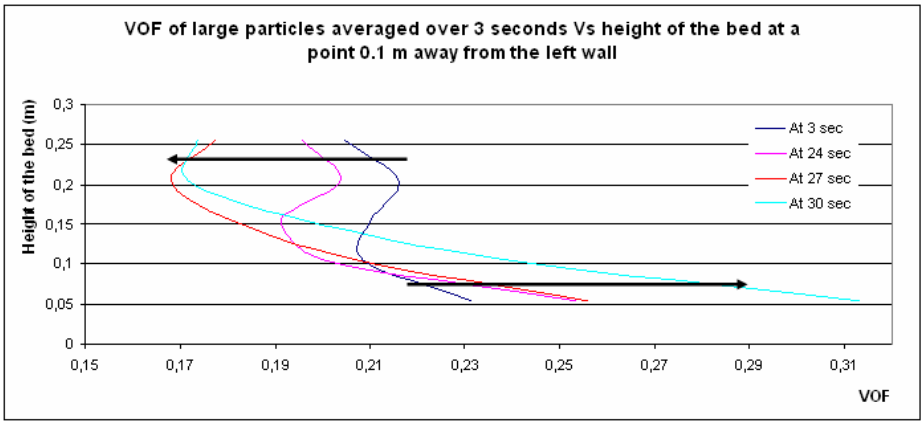

Figure G.2: Progree of particle segregation along the height of the bed at a radial position 0.05 m away from a wall with respect to the average particles in the simulation P2

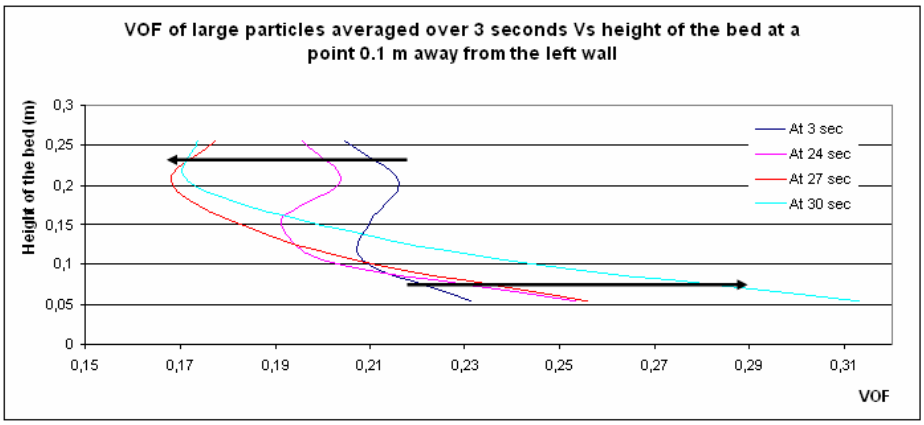

Figure G.3: Progree of particle segregation along the height of the bed at a radial position 0.1 m away from a wall with respect to the average particles in the simulation P2

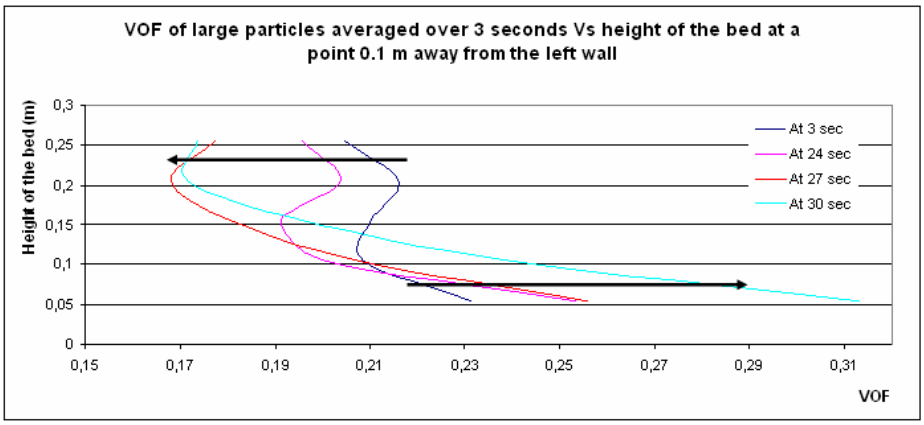

Figure G.4: Progree of particle segregation along the height of the bed at a radial position 0.05 m away from a wall with respect to the small particles in the simulation P3

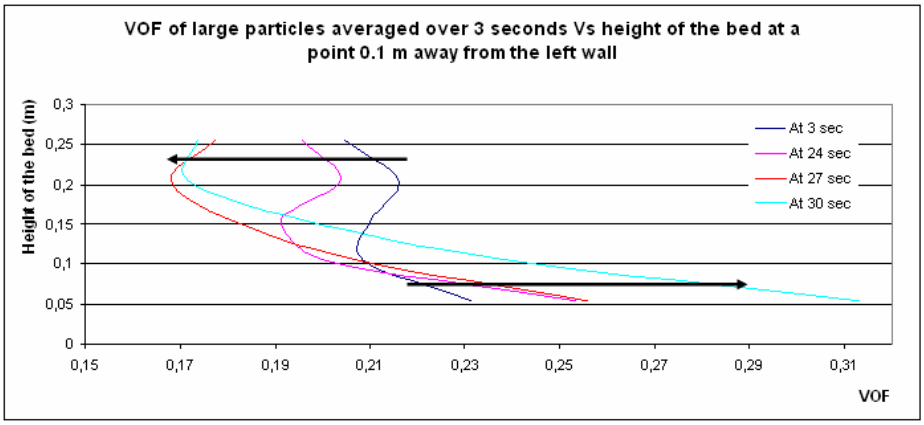

Figure G.5: Progree of particle segregation along the height of the bed at a radial position 0.05 m away from a wall with respect to the large particles in the simulation P3

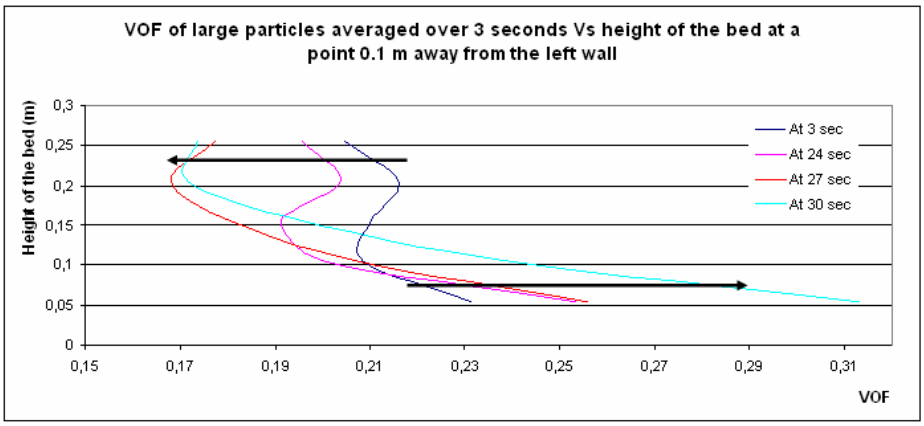

Figure G.6: Progree of particle segregation along the height of the bed at a radial position 0.1 m away from a wall with respect to the largel particles in the simulation P3

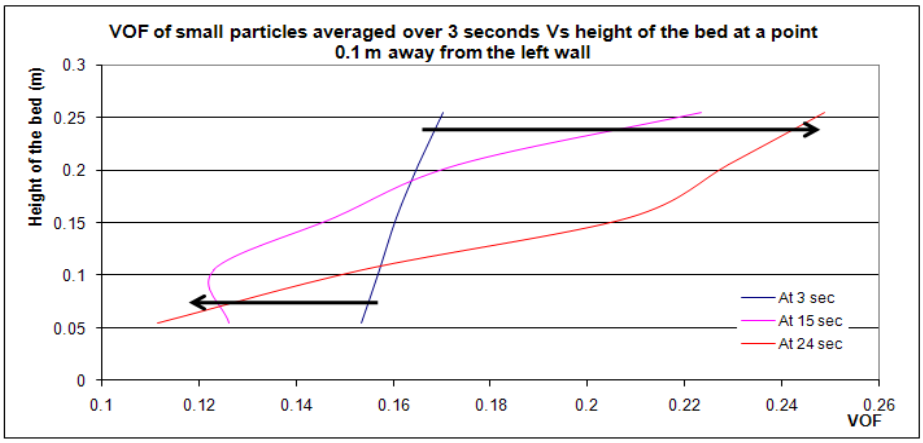

Figure G.7: Progree of particle segregation along the height of the bed at a radial position 0.05 m away from a wall with respect to the small particles in the simulation P4

G.1.3 Simulation P4

Each solid phase has presented separately for the convenience of reading due to the large number of plots available.

Small Particles

Figures G.7 and G.8 shows the selected curves to present the progress of particle segregation.

Medium Particles

Figures G.9 and G.10 shows the selected curves to present the progress of particle segregation.

Large Particles

Figures G.11 and G.12 shows the selected curves to present the progress of particle segregation.

G.1.4 Simulation P5

Each solid phase has presented separately for the convenience of reading due to the large number of plots available.

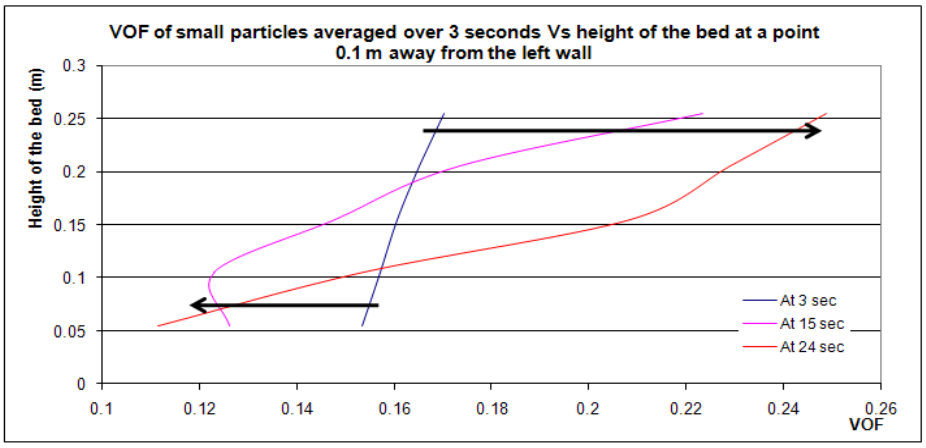

Figure G.8: Progree of particle segregation along the height of the bed at a radial position 0.1 m away from a wall with respect to the small particles in the simulation P4

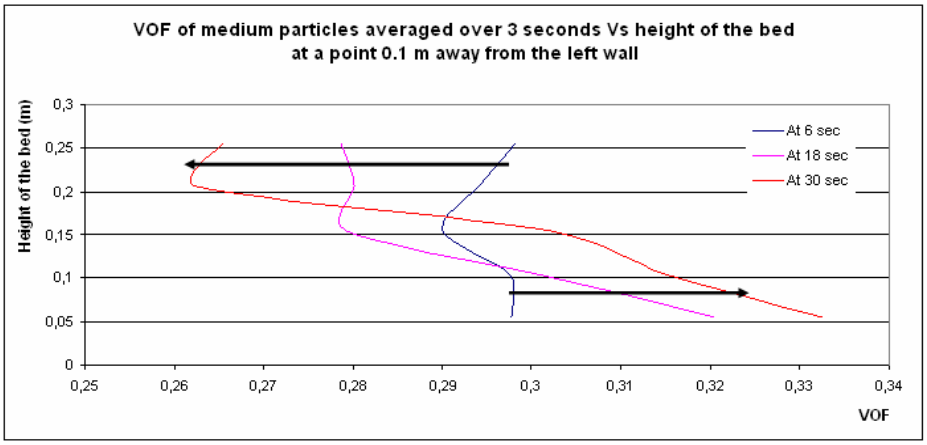

Figure G.9: Progree of particle segregation along the height of the bed at a radial position 0.05 m away from a wall with respect to the medium particles in the simulation P4

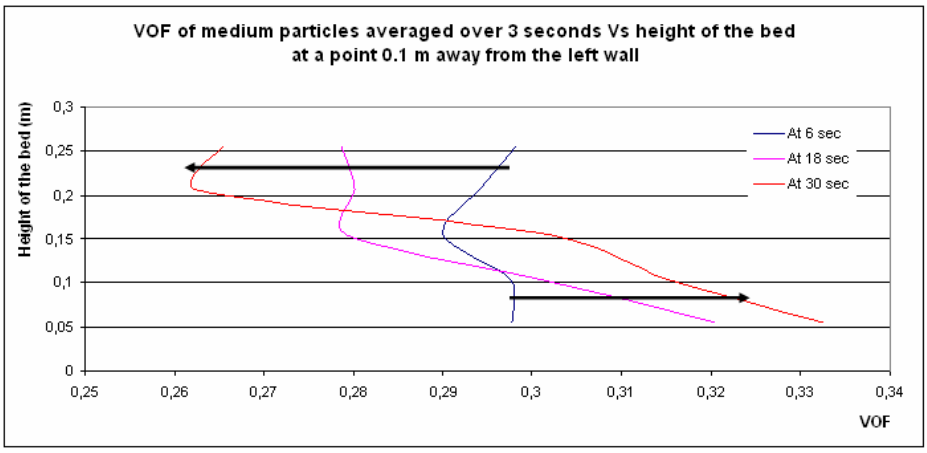

Figure G.10: Progree of particle segregation along the height of the bed at a radial position 0.1 m away from a wall with respect to the medium particles in the simulation P4

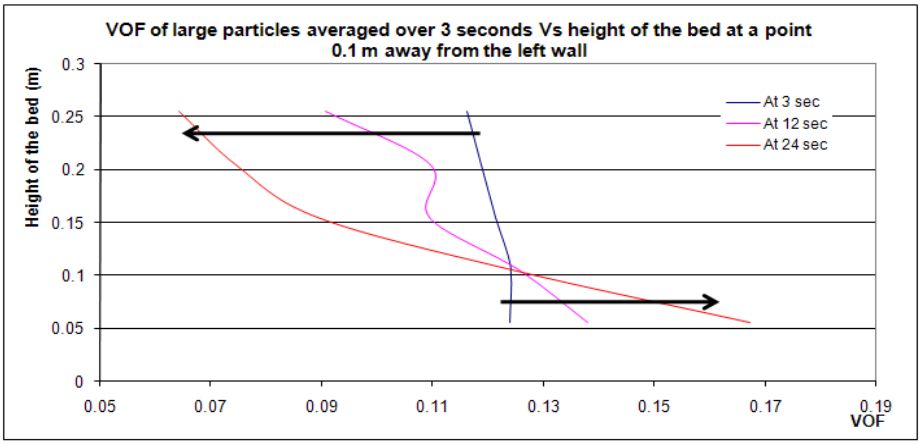

Figure G.11: Progree of particle segregation along the height of the bed at a radial position 0.05 m away from a wall with respect to the large particles in the simulation P4

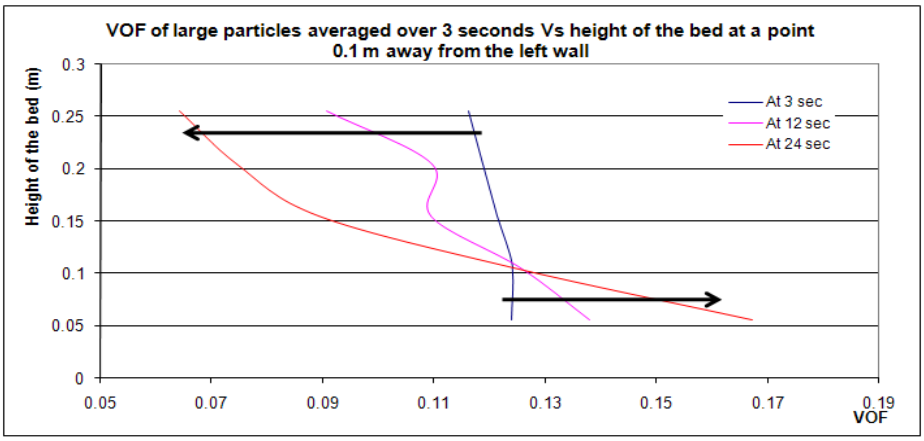

Figure G.12: Progree of particle segregation along the height of the bed at a radial position 0.1 m away from a wall with respect to the large particles in the simulation P4

Small Particles

Figures G.19 and G.14 shows the selected curves to present the progress of particle segregation.

Smaller Portion of the Medium Particles

Figures G.15 and G.16 shows the selected curves to present the progress of particle segregation.

Large Portion of the Medium Particles

Figures G.17 and G.18 shows the selected curves to present the progress of particle segregation.

Large Particles

Figures G.19 and G.20 shows the selected curves to present the progress of particle segregation.

G.2 Segregation at a Point

Figures G.21, G.22, G.23, G.24, G.25 and G.26 display the particle segregation in selected points closer to the top and bottom of the particle bed of the simulations.

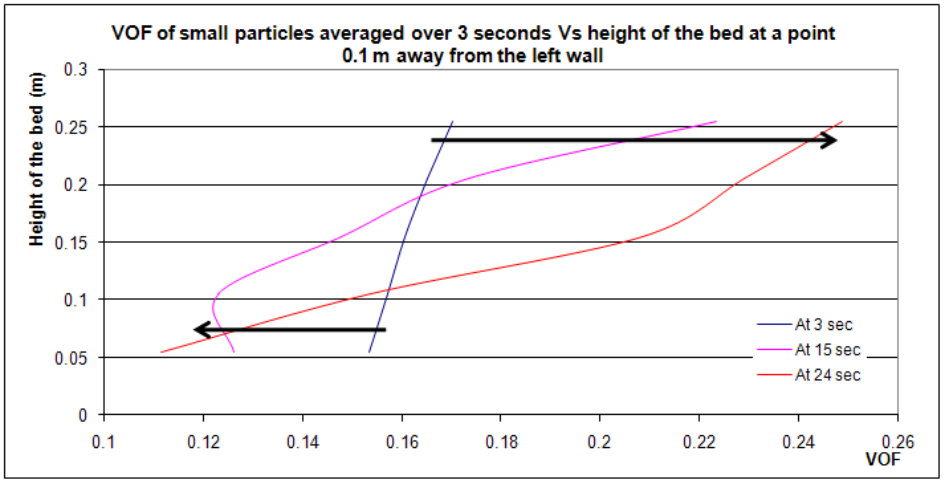

Figure G.13: Progree of particle segregation along the height of the bed at a radial position 0.05 m away from a wall with respect to the small particles in the simulation P5

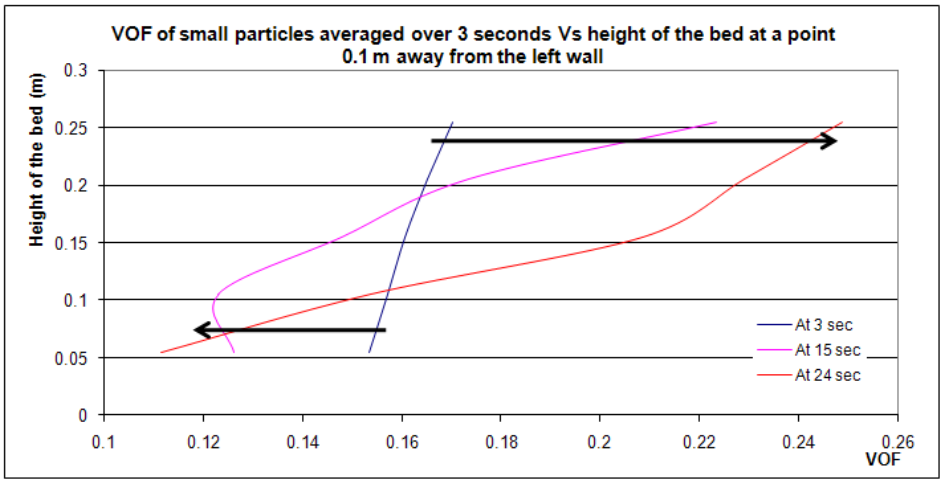

Figure G.14: Progree of particle segregation along the height of the bed at a radial position 0.1 m away from a wall with respect to the small particles in the simulation P5

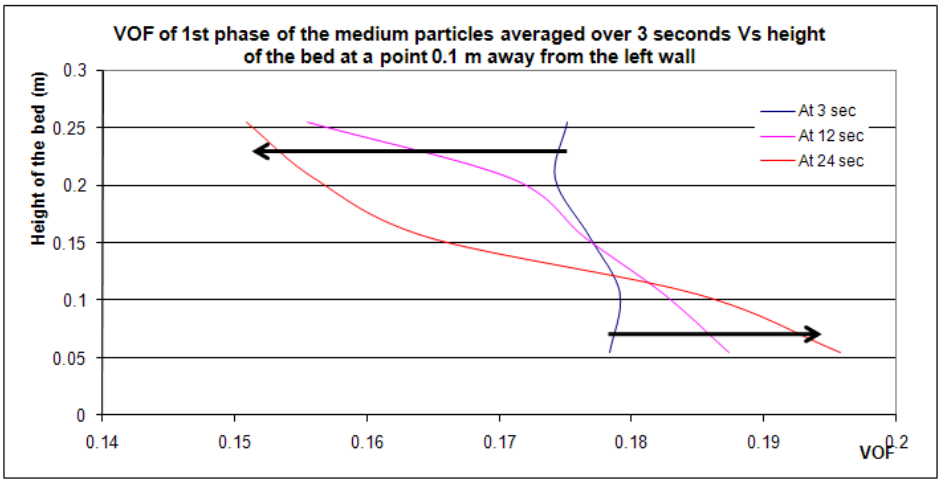

Figure G.15: Progree of particle segregation along the height of the bed at a radial position 0.05 m away from a wall with respect to the small portion of the medium particles in the simulation P5

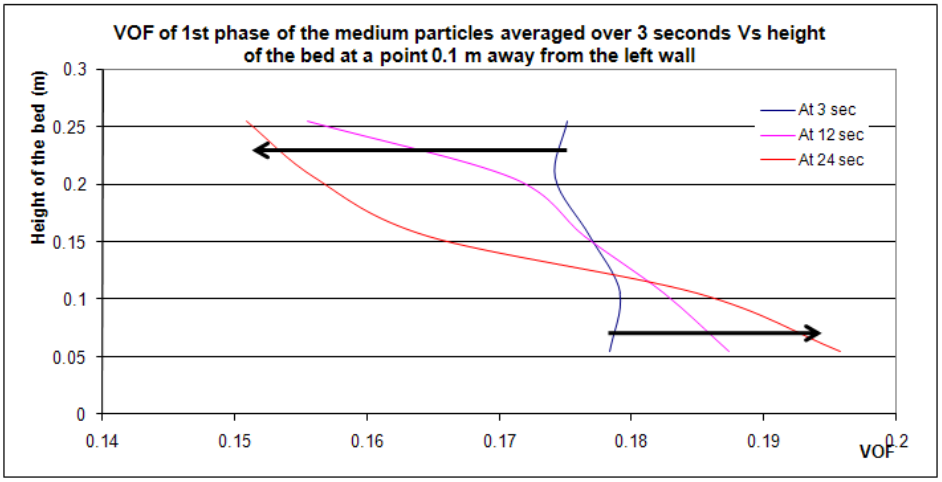

Figure G.16: Progree of particle segregation along the height of the bed at a radial position 0.1 m away from a wall with respect to the small portion of the medium particles in the simulation P5

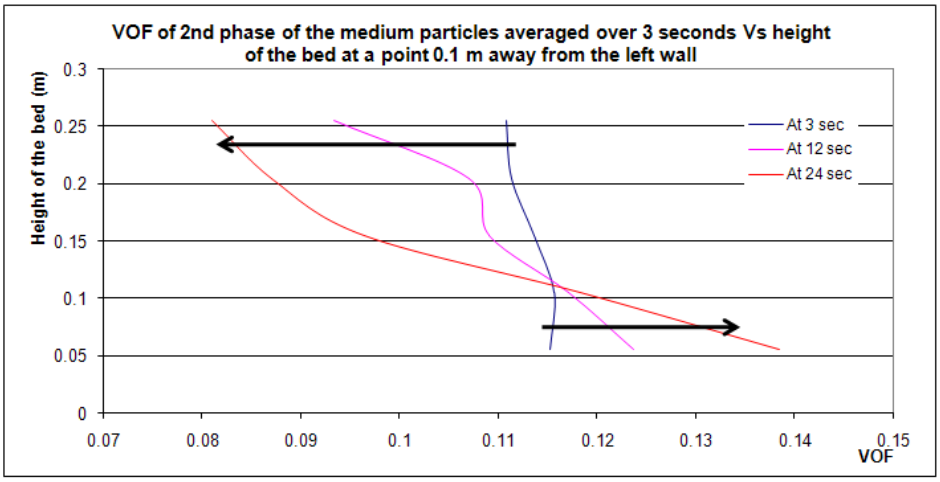

Figure G.17: Progree of particle segregation along the height of the bed at a radial position 0.05 m away from a wall with respect to the large portion of the medium particles in the simulation P5

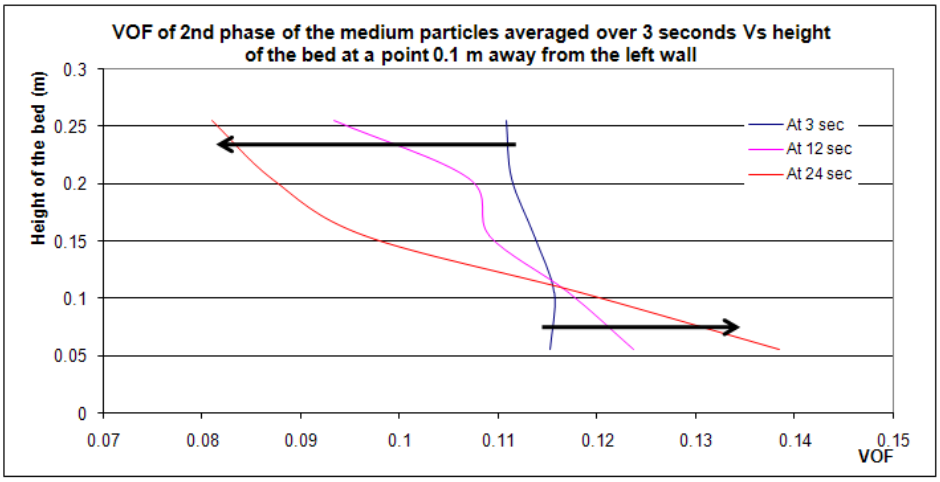

Figure G.18: Progree of particle segregation along the height of the bed at a radial position 0.1 m away from a wall with respect to the large portion of the medium particles in the simulation P5

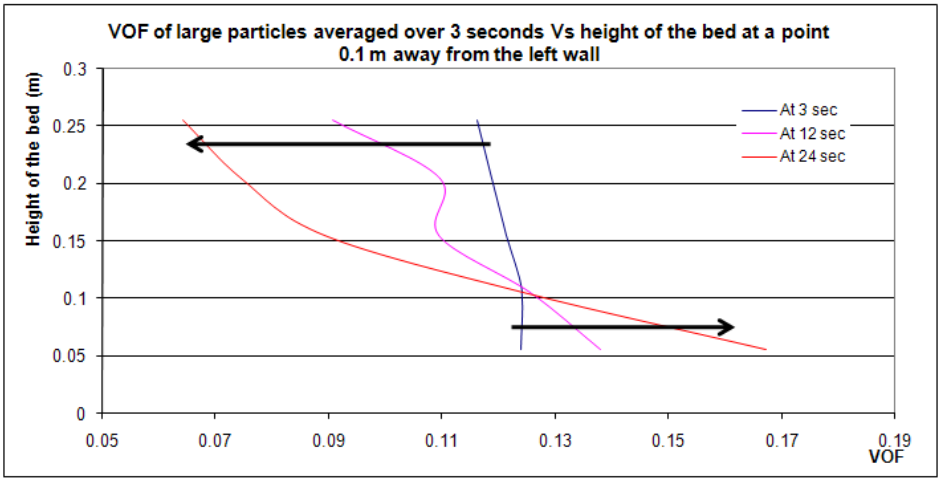

Figure G.19: Progree of particle segregation along the height of the bed at a radial position 0.05 m away from a wall with respect to the large particles in the simulation P5

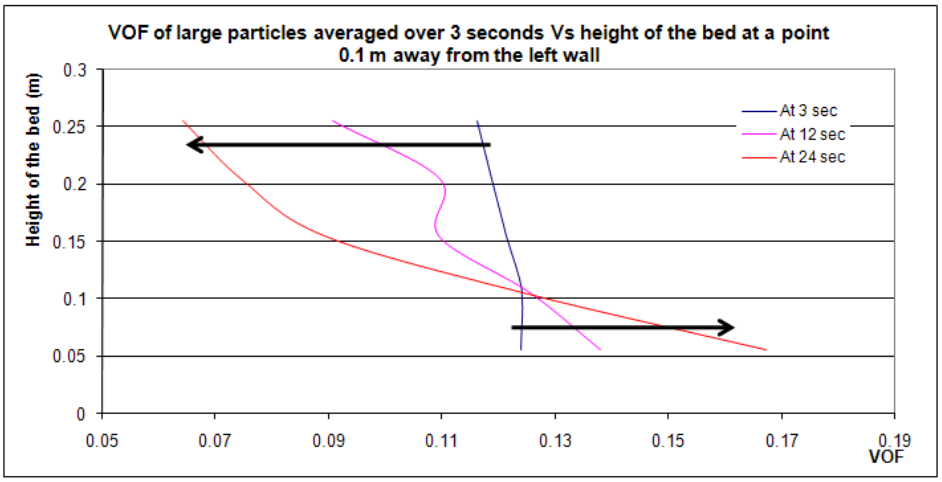

Figure G.20: Progree of particle segregation along the height of the bed at a radial position 0.1 m away from a wall with respect to the large particles in the simulation P5

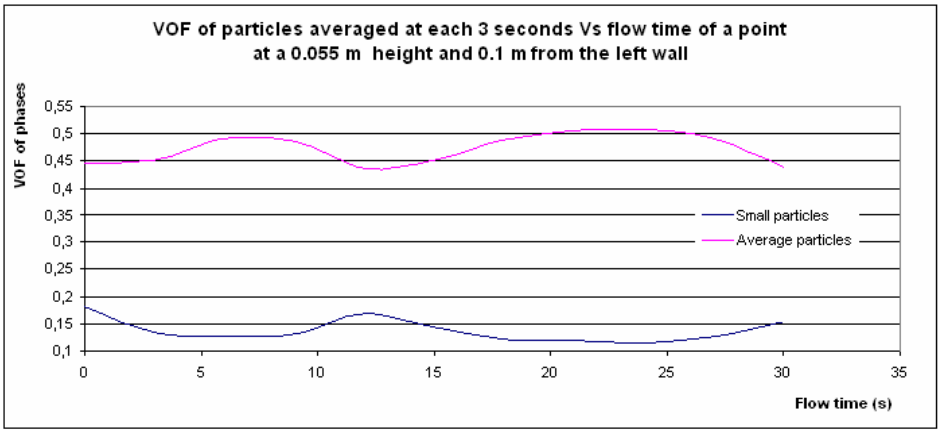

Figure G.21: VOF of particles as a function of time at a point close to the bottom of the bed in the simulation P2

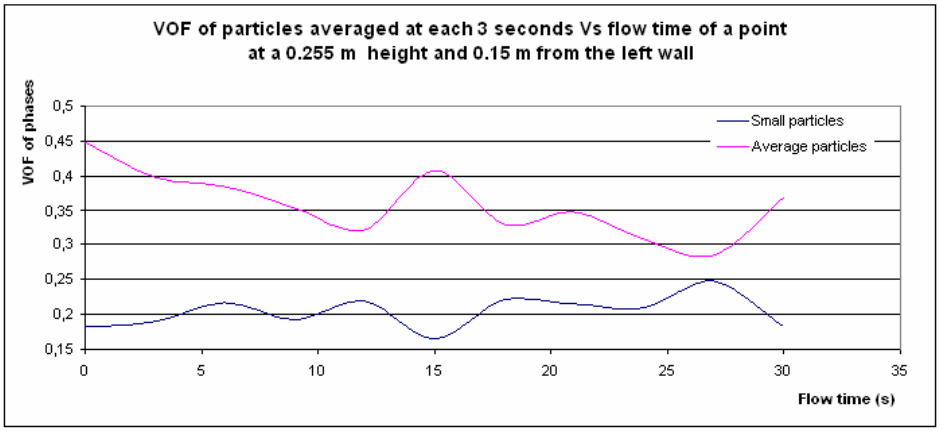

Figure G.22: VOF of particles as a function of time at a point close to the top of the bed in the simulation P2

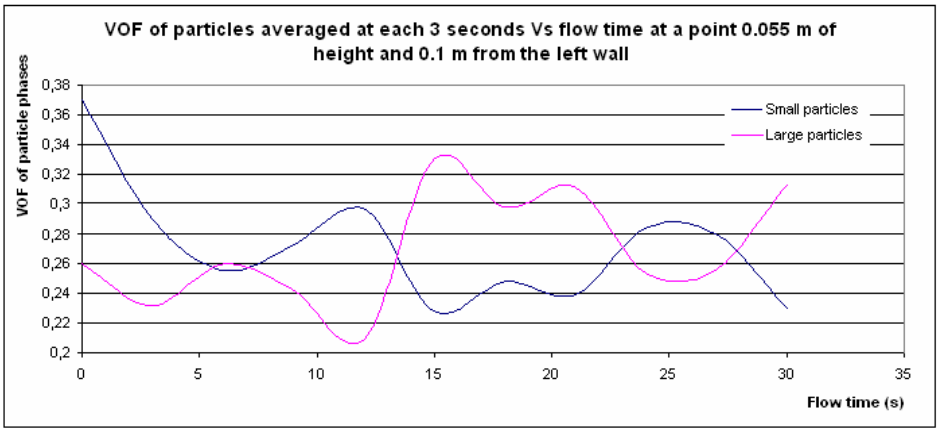

Figure G.23: VOF of particles as a function of time at a point close to the bottom of the bed in the simulation P3

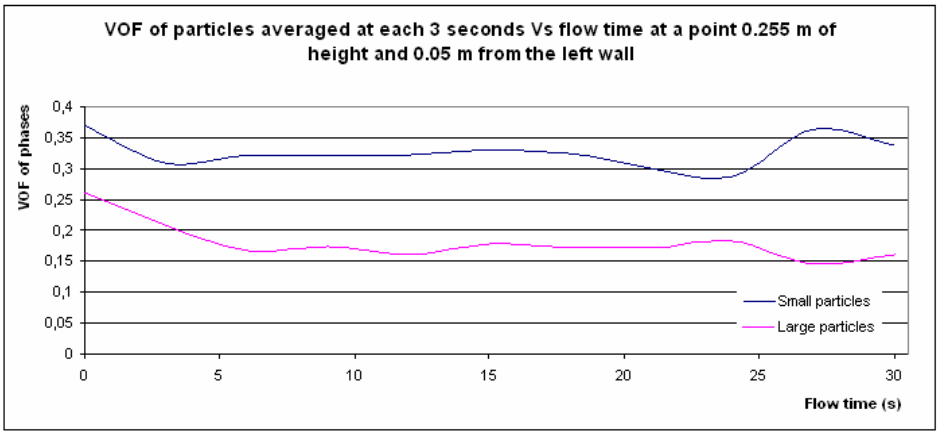

Figure G.24: VOF of particles as a function of time at a point close to the top of the bed in the simulation P3

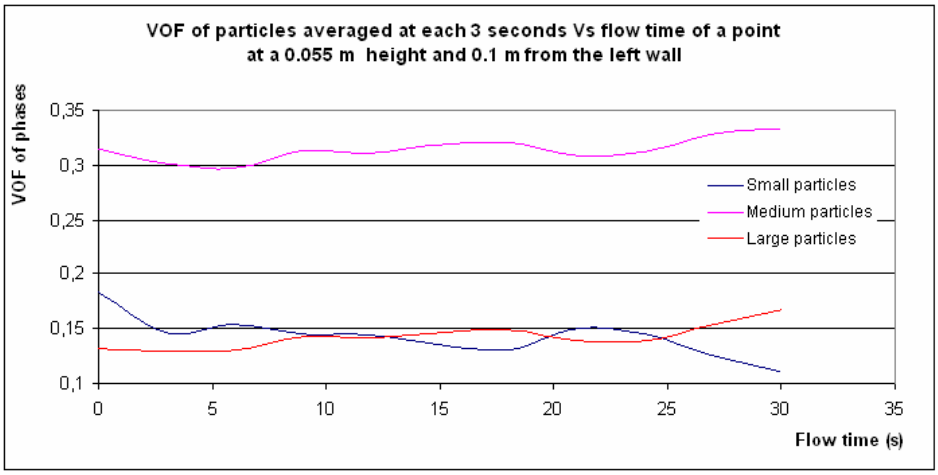

Figure G.25: VOF of particles as a function of time at a point close to the bottom of the bed in the simulation P4

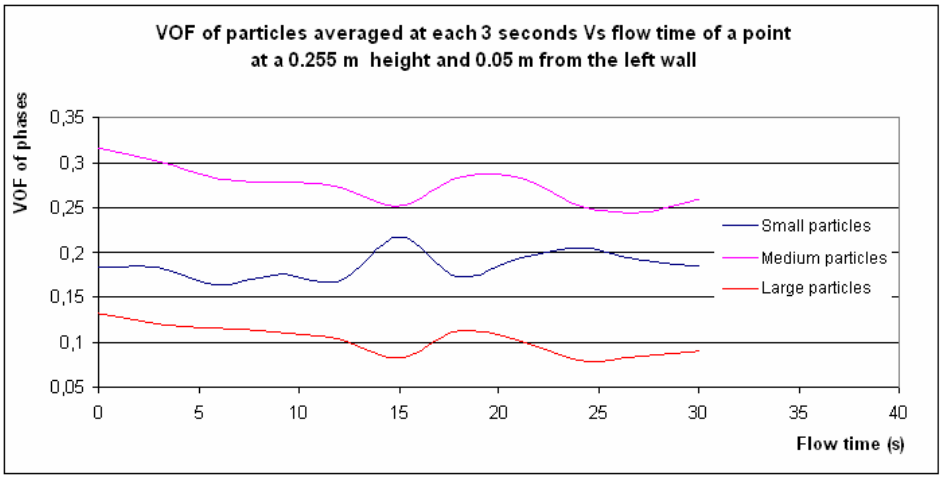

Figure G.26: VOF of particles as a function of time at a point close to the top of the bed in the simulation P4

Appendix H

Abstract for SIMS Conference

Verification of the Importance of Introducing Particle Size Distributions to Bubbling Fluidized Bed Simulations

D. G. A. S. U. Ariyarathna[a], W. J. Wu[a], B.M. Halvorsen[a,b]

[a] *Telemark University College*

[b] *Telemark Technology R&D Centre* $(Tel - Tek)$, *Norway*

Abstract

Fluidized beds are widely used in industrial operations due to their ability to give good mixing and a high contact area between the phases. The excellent controlling ability of temperature allows good operating conditions for solid catalyzed gas phase reactions and also the ease of the design.

Powders used in industrial fluidized beds have a particle size distribution, and the particle size distribution influence significantly on the flow behavior. In modelling of fluidized beds a mean particle diameter is often used, and important information about flow behavior can therefore be lost. The objective of this work is to study the influence of including particle size distribution in the simulation of a 2-D bubbling fluidized bed. Related to this work a series of simulations are performed using the commercial CFD software FLUENT version 6.3. The model used is based on a multi-fluid Eulerian description of the phases. The Shaeffer model and Syamlal O'Brien model are used as the frictional viscosity model and the granular viscosity model respectively. The drag model developed by Syamlal & O'Brien is used.

A 2-D wire frame mesh with the dimensions, 0.20 m and 1.5 m as width and height is used. The particle bed height is 0.28 m. A mean particle diameter of 488 μm and the superficial gas velocity of 0.134 m/s are used in all the simulations. The simulations are run with one, two, three and four particle phases. The particle size distribution is accounted for by including multiple particle phases. The computational results are compared to results from experiments performed by Mr. W.J. Wu at Telemark University College, Norway. A

fluidized bed which is approximated as a 2-D fluidized bed by having a depth of 0.025 m is used for the experiments.

The computational results are compared with each other with respect to the bubble appearance, bubble distribution, bubble velocity, bed expansion and particle segregation. The comparison shows that the results vary significantly depending on the number of particle phases used.

Computational results of bubble velocity, bubble distribution, bed expansion and particle segregation are compared to the experimental data. The results from the simulations with three and four particle phases agree well with the experimental results according to bed expansion and bubble behavior. In the simulations with multiple particle phases, the segregation of particles is clearly visible and show similarities to the experiments. The results show that the segregation of particles influences on the flow behavior and bubble distribution in the bed. The consequences of segregation can only be studied by using more than one particle phase in the simulations.

The simulations show the importance of accounting for the particle size distribution in the computational model. By using one particle size, important information of the flow behavior is lost, and the results deviate significantly from the experiments.

Appendix I

Abstract to the AICHE – 2008 Annual Meeting

Influence from Particle Size Distributions on the CFD Simulations and Experiments of Bubbling Fluidized Beds

D. G. A. S. U. Ariyarathna[a], W. J. Wu[a], B.M. Halvorsen[a,b]

[a] *Telemark University College*

[b] *Telemark Technology R&D Centre* $(Tel - Tek)$, *Norway*

Abstract

Fluidized beds have an enormous role in process industry. Good mixing ability and high contact area between the phases are among the important features of the fluidized beds. The efficiency of fluidized beds depends on bubble behavior in the particle phase. Industrial fluidized beds in common normally use powders with size distributions. The size and size distributions of particles used in the bed may lead to different bubble behaviors. Because of that it is important to study the influence on bubble behavior from particle size distribution in fluidized beds.

In addition to that it is important to study the influence on the simulations of fluidized beds from particle size distributions. That is because, in modelling of fluidized beds a mean particle diameter is often used, and important information about flow behavior can therefore be lost.

A series of experiments are performed in order to check the effect from particle size distribution on bubble behavior. A lab-scale fluidized bed which is approximated as a 2-D fluidized bed by having a depth of 0.025 m with a uniform air distributor is used along with a video camera to record the bubble behavior in the bed. Several simulations also carried out in order to analyze the influence from the particle size distribution on the simulated results. A 2-D wire frame mesh with the same dimensions for the particle bed is used for the simulations in the commercial CFD software FLUENT 6.3. The model used is based on a multi-fluid Eulerian description of the phases. The drag model developed by Syamlal & O'Brien is used. The particle size distribution is accounted for by

including multiple particle phases.

The experiments and simulations are carried out in Telemark University College, Norway. Spherical glass particles with a density of 2485 kg/m^3 are considered. The mixture combinations used give a mean particle diameter of 488 μm. The superficial gas velocity is 0.134 m/s in magnitude.

The computational and experimental results are analyzed separately and compared with each other with respect to the volume fraction changes along the bed with time, particle segregation and bubble frequency. The analysis shows that the computational results vary significantly depending on the number of particle phases used and the experimental results are highly dependent on the particle size distribution used. The results from the simulations with three and four particle phases agree well with the experimental results.

The simulations and experiments show that the particle size distributions significantly influence on the bubble behavior and particle segregation.